

12-2013

DESIGN AND SYNTHESIS OF POLYMER - MAGNETIC NANOPARTICLE COMPOSITES FOR USE IN BIOMEDICAL APPLICATIONS

Roland Stone

Clemson University, rolndstone@gmail.com

Follow this and additional works at: https://tigerprints.clemson.edu/all_dissertations



Part of the [Materials Science and Engineering Commons](#)

Recommended Citation

Stone, Roland, "DESIGN AND SYNTHESIS OF POLYMER - MAGNETIC NANOPARTICLE COMPOSITES FOR USE IN BIOMEDICAL APPLICATIONS" (2013). *All Dissertations*. 1248.

https://tigerprints.clemson.edu/all_dissertations/1248

This Dissertation is brought to you for free and open access by the Dissertations at TigerPrints. It has been accepted for inclusion in All Dissertations by an authorized administrator of TigerPrints. For more information, please contact kokeefe@clemson.edu.

DESIGN AND SYNTHESIS OF POLYMER - MAGNETIC NANOPARTICLE
COMPOSITES FOR USE IN BIOMEDICAL APPLICATIONS

A Dissertation
Presented to
the Graduate School of
Clemson University

In Partial Fulfillment
of the Requirements for the Degree
Doctor of Philosophy in Polymer and Fiber Science

by
Roland Christopher Stone
December 2013

Accepted by:
Dr. Olin Thompson Mefford, Committee Chair
Dr. Frank Alexis
Dr. Gary Lickfield
Dr. Igor Luzinov

ABSTRACT

The future of diagnostics and therapeutic drugs in biomedicine is nanoparticles. These nanoparticles come in many different shapes, sizes, and combination of materials. Magnetic nanoparticles have been studied for many years for use in biomedicine, not only for their high surface area, but also because of its unique magnetic properties. They can magnetically interact with their environment, be guided to a specific location, and manipulated to release energy in the form of heat. To ensure that these magnetic nanoparticles survive in the circulatory system, they must be modified with materials to make them colloidally stable in water and shield them from the body's immune response to foreign objects.

The purpose of this project is to design and synthesize a ligand for the modification of iron oxide nanoparticles with three important characteristics: 1) water-dispersable, 2) biologically stable, and 3) functional surface. This was accomplished by synthesizing specialized heterobifunctional polyethylene oxide (PEO) that has a catechol on one end to bind strongly to iron oxide nanoparticles and an alkyne on the other end to provide further functionality. This design allows for easy customization of the particles surface, using "click chemistry," with targeting and fluorescent moieties for any desired application.

The work reported discusses the techniques used for synthesizing a variety of heterobifunctional PEO via anionic ring opening polymerization of ethylene oxide and subsequent end group modifications that ultimately led to the design of a universal ligand for iron oxide nanoparticles, with improved stability in biological environments, that can

be used in many biomedical applications. These universal magnetic nanoparticles were modified with different fluorescent dyes for imaging biofilms, carbohydrates for targeting bacteria, and radiotracers for multifunctional diagnostic probes to demonstrate the versatility of this surface.

ACKNOWLEDGEMENTS

First and foremost, I would like to give all of my gratitude to my research advisor, Dr. Thompson Mefford. He took a chance on an inexperienced researcher and motivated me to do things that I never imagined possible. I can never thank him enough for his support and understanding through an extremely difficult time in my life.

I am also very grateful for my research committee, Dr. Frank Alexis, Dr. Gary Lickfield, and Dr. Igor Luziov for their guidance, time, and expertise throughout this project.

I would not have made it through graduate school without the support of my labmates, Bin Qi, Steven Saville, and Dan D'Unger. We were a very collaborative group and supported each other constantly, whether it would be supplying materials, characterization, or discussing research ideas.

I also have to show my gratitude to all of the lifelong friends I have made in the Department of Materials Science and Engineering during my 8 years at Clemson University. I will never forget the many after work hours spent at Nick's and of course the frequent weekend cookouts at Bob Bowen's spent with brilliant future scientists and great friends.

Thank you to Dr. Jeremy Tzeng's research group and Dr. Tamara McNeal's research group of the Department of Biological Sciences at Clemson University. Thank you to Dr. Urs Häfeli's research group of Department of Pharmaceutical Sciences at the University of British Columbia. Special thanks to Yash Raval in the Department of Biological Sciences for TEM of the modified magnetic nanoparticles and bacteria work,

George Huang for help with cell viability studies on the polymer-magnetic nanoparticle complexes. Thank you to Brennen Jenkins of the Department of Biological Sciences at Clemson University for the biofilm images treated with the particles I supplied them. Thank you to Katayoun Saatchi for radiolabeling data on the particles I supplied them. Thank you Ashley Hearing for the drawings of the different trisaccharades. Thank you to Kim Ivey in Material Science and Engineering at Clemson University for GPC of the polymers and particles, David Trebatoski of University of Wisconsin for his summer REU work on the biostability studies using the DLS, Bin Qi in Material Science and Engineering at Clemson University for synthesis and characterization of magnetic nanoparticles, and Dr. Steven Foulger for supplying the azido-modified dyes used in the particle modification.

DEDICATION

This work is dedicated to my grandfather, the late John Carl Marshall. He was God fearing man who saw the value in hard work and putting others first. Without his support through my undergraduate studies, I would have never imagined furthering my education.

This work is also dedicated to my loving mother and father for their constant support and guidance. They have never doubted my decisions in any aspects of my life and I would not be the man I am today without them.

I would also like to dedicate this work to my dearest friends and their families, the Whitehead's, the Abrams', the Todd's, the Joline's, and the Olesh's for always being there for me and treating me as part of their families. I cannot thank them enough for all of their love and support they have given to me from the first time I befriended their children in middle school.

Finally, I would like to dedicate this work to my love, Jennifer Olesh. I am so grateful for her love and support to get me through a time in my life that I would not have been able to handle on my own. I love you, most ardently.

TABLE OF CONTENTS

	Page
ABSTRACT	I
ACKNOWLEDGEMENTS.....	III
DEDICATION.....	V
LIST OF TABLES.....	X
LIST OF FIGURES	XI
CHAPTER 1. INTRODUCTION MAGNETIC NANOPARTICLES FOR TARGETED MAGNETIC HYPERTHERMIA.....	1
1.1. ABSTRACT	1
1.2. MAGNETIC HYPERTHERMIA.....	2
1.3. INORGANIC MAGNETIC NANOPARTICLES USED IN BIOMEDICAL APPLICATIONS	2
1.4. NANOPARTICLE SIZE EFFECTS ON MAGNETIC NANOPARTICLES..	4
1.5. MEASURING HEATING EFFICIENCY OF MAGNETIC NANOPARTICLES.....	6
1.6. PARTICLE MODIFICATION.....	9
1.7. SIZE AND SURFACE CHARGE EFFECTS ON STABILITY.....	13
1.8. MOLECULAR WEIGHT AND SURFACE CHARGE EFFECTS ON STABILITY	14
1.9. IMPORTANCE OF POLYETHYLENE GLYCOL IN THERAPEUTICS...	16
1.10. “CLICK CHEMISTRY”	18
1.11. OVERVIEW	20
CHAPTER 2.SYNTHETIC TECHNIQUES USED TO PRODUCE HETEROBIFUNCTIONAL POLYETHYLNE OXIDE OLIGOMERS	21

2.1. ABSTRACT	21
2.2. INTRODUCTION	21
2.3. MATERIALS AND CHARACTERIZATION	23
2.3.1 Materials	23
2.3.2. Potassium naphthalenide preparation	25
2.3.3. Characterization Techniques	25
2.4. ANIONIC RING OPENING POLYMERIZATION OF ETHYLENE OXIDE USING TERT-BUTYL MERCAPTAN	27
2.4.1 Experimental.....	27
2.4.2. Results and Discussion	28
2.5. ANIONIC RING OPENING POLYMERIZATION OF ETHYLENE OXIDE USING ALLYL ALCOHOL	30
2.5.1 Experimental.....	30
2.5.2. Results and Discussion	30
2.6. ANIONIC RING OPENING POLYMERIZATION OF ETHYLENE OXIDE USING TETRABUTYLAMMONIUM AZIDE.....	32
2.6.1. Experimental.....	32
2.6.2. Results and Discussion	33
2.7. ANIONIC RING OPENING POLYMERIZATION OF ETHYLENE OXIDE USING HYDROXYPYRILTRIVINYLSILANE (HPTVS) AS INITIATOR	37
2.7.1. Experimental.....	37
2.7.2. Results and Discussion	40
2.8. ANIONIC RING OPENING POLYMERIZATION OF ETHYLENE OXIDE USING 2-(TETRAHYDRO-2H-PYRAN-2-YLOXY)ETHANOL (THP) AS INITIATOR	46
2.8.1. Experimental.....	46
2.7.2. Results and Discussion	46
2.9. ANIONIC RING OPENING POLYMERIZATION OF ETHYLENE OXIDE USING POTASSIUM BIS(TRIMETHYLSILYL) AMIDE AS INITIATOR	48

2.9.1. Experimental.....	48
2.9.2. Results and Discussion.....	49
2.10. CREATING HETEROBIFUNCTIONALITY THROUGH END GROUP MODIFICATION	51
2.10.1 Modification of an alcohol terminus to a carboxylic acid.....	51
2.10.2. Modification of Alcohol Terminus with NitroDOPA	52
2.10.3. Modification of the Alcohol Terminus to an Alkyne	54
2.10.4. Modification of the Alcohol Terminus to a Methacrylate.....	56
2.11. CONCLUSION	57
 CHAPTER 3. SYNTHESIS AND CHARACTERIZATION OF HETEROBIFUNCTIONAL POLY(ETHYLENE OXIDE) PLATFORM FOR BIOMEDICAL MAGNETIC NANOPARTICLES	59
3.1. ABSTRACT	59
3.2. INTRODUCTION.....	59
3.3. EXPERIMENTAL.....	61
3.3.1. Synthesis of nitroDOPA	61
3.3.2. Synthesis of THP-PEO-OH.....	61
3.3.3. Synthesis of THP-PEO-Alkyne	62
3.3.4. Deprotection of THP-PEO-Alkyne	63
3.3.5. Synthesis of Alkyne-PEO-COOH	64
3.3.6. Synthesis of Alkyne-PEO-NHS.....	64
3.3.7. Synthesis of Alkyne-PEO-NitroDOPA	65
3.3.8. Synthesis of magnetite nanoparticles	66
3.3.9. Modification of magnetite nanoparticles.....	66
3.3.10. Functionalization of alkyne-PEO-nitroDOPA coated magnetic nanoparticles with azido-functionalized dyes	67
3.4. RESULTS AND DISCUSSION.....	67
3.5. CONCLUSIONS	76

CHAPTER 4. SYNTHESIS AND CHARACTERIZATION OF MULTI-ANCHORED HETEROBIFUNCTIONAL POLY(ETHYLENE OXIDE) FOR ENHANCED STABILITY AND FUNCTIONALITY OF MAGNETIC NANOPARTICLES.....	78
4.1. ABSTRACT	78
4.2. INTRODUCTION	78
4.3. EXPERIMENTAL.....	81
4.3.4. Modification of Protected amine-PEO with alkyne	81
4.3.5. Deprotection of amine-PEO-alkyne	82
4.3.6. Modification of poly(acrylic acid) with amine-PEO-alkyne	82
4.3.7. Modification of PAA-PEO-alkyne with NitroDOPA.....	83
4.3.8. Modification of Magnetic Nanoparticles with Polymer	83
4.3.9. Cell Viability Studies.....	84
4.3.10. Modification of particles with Azido-Cy5.5 Dye.....	84
4.4. RESULTS AND DISCUSSION.....	85
4.5. CONCLUSIONS	99
CHAPTER 5. VERSATILITY OF A MULTI-ANCHORED HETEROBIFUNCTIONAL POLY(ETHYLENE OXIDE) MODIFIED MAGNETIC NANOPARTICLES	100
INTRODUCTION	100
BACTERIAL AGGREGATION AND TREATMENT USING MAGNETIC HYPERTHERMIA	101
INTERACTIONS OF MAGNETIC NANOPARTICLES IN BACTERIAL BIOFILM	109
MULTIFUNCTIONAL DIAGNOSTIC PROBE FOR SPECT/MR IMAGING	114
CHAPTER 6. FUTURE WORK	117
CHAPTER 7. CONCLUSIONS	124
REFERENCES	126

LIST OF TABLES

	Page
Table 3.1. DLS of magnetic nanoparticles before and after modification.....	72
Table 4.1 Presents the results of the time dependence studies done in a 50% FBS in magnetic nanoparticles solution (v/v).....	93

LIST OF FIGURES

	Page
Figure 1.1 (A) Néel relaxation and (B) Brownian motion mechanisms when exposed to an AC field.....	4
Figure 1.2. General schematic of AC calorimeter that can be used to measure SAR.	7
Figure 1.3. The interaction potential between magnetic nanoparticles can be determined by adding the potential energies of the particles as a function of their distance.	13
Figure 1.4. Schematic of a 1,3-dipolar cycloaddition of alkyne and azide yielding a triazole.	19
Figure 2.1. Partial derivatization of diols of polyethylene glycol to create heterobifunctionality.....	22
Figure 2.2. Anionic ring opening polymerization using an initiator with X functionality and then terminating with a functionality of Y.....	23
Figure 2.3. Anionic ring opening polymerization of ethylene oxide using tert-butyl mercaptan.....	28
Figure 2.4. ¹ HNMR spectra of tert-butyl-thiol initiated PEO.....	29
Figure 2.5. Anionic ring opening polymerization of ethylene oxide using allyl alcohol as an initiator.....	31
Figure 2.6. Anionic ring opening polymerization of ethylene oxide using allyl alcohol.....	32
Figure 2.7. Coordination ring opening polymerization using tetrabutylammonium azide and triisobutylaluminum catalyst.....	34
Figure 2.8. ¹ HNMR of anionic ring opening polymerization of ethylene oxide using tetrabutylammonium azide and triisobutylaluminum catalyst.....	35
Figure 2.9. ¹³ CNMR spectra of anionic ring opening polymerization of ethylene oxide using tetrabutylammonium azide and triisobutylaluminum catalyst.....	36
Figure 2.10. FTIR spectra of anionic ring opening polymerization of ethylene oxide using tetrabutylammonium azide and triisobutylaluminum catalyst.....	37
Figure 2.11. I) Synthesis of 3-chloropropyltrivinylsilane (CPTVS), II) 3-iodopropyltrivinylsilane (IPTVS), III) 3-hydroxypropyltrivinylsilane (HPTVS).....	40

Figure 2.12. ¹ HNMR spectrum of chloropropyltrivinylsilane.....	42
Figure 2.13. ¹ HNMR spectrum of iodopropyltrivinylsilane.....	43
Figure 2.14. ¹ HNMR spectrum of hydroxypropyltrivinylsilane.....	44
Figure 2.15. Anionic ring opening polymerization of ethylene oxide using HPTVS	44
Figure 2.16. ¹ HNMR of the anionic polymerization of ethylene oxide initiated by HPTVS.....	45
Figure 2.17. Anionic ring opening polymerization of ethylene oxide using 2	47
Figure 2.18. ¹ HNMR spectrum of anionic ring opening polymerization of ethylene oxide using 2-(tetrahydro-2H-pyran-2-yloxy)ethanoxide	48
Figure 2.19. Anionic ring opening polymerizaion of ethylene oxide using potassium bis(trimethylsilyl)amide.....	49
Figure 2.20. ¹ HNMR spectrum of the anionic ring opening polymerization of ethylene oxide using potassium bis(trimethylsilyl)amide as an initiator.	50
Figure 2.21. End group modification of THP-PEO-OH with carboxylic acid using succinic anhydride.	51
Figure 2.22. End group modification of THP-PEO-COOH with NHS intermediate.	53
Figure 2.23. End group modification of THP-PEO-NHS with nitroDOPA.	54
Figure 2.24. End group modification of THP-PEO-OH with propargyl bromide to give alkyne functionality.	55
Figure 2.25. End group modification of PEO-OH with methacrylol chloride.	57
Figure 3.1. Anionic ring opening polymerization of ethylene oxide using THP initiator.	61
Figure 3.2. End group modification of THP-PEO-OH with propargyl bromide.	62
Figure 3.3. Cleavage of tetrahydropyranol to yield alkyne-PEO-OH	63
Figure 3.4. Modification of alcohol terminus with carboxylic acid using succinic anhydride.	64
Figure 3.5. PEO-alkyne modified with NHS intermediate.....	64

Figure 3.6. Modification of PEO with nitroDOPA.....	65
Figure 3.7. ¹³ CNMR spectra of nitroDOPA in D ₂ O	68
Figure 3.8. Interferogram of DOPA (top) and nitroDOPA (bottom). Symmetric and asymmetric stretching peaks at 1330 and 1532 cm ⁻¹ confirm nitration.....	69
Figure 3.9. TEM micrograph of iron oxide nanoparticles synthesized via thermal decomposition with a mean size of 7.2nm ± 0.9.	70
Figure 3.10. Schematic of a magnetic nanoparticle modified with alkyne-PEO-nitroDOPA (left) and TEM micrograph of particles after modified with alkyne-PEO-nitroDOPA (right).....	71
Figure 3.11. Thermograph of particles modified with alkyne-PEO-nitroDOPA	73
Figure 3.12. (Left) Hydrodynamic diameter by intensity of magnetic nanoparticles before and after modification with alkyne-PEO-nitroDOPA; size data chart available (Right) Hydrodynamic diameter by intensity of the particles titrated with PBS, FBS, and BSA.....	74
Figure 3.13. Schematic of azide modified dyes used to modify magnetic nanoparticles using “click chemistry.” A) carbazole modified with an azide and B) fluorescein modified with an azide.	75
Figure 3.14. Image on the left shows a photoluminescence spectrum of particles before and after functionalization with fluorescein. Image on the right represents the final construction of magnetic nanoparticle with functional surface modified with a fluorophore.	75
Figure 3.15. Photoluminescence of mono-anchored nanoparticles after modification with A) carbazole dye (348 and 363 nm) and B) fluorescein dye (417 nm).	76
Figure 4.1. Schematic of synthesis and end group modification to yield heterobifunctional PEO (amine-PEO-alkyne)	86
Figure 4.2. Schematic of step taken to synthesize multi-anchored particles. 1) Modification of PAA with amine-PEO-alkyne. 2) Modification of PAA-PEO-alkyne with nitroDOPA. 3) Particle modification with multi-anchored particles.....	87
Figure 4.3. FTIR spectra of PAA (red) and PAA-PEO-alkyne (blue). Peak at 1728 cm ⁻¹ is attributed to carboxyl from PAA, and the peaks at 1648 and 1531 cm ⁻¹ are attributed to the carboxyl amide bond between amine-PEO-alkyne.	88

Figure 4.4. TEM micrograph (left) of multi-anchored particles and DLS (right) of the modified particles in DI water.	89
Figure 4.5. TGA thermogram of multi-anchored magnetic nanoparticles, 81.3% weight loss.	90
Figure 4.6. FTIR spectrum of multi-anchored particles. A) Alkyne group on the surface of the particle. B) Carbonyl stretching of PAA (1711 cm^{-1}). C and D) Amide-carbonyl stretch (1643 and 1561 cm^{-1}) indicating modification of PAA.	91
Figure 4.7. Stability studies comparing mono and multi-anchored particles. A) DLS of mono-functional particles in 50% by volume PBS at $37\text{ }^{\circ}\text{C}$; B) DLS of multi-functional particles in 50% by volume PBS at $37\text{ }^{\circ}\text{C}$; C) DLS of mono-anchored particles titrated with PBS from 0-100% by volume; D) DLS of multi-anchored particles titrated with PBS from 0-100% by volume;.....	92
Figure 4.8. Cell viability of L929 cells after exposure with multi-anchored particles for 24 and 48 hours at different concentration of iron. (mean \pm standard dev.; n=3)	95
Figure 4.9. Micrographs of cells incubated with multi-anchored magnetic nanoparticles after 24 hours. A) Control, B) $63\text{ mg of Fe}_3\text{O}_4\text{ mL}^{-1}$, respectively. All scale bars are 100 micrometers. Green circle shows an example of a living cell and red circle shows a dead cell.	97
Figure 4.10. Micrographs of cells incubated with multi-anchored magnetic nanoparticles after 48 hours. A) Control, B) $63\text{ mg of Fe}_3\text{O}_4\text{ mL}^{-1}$, respectively. All scale bars are 100 micrometers. All scale bars are 100 micrometers. Green circle shows an example of a living cell and red circle shows a dead cell.....	97
Figure 4.11. Photoluminescence of multi-anchored particles before and after being modified with Cy5.5 using “click chemistry.”	98
Figure 5.1. Schematic summarizing the flexibility of the heterobifunctional PEO scaffolding used to modify magnetic nanoparticles. A) magnetic nanoparticle modified with alkyne-PEO-nitroDOPA, B) micrograph of clustered <i>E. coli</i> using magnetic nanoparticles functionalized with Tr-32, C) 3D fluorescent imaging of biofilms treated with magnetic nanoparticles with Cy5.5 dye, and D) Chelated ^{64}Ga ligand used to modify magnetic nanoparticles for SPECT/MR imaging.	101
Figure 5.2. Structure of Tr32 tri-saccharides that was used to target <i>E. coli</i> K99 bacteria.	102
Figure 5.3. Fluorescence (left column) and phase-contrast (right column) microscopy of A) <i>E. coli</i> K99 in PBS, B) <i>E. coli</i> K99 with mono-anchored particles (unmodified),	

C) <i>E. coli</i> O157:H7 with Tr-32 modified particles, D) <i>E. coli</i> K99 with Tr-32 modified particles. All scale bars are 100µm.	104
Figure 5.4. <i>E. coli</i> treatment with mono-anchored particles (unmodified) and Tr-32 modified particles. Data represented as Mean ± SD (n=3).....	105
Figure 5.5. Hyperthermia treatment of <i>E. coli</i> with mono-anchored particles (unmodified) and Tr-32 modified particles. Data represented as mean ± SD (n=3) (p<0.001)	107
Figure 5.6. A) MTS assay of mono-anchored nanoparticles in human colon cells (CCD18-Co). B) MTS assay of Tr-32 modified nanoparticles in human colon cells (CCD18-Co).	108
Figure 5.7. 3D Micrographs of <i>L. pneumophila</i> before and after treated with nanoparticles. A) Confocal micrograph of biofilm control. B) Confocal micrograph of biofilm treated with 1 µg of Fe/L of Cy5.5 modified magnetic nanoparticles. C) GSD micrograph of control. D) GSD micrograph of biofilm treated with 1 µg of Fe/L of Cy5.5 modified magnetic nanoparticles.	111
Figure 5.8. A) Biomass, B) Thickness, and C) Roughness analysis of biofilms before and after Cy5.5 particles were added. Data represented as Mean ± SD (n=3).....	112
Figure 5.9. Side profile of GSD image of biofilm (green) modified with Cy5.5 magnetic nanoparticles (red)	114
Figure 5.10. Schematic 1,4,7-triazacyclononane-1,4,7-triacetate (NOTA) ligand that is commonly used to chelate ⁶⁷ Ga radiotracer.....	115
Figure 6.1. Proposed anionic ring opening polymerization of ethylene oxide using a protected propargyl alcohol as an initiator.	118
Figure 6.2. Magnetic nanoparticle functionalized with a variety of functionalities on the same nanoparticle. From top to bottom: moiety that can chelate different metals, folic acid to target overexpressed folate receptors, and Cy5 NIR dye that can be used for imaging through human tissue.	119
Figure 6.3. Schematic of ATRP polymerization of PEO-alkyne and catechol-methacrylate block copolymer.....	120
Figure 6.4. Schematic of clustered nanoparticles via “click chemistry” using a bis-azide to link the alkyne surface of the magnetic nanoparticles.....	121

Figure 6.5. Magnetic nanoparticle displaying a surface with a combination of alkyne for functionalization with a targeting or fluorescent moiety and amines for aiding in internalization. 122

CHAPTER 1. INTRODUCTION MAGNETIC NANOPARTICLES FOR TARGETED MAGNETIC HYPERTHERMIA

1.1. ABSTRACT

Nanotechnology provides a unique approach to solving some of the world's biggest problems. One of the largest research areas currently utilizing nanotechnology in the form of nanoparticles, particles smaller than 100 nm, is biomedicine. Typically these nanoparticles are used as a vessel for carrying therapeutic drugs for treatment or diagnostic dyes for imaging because of the large surface area available to carry these agents. Much work has been done into the synthesis of nanoparticles using inorganic, magnetic materials that adds magnetic component that can be manipulated in a magnetic field. For biomedicine, they offer a new functionality that can be taken advantage of for delivery (magnetic targeting), therapy (magnetic hyperthermia), and diagnostics (contrast agents) that was not available before. Unfortunately, many of these magnetic nanoparticles are synthesized using hydrophobic ligands that are incompatible for biomedical applications and require water-soluble coatings to improve biocompatibility. This chapter will provide background information about the different types of inorganic materials used in magnetic nanoparticles, surface coatings used to make them more biocompatible, how their size and surface can affect delivery and treatment, the importance of polyethylene oxide (PEO) for biological stability of drugs, and how "click chemistry" has revolutionized drug conjugation.

1.2. MAGNETIC HYPERTHERMIA

The application of alternating magnetic fields to magnetic materials, known as magnetic hyperthermia, was first investigated by Gilchrist et al. in 1957.¹ The general procedure for magnetic hyperthermia involves the accumulation of magnetic nanoparticles via the local application of a magnetic field or surface functionalization with targeting ligands that specifically bind to cell or tissue receptors after systemic or local administration. Once the magnetic nanoparticles (MNPs) are in the desired location, an alternating magnetic field of specified field and frequency is applied to generate heat and increase the temperature of the surrounding diseased tissue. Ideally, the tissue is heated to approximately 42°C for at least 30 minutes.² This targeted “fever” results in the destruction of cancer or other unwanted cells and tissue. Magnetic hyperthermia has been successively demonstrated in numerous cancerous treatments in vitro and in vivo, such as melanoma,³ glioma,⁴ and human colonic adenocarcinoma.⁵

1.3. INORGANIC MAGNETIC NANOPARTICLES USED IN BIOMEDICAL APPLICATIONS

Since metal-oxides were synthesized into nanoparticles, they have been of interest in the medical field for use in imaging and drug delivery due to their response to applied magnetic fields. Examples of different inorganic nanometer sized particles developed for magnetic applications are iron platinum,⁶⁻¹⁰ iron palladium,¹¹ cobalt platinum,^{12,13} cobalt oxide,¹⁴ and manganese based nanoparticles.^{15,16} Although these particles exhibit superior magnetic properties, they are not as biocompatible as iron oxide based nanoparticles (IONP),¹⁷ i.e. magnetite (Fe_3O_4),¹⁸ and maghemite ($\gamma\text{-Fe}_2\text{O}_3$).¹⁹ IONPs have been used for years in magnetic resonance imaging (MRI) contrast agents to improve medical

diagnostics.^{20,21} There has also been recent interest in the use of these same particles in magnetic cell separation^{22,23} and magnetic hyperthermia for cancer therapy.^{2,24-26}

Other substituted ferrites, CoFe_2O_4 ,²⁶ MnFe_2O_4 ,²⁷ and NiFe_2O_4 ²⁸ are being studied for their use in contrast agents and magnetic hyperthermia because of their high specific absorption rate (SAR) and biocompatibility once modified with a stabilizing layer. Pradhan et al. compared the magnetic heating properties and biocompatibility of Fe_3O_4 , CoFe_2O_4 , and MnFe_2O_4 modified with lauric acid. They discovered that Fe_3O_4 and MnFe_2O_4 had the higher SARs, 120 and 97 W g^{-1} ferrite, respectively. CoFe_2O_4 not only had the lowest SAR at 37 W g^{-1} ferrite, but the percent viability was the lowest for every concentration studied.²⁹ Buckley et al. has also shown that nickel zinc ferrite nanoparticles can be used in shape memory polymers for medical stents and intravascular actuators.³⁰

Noble metals such as gold and silver have also been synthesized into nanoparticles that have distinct optical (e.g. plasmonic) and surface properties for biological applications.³¹ Gold is useful as a tracer and silver nanoparticles are very strong light absorbers and scatterers.^{25,32-34} These nanoparticles are used in catalysis and chemical sensing, as shells for magnetic nanoparticles to improve ligand binding, and in exploiting magnetic and optical properties.^{35,36} These properties make them ideal for biological conjugation and labeling applications using photothermal imaging, dark field microscopy, and fluorescent microscopy.³⁷

Metal oxide magnetic nanoparticles are synthesized using different methods based upon the application of the IONP system. One of the most common procedures used to

create IONPs involves co-precipitation of iron (II) chloride and iron (III) chloride from a basic solution in water.^{38,39} This method generally produces MNPs with a charged surface and polydispersity. More advanced synthetic methods have been developed to produce size controlled, monodispersed nanoparticles by the decomposition of metal precursors in high boiling point (~300°C) solvents and surfactants.^{15,18} The surfactants that are generally used are fatty hydrocarbons that produce hydrophobic particles. These hydrophobic surfaces are unsuitable for the aqueous environment of the body and require further surface modification.

1.4. NANOPARTICLE SIZE EFFECTS ON MAGNETIC NANOPARTICLES

Literature suggests that Néel relaxation of the magnetic moments, (Figure 2A) has the most influence on the heating of single domain particles, whereas Brownian losses (Figure 2B) brought about by particle rotation against viscous forces do not contribute to frequencies suggested for medical applications; the MNPs must be larger.⁴⁰

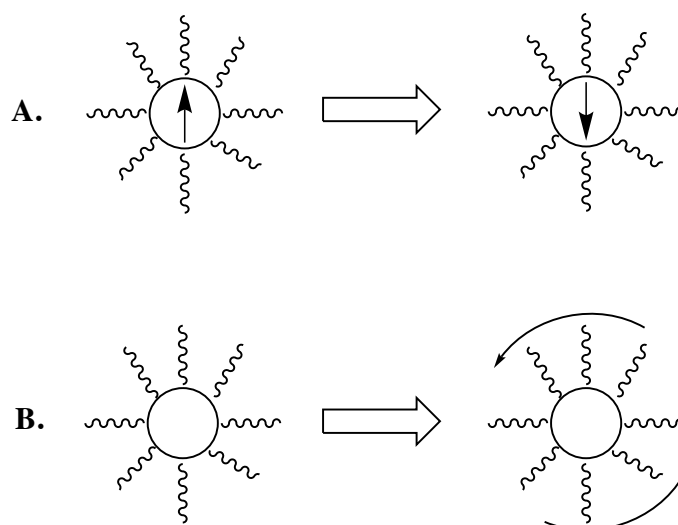


Figure 1.1 (A) Néel relaxation and (B) Brownian motion mechanisms when exposed to an AC field

In a recent study comparing the heating rates of 16 commercially available MNPs systems,⁴¹ the Pankhurst group found that the Resovist (Bayer-Schering) and Nanomag-D-spio100 (MicroMod) particles produced the greatest power generated per mass. Both systems consist of clusters of 6-12 nm diameter IONPs coated with cyclodextran for a hydrodynamic diameter of 60-90 nm. Both also had high magnetic crystalline diameters determined via fitting of superconducting quantum interference device (SQUID) hysteresis loops. While these high crystalline diameters are perhaps due to single domain effects, this phenomenon could also indicate close particle clustering, resulting in behavior analogous to that of multi-domain structures. Such behavior supports the hypothesis that clustering nanoparticles are a major catalyst in the heating rate and efficiency in magnetic hyperthermia. Additional research on particle interaction affecting the heating rate and efficiency in magnetic hyperthermia has been reported.⁴² Particles with a small particle interaction radii determined by small angle neutron scattering (SANS) exhibited heating rates seven times as great as particles with larger radii. The authors theorized that close interactions could significantly enhance dipole interactions as well confining heat output to a smaller area.⁴² Eggeman et al., comparing well-stabilized monodispersed particles to highly clustered commercially available particles, found that the clustered particles exhibited significantly greater heating than their well dispersed counterparts.⁴³ These findings suggest that the composition and size of the particles is insufficient for predicting particle response to alternating magnetic fields.

1.5. MEASURING HEATING EFFICIENCY OF MAGNETIC NANOPARTICLES

One way of characterizing magnetic particle-polymer complexes is by calculating the power generated per mass of magnetic material. The power generated by a solution of MNPs with the application of an alternating magnetic field can be described as the volumetric power dissipation, P , in watts per unit volume,⁴⁴ shown below.

$$P = \frac{\mu_0 \omega^2 \tau H_0^2 \chi_0}{2(1 + (\omega\tau)^2)}$$

where μ_0 is the permeability of free space (1.26×10^{-6} kg m s⁻² A⁻²), ω is the frequency of the magnetic field, τ is the relaxation time, H_0 is the magnetic field intensity, and χ_0 is the magnetic susceptibility.

Because not every MNPs system is identical, the heating efficiency of particles is given by the specific absorption rate (SAR) or specific loss power (SLP).⁴⁵⁻⁴⁸

$$SAR = C \frac{m_{sample}}{m_{iron\ oxide}} \left(\frac{dT}{dt} \right)$$

where C is the specific heat capacity of the media (e.g., 4.186 J g⁻¹ °C⁻¹), m_{sample} is the mass of the sample, $m_{iron\ oxide}$ is the mass of iron oxide determined magnetically, and dT/dt is the slope of the heating curve.

To measure the SAR of a MNP solution, an alternating magnetic field system is utilized. These consist of a copper induction coil that wraps around the sample, capacitors to form a resonance circuit, and a power supply. The induction coil is wrapped around the sample holder that is temperature controlled by recirculating water, Figure 1.2. An example of a capacitance network, used by Ivkov et al., created an oscillation of ~153 kHz and used a 0-25 kW generator to power it.⁴⁹ The sample chamber's magnetic field is

mapped with a magnetic probe to measure the field produced in the induction coil. An infrared thermocouple is used to monitor temperature change over time of the magnetic fluid.^{40,41,45,46,48,50-52} Studies show that higher heating rates are obtained by decreasing the polydispersity and “optimizing the size for a given set of conditions, most specifically the frequency of the AC-field.”⁴⁵

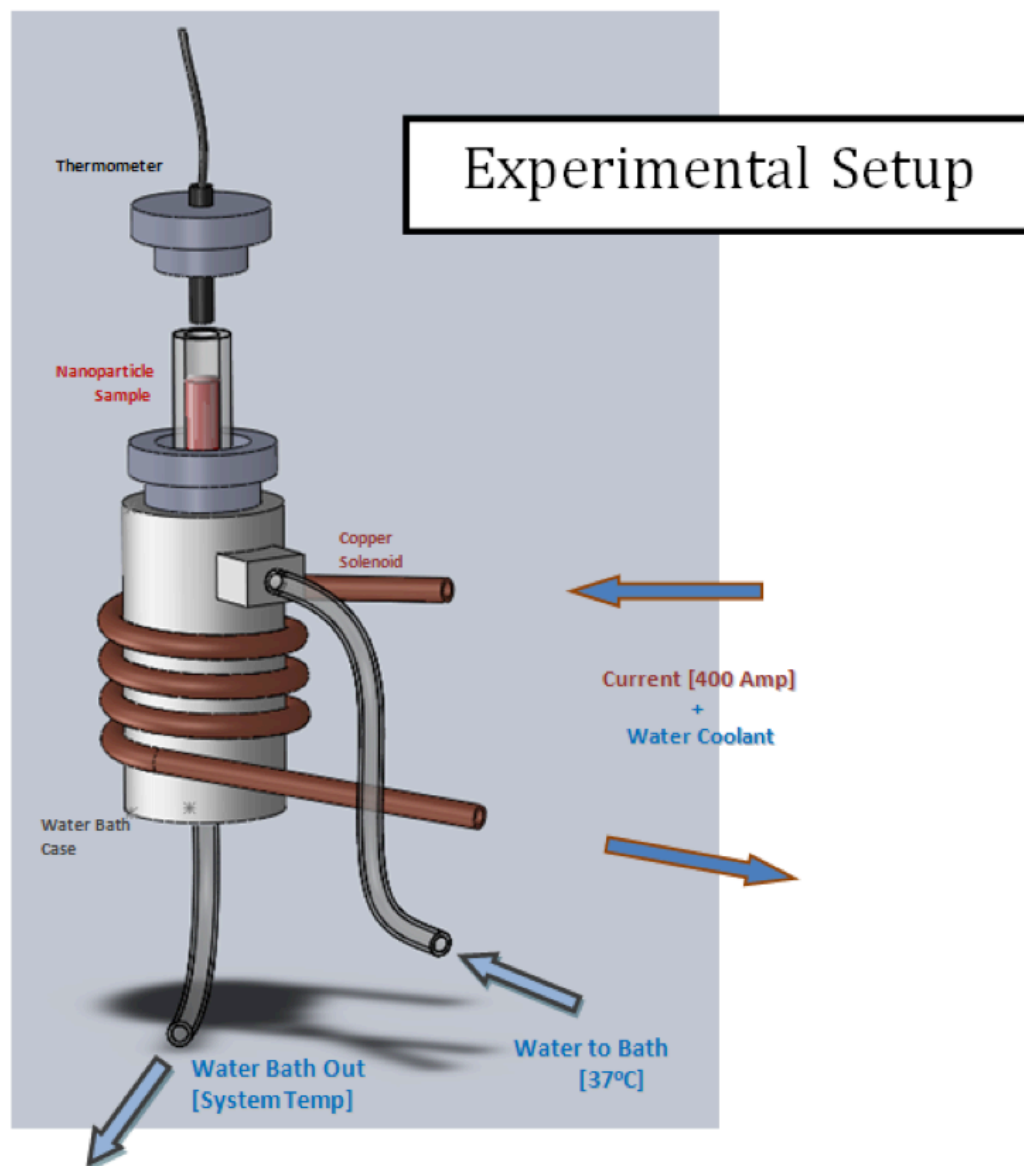


Figure 1.2. General schematic of AC calorimeter that can be used to measure SAR.

Currently, there is one unit magnetic hyperthermia applicator in clinical use [MFH300F].⁵³ This system uses an alternating magnetic field with a frequency of 100 kHz and variable field strength of 0-18 kA m⁻¹. To measure heating rate in situ, fiber optic thermocouples were surgically positioned into the prostate, urethra, rectum, perineum, scrotum and left ear and monitored with software. The temperature could be read at a constant field strength or even allow the researchers to adjust the field strength to reach any desired temperature.

Though current MNPs systems used for magnetic hyperthermia studies are generally polydisperse in size, it is speculated that more monodispersed particles will create a more efficient therapeutic system.⁴⁴ While some experimental protocols have been used to report the heating efficiencies of these materials like SAR, the field lacks a consistent and accepted manner to characterize the heating efficiency that can be reproduced throughout the community. For example, the SAR value reported by one instrument may be different than that reported for the same material by an instrument operating at a different field and frequency of the first measurement. In addition the SAR value does not include specifics regarding “size, size distribution, shape and chemical composition of particles, frequency and amplitude of magnetic field”.⁴⁶ General equations describe SAR as the heat capacity of the material multiplied by the change in temperature over some given time. M. Ma et al. described the equation that uses a mass weighted mean value of the heat capacity of the particles and solvent.⁴⁸ Because the SAR value can be altered for the same sample by merely modifying the field frequency and strength, the intrinsic loss power (ILP) was developed to better compare between

experiments by adding field (H) and frequency (f) to the equation, but only at frequencies below two megahertz and a polydispersity of 0.1.⁴¹

$$ILP = \frac{SAR}{H^2 f}$$

While the ILP offers an alternative to reporting SAR, it does not resolve the issues related to difference in instrumentation. For example, the ILP normalization is only effective in the linear region according to Eggemen et al.⁴³ They found that the size, composition, and shape are not enough to predict the effects they have on heating in an alternating magnetic field.

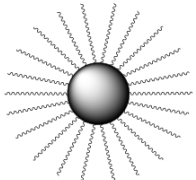
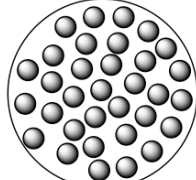
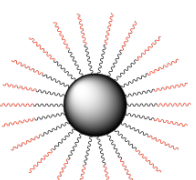
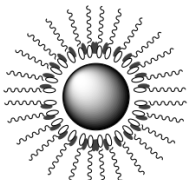
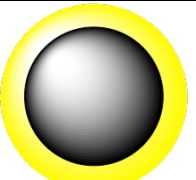
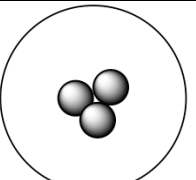
1.6. PARTICLE MODIFICATION

Nanoparticle systems used for targeted drug delivery have historically been liposomes, polymer-drug conjugates, and micelles that deliver a drug encapsulated into the core of the nanoparticle. Liposomes are made up of a phospholipid bilayer that comprise of lipids that have a fatty hydrocarbon tail and a hydrophilic head group; these separate an aqueous internal compartment from an aqueous bulk. Micelles are comprised of a lipid monolayer that has a fatty core and a charged hydrophilic surface.

Surface modification of nanoparticles is critical to improving stability, biocompatibility, and success in targeted magnetic hyperthermia, which is discussed later in this review. The nanoparticle complexes described here are a core-shell structure, in which iron oxide is the core and the shell is comprised of polymeric coatings. Examples of these core-shell complexes can be found in Table 1. MNPs have been modified with a variety of ligands using different synthetic routes. One commonly used method for surface coating is the physical adsorption of material onto the surface of the particle.

Another such method to coat MNP surfaces also involves covalently or electrostatically bonding a polymer to the particle surface. Electrostatically binding of a polymer to modify IONPs has been reported with different polymer ligands using end and side chain functional groups such as carboxylates,⁵⁴ alcohols,⁵⁵ amines,⁵⁶ and phosphates.^{57,58} For example, dextran has been shown to adsorb to the surface of IONP to create a dispersible complex in a biological system.⁵⁹ Dextran has been used to modify coprecipitation MNPs for biological systems currently used in MRI contrast agents.²⁰ Unfortunately, some of these binding groups can be displaced by other anions such as phosphates and silicates.⁶⁰ Once in contact with biological fluids, however, this displacement of the polymer coating on the surface of the magnetic nanoparticles can lead to IONP instability and aggregate formation. The advantage of chemical adsorption over physical adsorption is strength of adhesion to the particle. The heat of adsorption is much higher for a chemical bond (-40 to -1000 kJ/mol) than physical interaction (-10 to -40 kJ/mol) of a molecule onto a surface.⁶¹ A binding group that shows great promise for binding biologically inert ligands are catechol derived anchor groups.⁶²⁻⁶⁴ Gu et al. has demonstrated that oleic acid and oleic amine on the surface of magnetite can be displaced with dopamine derivatives that bind tightly to iron oxide surfaces.⁶⁵ Amstad et al. used dopamine as an anchor for adsorption of PEG onto the surface of magnetite and showed stability of particles in physiological conditions.⁶⁶

Table 1. Representative schematics of existing magnetic nanoparticle complexes

Particle Complex	Description
	Magnetic nanoparticle coated with hydrophilic polymer ligand ^{7,57,67-69}
	Multiple magnetic nanoparticles encapsulated in cross-linked polymer matrix ^{70,71}
	Single magnetic nanoparticle with copolymer ligands; PEO/PLA, PEO/PGMA ^{72,73}
	Ligands with hydrophobic head and hydrophilic tail to encapsulate particle ^{25,74}
	Nobel metal coated magnetic nanoparticle ^{31,35,36}
	Controlled clustering of nanoparticles, and then coated with polymer shell ⁷⁵

Biologically inert polymers have been used to modify IONPs for magnetic hyperthermia, which is advantageous for controlling the particles size and functionality that permits multiple applications. Polyethylene glycol (PEG) is one such polymer being explored for use biological particle systems. Because of its solubility in water, low immunogenicity, and fast renal clearance, PEG is ideal for biomedical applications.⁷⁶ Many multifunctional PEG ligands have been synthesized, some of which are commercially available, for modifying MNPs.

Block copolymers have been exploited for altering solubility and thermal properties for entrapment and controlled release of drugs, a concept also applied to the encapsulation of MNPs. Triblock copolymers of polyethylene glycol and polypropylene oxide (PPO), commonly known as a pluronic, have been used in multiple applications (i.e. detergency, emulsification and drug delivery systems).⁷⁷ This amphiphilic polymer has been utilized to create a polymer shell that is biocompatible and can be modified for targeting purposes. Pluronic have also been studied for the use in temperature-controlled release of drugs; when the polymer is above its critical micelle temperature, the polymer collapses on itself to contain the drug. Once the MNPs are accumulated in the diseased tissue, the temperature is decreased to extend the ligands and release the drug.^{72,73} Another polymer system of interest for the temperature-controlled release of drugs is random block copolymer composed of poly(N-isopropylacrylamide) (pNIPAAm) with hydrophilic monomers. These thermo-sensitive block copolymer have a lower critical solution temperature (LCST) in which the polymer, above the LCST converts to a coiled formation as opposed to extended chain formation.⁷⁸ Meyer et al. have combined

PNIPAAm and PEG as a copolymer to encapsulate MNPs and drugs simultaneously. When these particles are subjected to an AC field, temperatures higher than LCST of the PNIPAAm are achieved, causing the polymer to coil and force the encapsulated drug into the surrounding tumor.⁷⁹

1.7. SIZE AND SURFACE CHARGE EFFECTS ON STABILITY

Designing a stable MNPs system requires a balance between repulsive and attractive forces within a colloidal system. According to a modified Derjaguin-Landau-Verwey-Overbeek (DLVO) theory, shown in Figure 1, these forces include van der Waals, electrostatic repulsion, steric repulsion, and magnetic attraction forces that mediate the stability of an MNPs system.⁷⁹ Magnetic interactions for superparamagnetic nanoparticles, ideally should be non-existent. Achieving a narrow size distribution of particles that have no net magnetic moment is difficult and will require an increase in the repulsion forces to decrease agglomeration due to magnetic interactions.⁸⁰

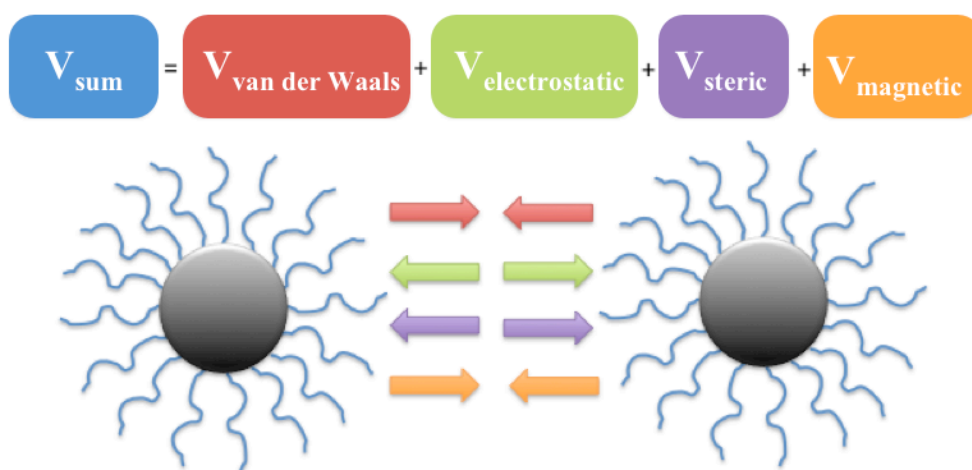


Figure 1.3. The interaction potential between magnetic nanoparticles can be determined by adding the potential energies of the particles as a function of their distance.

By calculating the potentials for the interaction between two particles in solution, it is possible to infer the effects of various parameters (i.e. core particle size, degree of coverage by stabilizing layer, molecular weight of the stabilizing polymer, solvent conditions, etc.). For example, the radius of the core of MNPs is critical for the colloidal stability of a system; indeed small portions (<1%) of the population of a polydisperse system may be responsible for agglomeration.⁶⁷

1.8. MOLECULAR WEIGHT AND SURFACE CHARGE EFFECTS ON STABILITY

Surface modification, using methods described previously, alters the MNPs in order to: i) reduce the immune response of the body; ii) enable the homogeneous suspension of the nanoparticles in physiological solutions; and iii) provide a stabilizing layer that prevents particle agglomeration. For example, Ditsch et al. coated 7.5nm diameter (polydispersity of 0.26) magnetite nanoparticles with block copolymers of sodium styrene sulfonate, sodium vinyl sulfonate and acrylic acid. It was discovered that at low molecular weights, e.g. <15 kDa, steric repulsion was not great enough such that particle clustering may occur. Steric repulsion was enhanced when the PEG molecular weight increased which resulted into a suspension of dispersed particles. However, if molecular weight is further increased, e.g. 30kDa, polymer chains begin to entangle and clustering would again occur in the system caused by entanglements of neighboring particles' brushes and thus bring the particles together.⁷⁵

Both the molecular weight and the structure of the surfactant affect particle stability,⁸¹ particularly in copolymers with hydrophobic and hydrophilic blocks, like PEG-PPO block copolymers. PEG is a linear polyether comprised of a repeat unit of two

methylene groups and an oxygen, which gives it hydrophilic properties. PPO has a very similar structure, but has a branched methyl group off of the methylene groups in the chain that makes it hydrophobic. The molecular weight necessary for minimum clustering will shift with a ratio change between the hydrophilic and hydrophobic segments in the polymer chain. If the hydrophilic segment is larger than the hydrophobic, an increase in the total molecular weight of polymer chains is required to minimize clustering.⁷⁵

When modifying nanoparticles with a polymer, the overall particle size can increase significantly, affecting the functionality of the system. Compared to the autonomous magnetic core, the magnetic field strength of coated IONPs decreases by a small percentage. For example, in the development of MRI contrast agents, Tong et al. used different molecular weight IONP polymer coatings to demonstrate diverse T_2 relaxivity. Using 5 and 14nm magnetite nanoparticles coated with PEG with molecular weights of 550, 750, 1000, 2000, and 5000 g mol^{-1} , respectively, they found that the particle system with the highest T_2 relaxivity— $385 \pm 39 \text{ s}^{-1}\text{mM}^{-1}$ —was the 14 nm diameter particle with 1000 g mol^{-1} coating. However, the indeterminate relationship between polymer molecular weight and T_2 relaxation rate suggests the necessity of additional study.⁸²

It should be noted that for each size of magnetite particle, a sufficient steric or electrostatic stabilizing layer is necessary to maintain good colloidal stability.⁶⁷ Electrostatic effects are a product of the surface chemistry⁸³ of the particle as well as the medium in which it is dispersed⁸⁴. Relying on electrostatic repulsion alone could be a

poor choice, as the high ionic strength of the body would result in weak colloidal stability. This insufficient repulsive energy is due to ionic screening of the electric double layer around the particle. Wiogo et al. completed size and zeta potential studies on magnetic nanoparticles with carboxylic acid on the surface in water, phosphate-buffered solution (PBS), and cell culture media (RPMI-1640) to show how the ionic nature of the body can cause suppression of the electrostatic double layer on a nanoparticle used for biomedical applications.⁸⁵ They found that in water, the zeta potential was -32 ± 5 mV and there was no significant size change after 16hrs. The same particles in PBS and cell culture media showed a ~ 10 mV decrease in zeta potential and a shift in the size distribution to larger size agglomerates.

1.9. IMPORTANCE OF POLYETHYLENE GLYCOL IN THERAPEUTICS

Polyethylene glycol (PEG) has been a FDA approved for use in a variety of cosmetics, pharmaceuticals, and even an additive in food.⁸⁶ Due to its structure, it shows low toxicity and has renal clearance, <30 kDa.⁸⁷ One of the initial applications of PEG was to overcome issues had with modifying polypeptides with liposomes for drug delivery.⁸⁸ The first PEGylation, a term describing the modification of small molecules with PEG, was done by Abuchowski et al. in 1976. Their group covalently attached monomethoxy terminated PEG, 1900 and 5000 g mol⁻¹, to bovine liver catalase and found that it enhanced the circulation time in the blood of mice with no negative immune response to the modified enzymes.⁸⁹ PEGylation is not only limited to enzymes, but has also been used to modify proteins to give it desirable drug delivery properties. A study on PEG in solution with proteins of similar molecular weight has found that the interaction

of water molecules with the polymer increases the size, protecting the proteins from immediate renal clearance and enzyme degradation.⁹⁰

Taking advantage of the unique biological properties of PEG, it can be linked to therapeutic agents to improve solubility, increase circulation in the body and decrease toxicity that are inherit in many small molecule drugs, including antitumor agents.⁹¹. Unfortunately, linking therapeutic agents to monofunctional PEG is limited in its efficiency because it can only rely on passive targeting to deliver the drug. Passive targeting takes advantage of irregular vascular structures in tumors to deliver the drug. Adding active targeting agents to drug complexes is needed to improve delivery efficiency. Active targeting requires a compound that will bind to over-expressed receptors found in tumors.⁹² One example of an active targeting compound is folic acid; many epithelial cancer cells, ie. ovary, kidney, colon, and lung, over-express folate receptors that have a high affinity for folic acid.⁹³ Synthesizing PEG that can carry a drug and target specific receptors was the next step in drug delivery. In 2007, a group from Rutgers University reported the modification of a bis-carboxyl PEG modified with doxorubicin and sialic acid that showed an increase in anticancer activity and bioavailability.⁹⁴ Improvement of therapeutic efficiency by attaching a targeting and drug to PEG was a huge advancement, but is limited by the extremely low drug loading that is inherent with a chain that can have a maximum of two functionalities. This has brought about the advancement of branched and multi-armed PEGs to provide multiple functional groups to increase the loading of therapeutic agents.⁹⁵

The use of polymers for the advancement of drug delivery naturally progressed into the development of polymeric nanoparticles for the same application. Polymeric nanoparticles, made up of conjugated⁹⁶ and amphiphilic block copolymers,⁹⁷ provide a large surface area and increased functionality that can be conjugated with a variety of drugs and targeting moieties.

1.10. “CLICK CHEMISTRY”

In a review by Kolb et al., they describe the foundation of the approach to “click chemistry” is to join small units together using selective and modular ‘blocks’ that can work in small and large scale applications.⁹⁸ Using “click chemistry” as the approach for combining two molecules together is ideal for optimizing drug development and conjugation.⁹⁹ Nucleophilic ring opening reactions, carbonyl chemistry, and cycloaddition are all examples of synthetic routes that are under the umbrella of “click chemistry,” as defined by Sharpless.^{98,100}

The reaction that is almost synonymous with “click chemistry” is the 1,3-dipolar cycloaddition of alkynes and azides yielding an triazole, developed by Huisgen.¹⁰⁰ Alkyne and azide functional groups are extremely stable in many synthetic conditions.¹⁰¹ Unfortunately, the reaction requires heat and creates a product of 1,4 and 1,5 regioisomers, making it difficult to purify.¹⁰¹ That was true until copper (I), created insitu using a reducing agent, was used to catalyze the reaction in water to yield 1,4-disubstituted 1,2,3-triazoles (>95% yield), an example is shown in Figure 1.3.¹⁰²

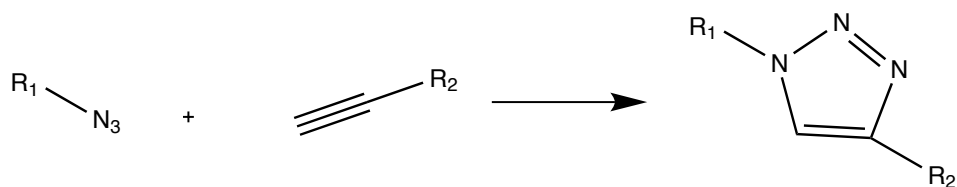


Figure 1.4. Schematic of a 1,3-dipolar cycloaddition of alkyne and azide yielding a triazole.

The mild reaction conditions of the copper catalyzed reaction of an alkyne and azide make it an ideal synthetic route for attaching biomolecules to each other, also referred to as bioconjugation. The triazole linkers are ideal for bioconjugation because they are soluble and stable in water as well as the harsh biological environments.¹⁰³ Cowpea mosaic virus (CPMV), a scaffold commonly used for testing bioconjugations, was modified with an alkyne and was tagged with an azide modified fluorescein, with a 100% efficiency.¹⁰⁴ DNA bioconjugation can be quite difficult and inefficient because it requires aqueous conditions. Seo et al. was able to tag a strand of DNA, for sequencing studies, modified with an alkyne and with a fluorophore modified with an azide, with a product yield of 91%.¹⁰⁵

These same reactions can be used to synthesize more efficient and specialized bioconjugated polymers for drug targeting and delivery. One research group used treated PDMS (hydrophobic) modified with an azide on both ends to attach PEG (hydrophilic) modified with an alkyne to produce a block copolymer that was used to create polymeric vesicles to carry hydrophobic drugs.¹⁰⁶ Cheng et al. synthesized a heterobifunctional PEG with an alcohol on one end and bromine on the other. The bromine terminus was then reacted with sodium azide, via a substitution reaction, to yield an azide terminus. Then using “click” chemistry, the azide-PEG was attached to a tri-alkyne to produce a three

arm PEG that provides three functionalities per macromolecule to increase drug loading.¹⁰⁷ Nanoparticles have also been synthesized to have either an alkyne or azide surface that can be easily modified with targeting agents (ie. folate)^{108,109} and dyes(ie. fluorescein)¹¹⁰ equipped with their respective counter functionality.¹¹¹⁻¹¹³

1.11. OVERVIEW

The following chapters will discuss the synthesis of heterobifunctional PEO for stabilizing magnetic nanoparticles for biological therapeutic and diagnostic applications. It will begin with the synthesis of a library of heterobifunctional PEO that were synthesized by the anionic ring opening polymerization of ethylene oxide using a variety of initiators that can produce thiol, azide, amine, alcohol, vinyl, and trivinyl end groups. Chapter 2 will also include different end group modification techniques important for creating functionalities that can be utilized for different applications. Chapter 3 will involve modifying magnetic nanoparticles with specialized heterobifunctional PEO that was synthesized using techniques in Chapter 2. These materials have a surface that can be built upon with diagnostic dyes and targeting moieties for biological applications. Chapter 4 builds upon the same scaffold that was developed in Chapter 3, but utilizes multiple binding groups to enhance biological stability while still maintaining functionality. Finally, the document will conclude with a discussion on how the design of these particles is not limited to just magnetic hyperthermia for the treatment of cancer, but that these particles can be used as an alternative to antibiotics, imaging in biofilms and a probe for emerging medical diagnostics.

CHAPTER 2.SYNTHETIC TECHNIQUES USED TO PRODUCE HETEROBIFUNCTIONAL POLYETHYLNE OXIDE OLIGOMERS

2.1. ABSTRACT

Polyethylene oxide (PEO) oligomers have become a desirable material in pharmaceutical and biomedical applications. The inert backbone in PEO provides a water-soluble platform that can be easily modified and survive in harsh biological environments.⁸⁸ Through various initiators and end group modifications, an assortment of heterobifunctional PEO can be synthesized and customized for any specialized application. This chapter discusses the synthesis and characterization of different heterobifunctional PEO for biological applications.

2.2. INTRODUCTION

Polyethylene glycol (PEG), also referred to as polyoxyethylene (POE) and polyethylene oxide (PEO), is a “linear or branched polyether often terminated with hydroxyl groups that are derived from neutralization of the terminal ether repeated unit in the chain.”¹¹⁴ PEG is generally used when describing lower molecular weight polyethers (<10000 g mol⁻¹) and PEO describes higher molecular weights (>10000 g mol⁻¹).¹¹⁵ The repeating units are relatively unreactive which allows for modification of the end groups without affecting the chain integrity. PEO is also soluble in water and many organic solvents, which allows for a variety of routes in chemical modification of its end groups.⁵⁴ Because of its solubility in water and capability of modification, PEO is ideal for biomedical applications; it has low immunogenicity, renal clearance in vivo, and is not biodegradable.⁷⁶

Creating a facile method for synthesis of heterobifunctional polyethylene oxide (PEO) is important for the functionalization of nanoparticles, which requires a strong binding group and then still have an end group that can be easily tailored to give a specific functionality. This research is vital in the successful integration of a material into biological environments and have the functionality to complete a task, ie targeting a specific site or fluorescent imaging. Using different initiators and end group modifications, a variety of heterobifunctionality can be customized for any application.

There are two ways of synthesizing heterobifunctional PEO. One method involves the partial derivatization of polyethylene glycol diols, Figure 2.1, and then statistically collecting the desired heterobifunctional oligomer. This method is time consuming and extremely inefficient giving very low yields.

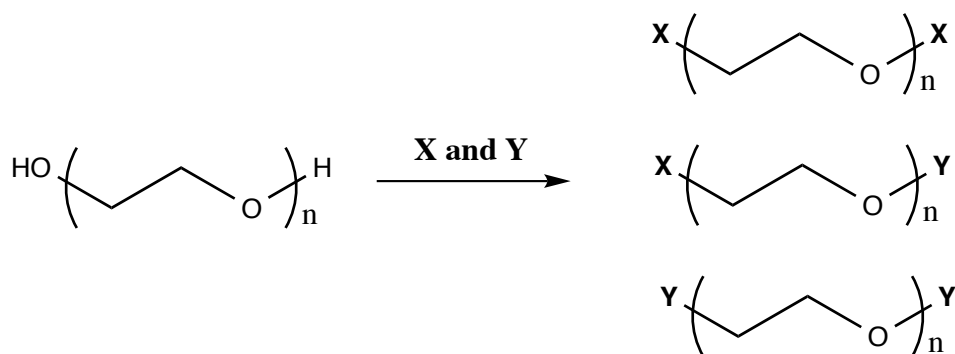


Figure 2.1. Partial derivatization of diols of polyethylene glycol to create heterobifunctionality.

The second method to creating heterobifunctional PEO is to initiate the polymerization of ethylene oxide (EO) using a functional initiator and, once propagation is complete, terminate with functional group as shown in Figure 2.2.¹¹⁶⁻¹¹⁹ Creating heterobifunctional PEO using this route generally has high yields and low

polydispersity.¹¹⁴ Because these reactions are living in nature, it is important to keep water out of the reaction to avoid the formation of PEO diols that can reduce the targeted molecular weight.⁷⁶

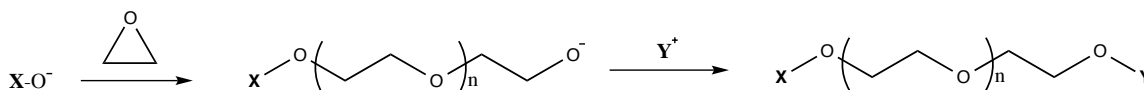


Figure 2.2. Anionic ring opening polymerization using an initiator with **X** functionality and then terminating with a functionality of **Y**.

The hydroxyl terminus is a great platform for synthesizing complex heterobifunctional end groups. The ease of hydroxyl modification allows for the conjugation of biomolecules by first modify the end group with carboxylic acid and then subsequently creating a succinimidyl ether intermediate¹²⁰ that can easily react with amines of many bioconjugates.^{121,122} The purpose of this chapter is to show different techniques used to synthesize specialized heterobifunctional PEO. A variety of anionic initiators and end group modifications that were used to create the desired heterobifunctionality are described in detail.

2.3. MATERIALS AND CHARACTERIZATION

2.3.1 Materials

Tetrahydrofuran (THF; B.D.H. ACS grade) was purified by reflux over sodium metal (Aldrich Chemistry; sodium lump in kerosene 99%) and benzophenone. Naphthalene (Aldrich Chemistry $\geq 99\%$) was purified by sublimation at 60 °C under vacuum. Bromophenol blue (Sigma Aldrich), hydrochloric acid (HCl; J.T. Baker, 1N volumetric solution), acetic acid (BDH, glacial ACS/USD/FCC), ethylene oxide (EO; Aldrich Chemistry), allyl alcohol (Sigma Aldrich, $\geq 99\%$), triisobutylaluminum (Aldrich

Chemistry, 25% w/w solution in toluene), tetrabutylammonium azide (Aldrich Chemistry), dichloromethane (DCM; EMD Millipore Chemicals, HPLC grade), diethyl ether (DEE; Macron Chemicals), toluene (BDH), 3-chloropropyltrichlorosilane, (Gelest, Inc.), vinylmagnesium bromide solution (Aldrich Chemistry, 1.0M in THF), ammonium chloride (Fisher Scientific, Certified ACS, Crystalline), magnesium sulfate (Mallinckrodt Chemicals, anhydrous powder), sodium chloride (Fisher Scientific, Certified ACS, Crystalline), sodium iodide (Sigma Aldrich, ACS reagent, $\geq 99.5\%$), sodium bicarbonate (J.T. Baker, anhydrous powder), hexamethylphosphoramide (HMPA; Aldrich Chemistry, 99%), acetone (Fisher Scientific, Certified ACS), (2-(tetrahydro-2H-pyran-2-yloxy)ethanol (THP; Aldrich Chemistry, purum $\geq 98\%$ (GC)), chloroform-D (CDCl_3 ; D,99.8%, Cambridge Isotope Laboratories Inc.), potassium bis(trimethylsilyl)amide solution (1M THF, Aldrich), and tert-butyl mercaptan (Aldrich Chemistry, 99%), 4-(dimethylamino) pyridine (DMAP; Fluka Analytical), N,N'-dicyclohexyl carbodiimide (DCC; Thermo Scientific), 1-((3-dimethylaminopropyl)-3-ethylcarbodiimide (EDC; Alfa Aesar, 98%), N-hydroxysuccinimide (NHS; Acros Organics 98+%), propargyl bromide solution (80% in toluene; Fluka), sodium hydride (NaH; Aldrich), dimethylformamide(DMF; 99.8%, Extra Dry over molecular sieves; Sigma Aldrich), methanol (absolute ACS reagent grade; Ricca Chemical Company), methacryol chloride (Fluka Analytical, $\geq 97.0\%$, GC, Contains $\sim 0.02\%$ 2,6-di-tert-butyl-4-methylphenol as stabilizer), and Spectrum Spectra/Por® molecular porous membrane tubing, MWCO of 1K, 12K-14K, and 50K g mol^{-1} was used as received.

2.3.2. Potassium naphthalenide preparation

Potassium naphthalenide was prepared in the follow way for all reactions.⁵⁷ To a 250 mL Erlenmeyer flask, 20g of naphthalene was put under vacuum at 60 °C until all naphthalene was sublimed onto the inside walls of the flask. The sublimed naphthalene (14.1 g, 0.11 mol) was then charged to a flame dried, 250 mL round bottom flask containing a stir bar. After submitted to a heavy purge of nitrogen, 100 mL of THF was added via syringe. Once naphthalene was completely dissolved, 3.96 g (0.10 mol) of potassium were added. The reaction was mixed for 12 hours at room temperature in darkness. The concentration of the solution was determined by titration, using 1 M HCl solution and bromophenol blue as an indicator, observing a color change from a deep blue to yellow.

2.3.3. Characterization Techniques

NMR spectroscopy was conducted using a Jeol ECX-300. Polymer samples were prepared by dissolving 50mg in 1 mL of deuterated chloroform and transferred into a 5mm economy, 7", NMR sample tube via glass pipet. Each sample was analyzed using 64 scans for ¹HNMR and 20000 scans for ¹³CNMR at 20 °C. The NMR was controlled by Delta NMR Processing and Control Software (v 4.3.6, Windows_NT). The spectra were analyzed with Delta NMR Processing and Control Software (v 5.0.1, Darwin-x86).

Fourier transform infrared spectroscopy (FTIR) using a Nicolet 6700 FTIR spectrometer. Spectra were acquired using attenuated total reflectance (ATR) on a diamond plate in air at room temperature. The wavelength recorded was from 550-4500cm⁻¹.

High-resolution transmission electron microscopy (TEM) images were acquired at an accelerating voltage of 300 kV on a Hitachi H-9500. TEM samples were prepared by dropping diluted hexane solutions onto a copper grid with carbon film. The mean size was acquired by averaging the diameter of 181 particles using FoveaPro image analysis software.

Photoluminescence (PL) spectra were collected using a Horiba Jobin-Yvon MicroHR spectrometer.

Thermogravimetric analysis (TGA) was accomplished using a Hi-Res TGA 2950 thermogravimetric analyzer from TA Instruments. Experiments were controlled via Thermal Advantage Instrument Control Software (v 1.3.0.205) and thermograms were analyzed using TA Universal Analysis 2000 (v 3.9A, build 3.9.0.9). All samples were run with TA Instruments' platinum sample pans, 100 μ L. The particles were exposed to nitrogen for 20 minutes, followed by a ramp to 100 $^{\circ}$ C at a rate of 20 $^{\circ}$ C min^{-1} , held isothermally for 60 minutes, and then ramped to 800 $^{\circ}$ C at a rate of 20 $^{\circ}$ C min^{-1} .

Dynamic Light Scattering (DLS) and Zeta Potential measurements were used to measure hydrodynamic diameter and surface charge of particles, respectively, using a Malvern Zetasizer Nano ZS (Model:ZEN3600). Measurements were controlled and analyzed with Dispersion Technology Software (DTS) (v. 5.10). Size measurements and zeta potential measurements for water-dispersed particles were done in a "Size & Zeta" folded capillary cell(DTS1060).

Gel permeation chromatography (GPC) was accomplished using a Waters Breeze system equipped with a UV/VIS and RI detector. Detection was done by differential

refractometer at 33 °C. Chloroform was the mobile phase at 1 mL min⁻¹ and the injection volume per sample was at 50µL using an autosampler. All standards were prepared at 0.5 mg mL⁻¹. All samples had concentrations of 1 mg mL⁻¹ in chloroform and filtered with 0.2 µm Teflon membrane filters. The column used was a Water Styragel HR column – 5E(effective MW range 2K to 4E6).

2.4. ANIONIC RING OPENING POLYMERIZATION OF ETHYLENE OXIDE USING TERT-BUTYL MERCAPTAN

2.4.1 Experimental

Ethylene oxide, 7.76 g (0.176 mol), was distilled into a 300 mL stainless steel Parr Reactor cooled to -40°C using an acetone dry ice bath, followed by the addition of 100 mL of THF. In a separate 50 mL flame dried, round bottom flask with stir bar and under nitrogen purge, 0.7 mL (6.21mmol) of t-butyl mercaptan was dissolved in 5 mL of THF. Next, 4.14 mL of a potassium naphthalenide solution (1.35 M) was added via syringe and stirred for 15 minutes. A white precipitate formed to indicate the formation of thiolates. The initiator solution was then charged to the reactor via syringe, and followed by 50 mL of THF. The reactor was brought to room temperature and reacted for 48 hours. Polymerization was terminated with 1.47 mL of 2.5 M acetic acid solution in THF. The reactor was then purged with nitrogen for 1hr. Solvent was removed by rotary evaporation, and the product was dissolved in 200 mL of chloroform. The solution was then washed with 150 mL of deionized water. The organic layer was then concentrated down and precipitated using cold DEE and the polymer was retrieved by filtration. The remaining polymer was dried in vacuum oven at 25 °C (yield: 6.38g). ¹HNMR (300 MHz,

CDCl₃, δ in ppm): 3.61 (m, (CH₂-CH₂-O)_n), 2.54 (t, CH₂-S-C-(CH₃)₃), 2.43 (s, CH₂-CH₂-OH), 1.29 (s, -CH₂-S-C-(CH₃)₃).

2.4.2. Results and Discussion

Polyethylene oxide is typically synthesized by nucleophilic attack on the methylene group using an anionic initiator. In this case, the anionic initiator was created using potassium naphthalenide and tert-butyl mercaptan, shown in Figure 2.3, the thiolate formation was confirmed by precipitation.¹¹⁸ After the initiator was added to the monomer solution, the reaction was performed under room temperature at 40 psi. After 48 hours, the change in pressure dropped about 7 psi, indicating that nearly all of the ethylene oxide has been consumed. Acetic acid was used to protonate and terminate the living polymer. The polymer solution was then washed with water to remove any acid and then precipitated multiple times to remove any unreacted initiator.

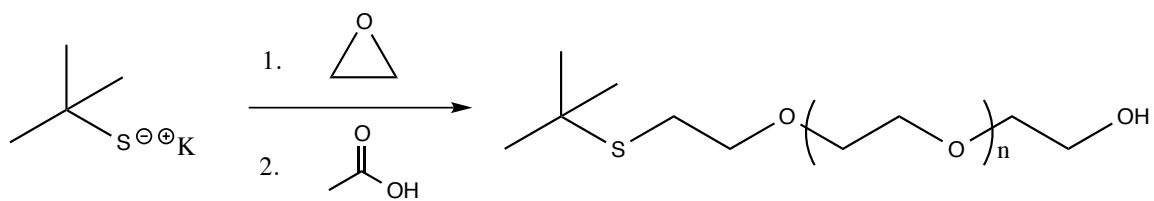


Figure 2.3. Anionic ring opening polymerization of ethylene oxide using tert-butyl mercaptan

End group characterization and molecular weight of the polymer was then analyzed using ¹HNMR. As seen in the spectrum in Figure 2.2, the two hydrogens of the methylene group adjacent to the thiol were observed as a triplet at 2.71 ppm. The three methyl groups in the protected group of the thiol have a chemical shift at 1.29 ppm (9H). There is also the characteristic shift at 3.61 ppm for the side-by-side methylene groups in

the backbone of polyethylene oxide. Comparing the relative integrations of the methylene and the protecting group of the tert-butyl mercaptan to the integration of the methylene groups in the polyethylene oxide, the number average molecular weight was calculated to be $\sim 1690 \text{ g mol}^{-1}$. The target molecular weight of 2500 g mol^{-1} was not met possibly due to sample preparation and polymerization execution. Although extreme caution was used to keep all reactants and glassware dry, oxygen may have been present which could cause premature chain termination, thus decreasing the overall molecular weight. There is also a good possibility that the reaction was not given sufficient time to propagate, leaving unreacted monomer.

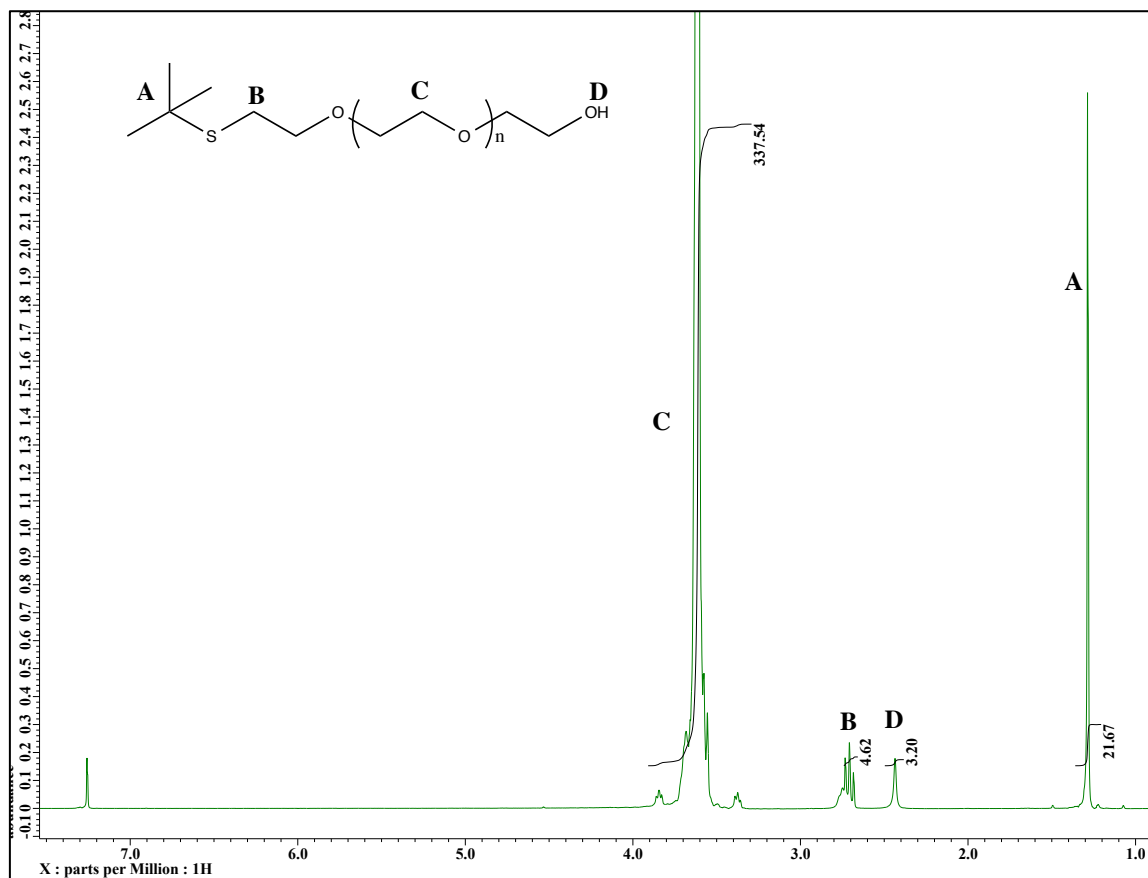


Figure 2.4. ^1H NMR spectra of tert-butyl-thiol initiated PEO

2.5. ANIONIC RING OPENING POLYMERIZATION OF ETHYLENE OXIDE USING ALLYL ALCOHOL

2.5.1 Experimental

Ethylene oxide, 9.12 g (0.207 mol), was distilled into 300 mL stainless steel Parr Reactor cooled to -40 °C using an acetone dry ice bath, followed by the addition of 100 mL of THF. In a separate 50 mL flame dried, round bottom flask with stir bar and under nitrogen purge, 0.22 mL (3.23 mmol) of allyl alcohol was dissolved in 10 mL of THF. Via syringe, 3.26 mL of potassium naphthalenide solution (0.9 M) was added and stirred for 10 minutes. The initiator solution was then charged to the reactor via syringe, and followed by 50 mL of THF. The reactor was brought to room temperature and reacted for 36 hours. Polymerization was terminated with 1.30 mL of 2.5 M acetic acid solution in THF. The reactor was then purged with nitrogen for 1 hour. Solvent was then removed by rotary evaporation, and the product was dissolved in 200 mL of chloroform. The solution was then washed with 150 mL of deionized water. The organic layer was then concentrated down and precipitated using cold DEE and the polymer was retrieved by filtration. The remaining polymer was dried in vacuum oven at 25 °C (yield: 5.855 g). ¹HNMR (300 MHz, CDCl₃, δ in ppm): 3.617 (m, (CH₂-CH₂-O)_n), 5.219 (m, CH₂=CH-CH₂-), 5.880(m, CH₂=CH-CH₂-), 4.00, (d, CH₂=CH-CH₂-), 2.611 (s, CH₂-CH₂-OH).

2.5.2. Results and Discussion

The synthesis of an allyl alcohol initiated PEO, shown in Figure 2.5,¹²³ with a target molecular weight of 2400 g mol⁻¹ was accomplished by first creating an alkoxide by putting it into solution with a slight deficiency of potassium naphthalenide. The

reaction was done under 57 psi at a temperature of 24 °C and after 3 days, the pressure dropped to 50 psi indicating the polymerization of ethylene oxide and yielded 5.8 g of PEO. The allyl end can act as an intermediate that can be modified with an amine or carboxylic acid using thiolated compounds through radical addition.⁷⁶

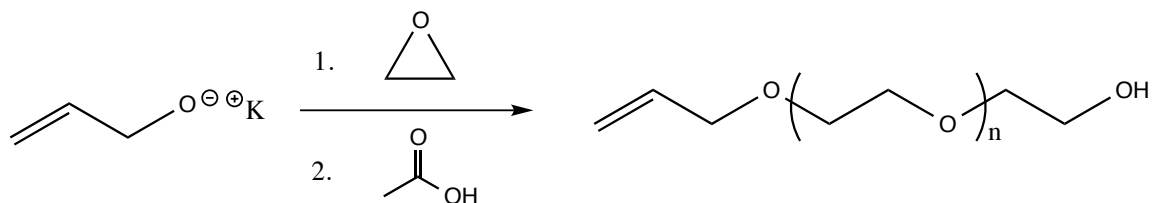


Figure 2.5. Anionic ring opening polymerization of ethylene oxide using allyl alcohol as an initiator.

Proton NMR was used to determine if the desired heterobifunctionality was accomplished. The hydrogens of the alkene were found at 5.88 (2H) and 5.23 ppm (1H). The adjacent methylene had a chemical shift of 4.00 ppm (2H) and the methylene shift of the PEO backbone was at 3.62 ppm (284H). The number average molecular weight was determined to be 3200 g mol^{-1} by comparing the integration of the chemical shifts of the alkene end group to the methylene hydrogen shifts of the PEO backbone. The number average molecular weight of the polymer was also determined by GPC, compared to PEO standards, to be 2138 g mol^{-1} with a PDI of 2.04.

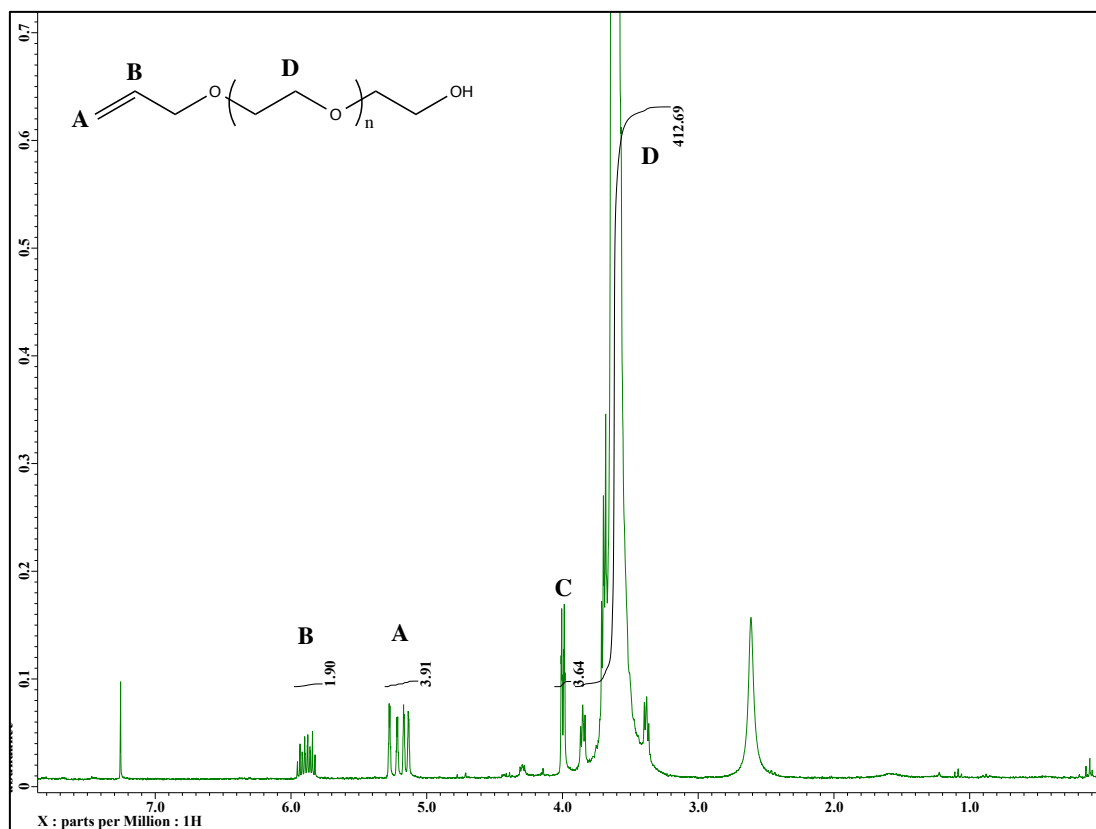


Figure 2.6. Anionic ring opening polymerization of ethylene oxide using allyl alcohol

2.6. ANIONIC RING OPENING POLYMERIZATION OF ETHYLENE OXIDE USING TETRABUTYLAMMONIUM AZIDE

2.6.1. Experimental

Using a modified procedure from Gervais et al.,¹¹⁷ ethylene oxide, 15.2 g (0.345 mol), was distilled into 300 mL stainless steel Parr Reactor cooled to -40°C using an acetone dry ice bath, followed by 100 mL of toluene. In a flamed dried 50 mL round bottom flask, 1.0 g (3.52 mmol) of tetrabutylammonium azide was dissolved in 15 mL of toluene and added to reactor. Triisobutylaluminum, 7.60 mL (7.04 mmol), was added via syringe and an increase in temperature was observed. The reactor was then brought to room temperature and reacted for 24 hours. The reactor was then purged with nitrogen

for 1 hour to remove unreacted monomer. The solution was vacuum filtered and the solvent was then removed by rotary evaporation, and dissolved in 200 mL of toluene. The resulting solution was then heated to 50 °C for 1 hour and then cooled to room temperature to precipitate the polymer to remove any unreacted tetrabutylammonium azide. The toluene was then removed by rotary evaporation and the product was dissolved in DCM and precipitated with cold DEE. The remaining polymer, 6.825 g, was dried in a vacuum oven at 25°C and characterized by ¹HNMR.

2.6.2. Results and Discussion

Synthesis of a heterobifunctional PEO with an azide has been done using end group modification, usually through a mesylated hydroxyl group that can be substituted with sodium azide.¹²³ Labbé et al. has done work on polymerizing oxiranes using tetrabutylammonium bromide and triisobutylaluminum.¹²⁴ The bromine terminus allowed for substitution with sodium azide to produce an azido end group.¹²⁵ This approach allowed for control of molecular weight and required fewer reactions to get desired functionality. Gervais et al. built upon the aforementioned work by using a tetrabutylammonium azide and triisobutylaluminum catalyst to directly polymerize ethylene oxide and propylene oxide with an azide.¹¹⁷

The direct synthesis of an azido-terminated PEO, Figure 2.7, was accomplished with coordination polymerization using a ratio 1:2 of tetrabutylammonium azide and triisobutylaluminum catalyst, respectively, to target a molecular weight of 6000 g mol⁻¹. The reaction was done for 24 hours at room temperature, where a decrease in pressure of about 10 psi was observed.

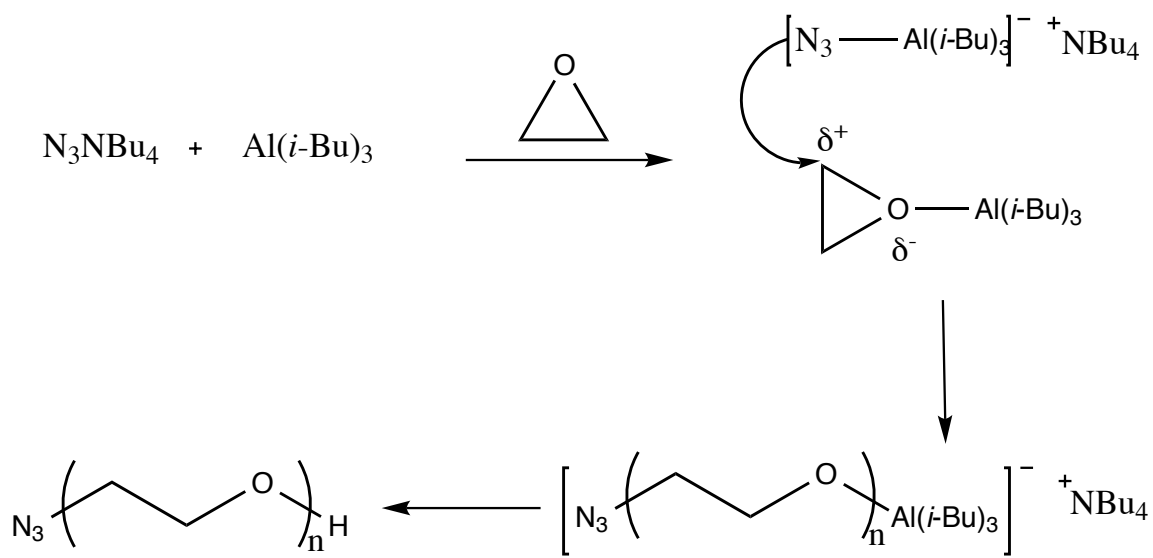


Figure 2.7. Coordination ring opening polymerization using tetrabutylammonium azide and triisobutylaluminum catalyst.

The molecular weight was determined by GPC, against polystyrene standards, to be 10188 g mol^{-1} with a PDI of 1.61. Proton and carbon NMR were used to confirm the azido-terminated PEO. The large peak at 3.64 ppm was the familiar methylene shift for PEO. Unfortunately, finding any indication of the presence of the azide was difficult to determine with $^1\text{H NMR}$, Figure 2.8. Via $^{13}\text{C NMR}$, Figure 2.9, the carbon from the methylene peak adjacent to the azide, has a chemical shift at 61.89 ppm. To make sure that the shift is not part of the noise of the spectrum, contact ATR was used to confirm the presence of an azide. In Figure 2.10, the characteristic antisymmetric stretch of the azide appears at 2100 cm^{-1} and the antisymmetric stretch of the ether in the polyethylene oxide appears at 1111 cm^{-1} .¹²⁶

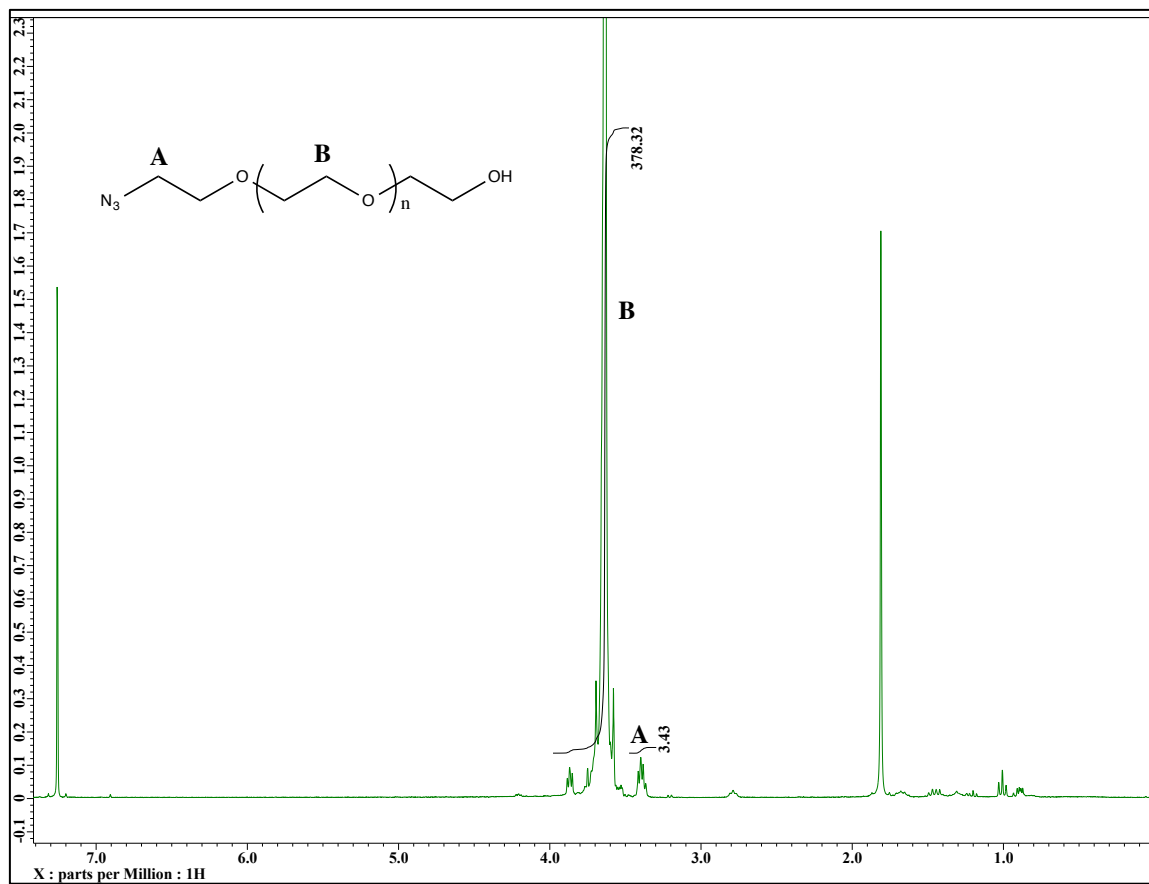


Figure 2.8. $^1\text{H NMR}$ of anionic ring opening polymerization of ethylene oxide using tetrabutylammonium azide and triisobutylaluminum catalyst.

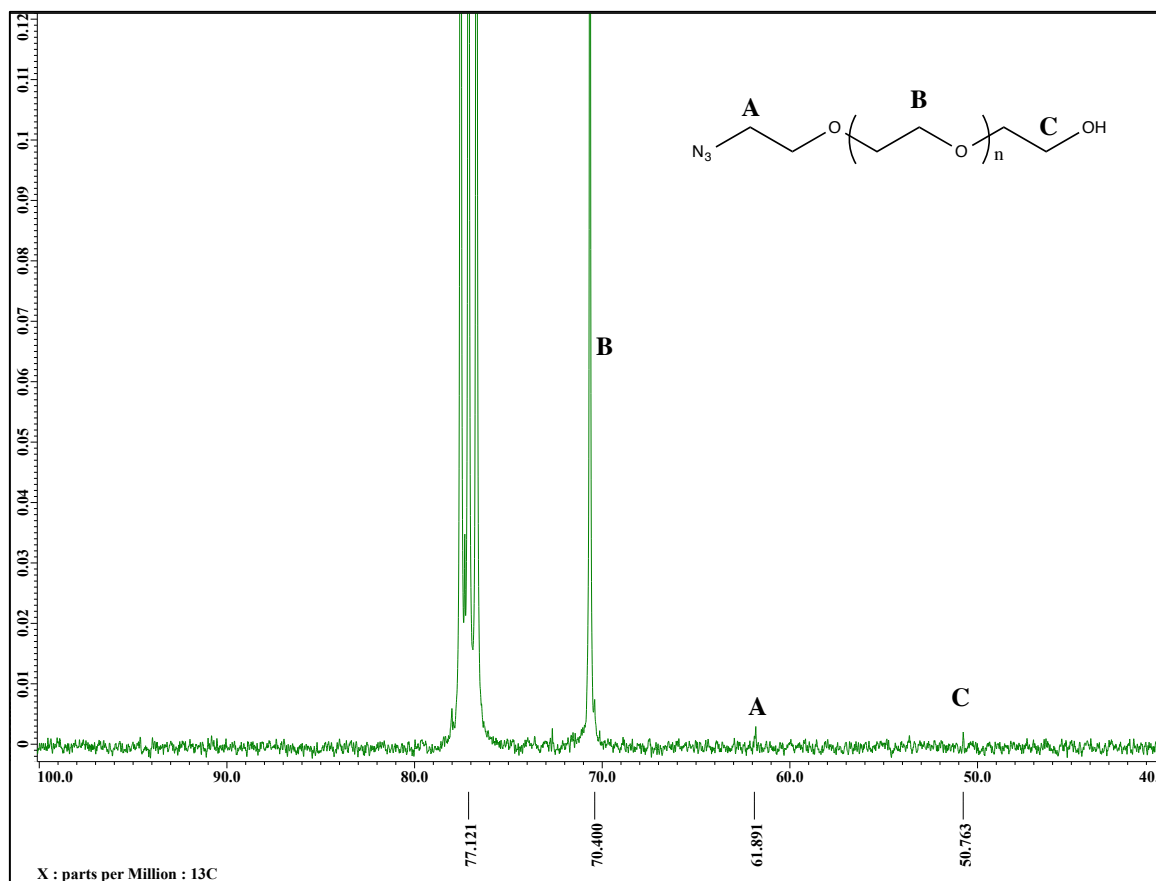


Figure 2.9. ^{13}C NMR spectra of anionic ring opening polymerization of ethylene oxide using tetrabutylammonium azide and triisobutylaluminum catalyst.

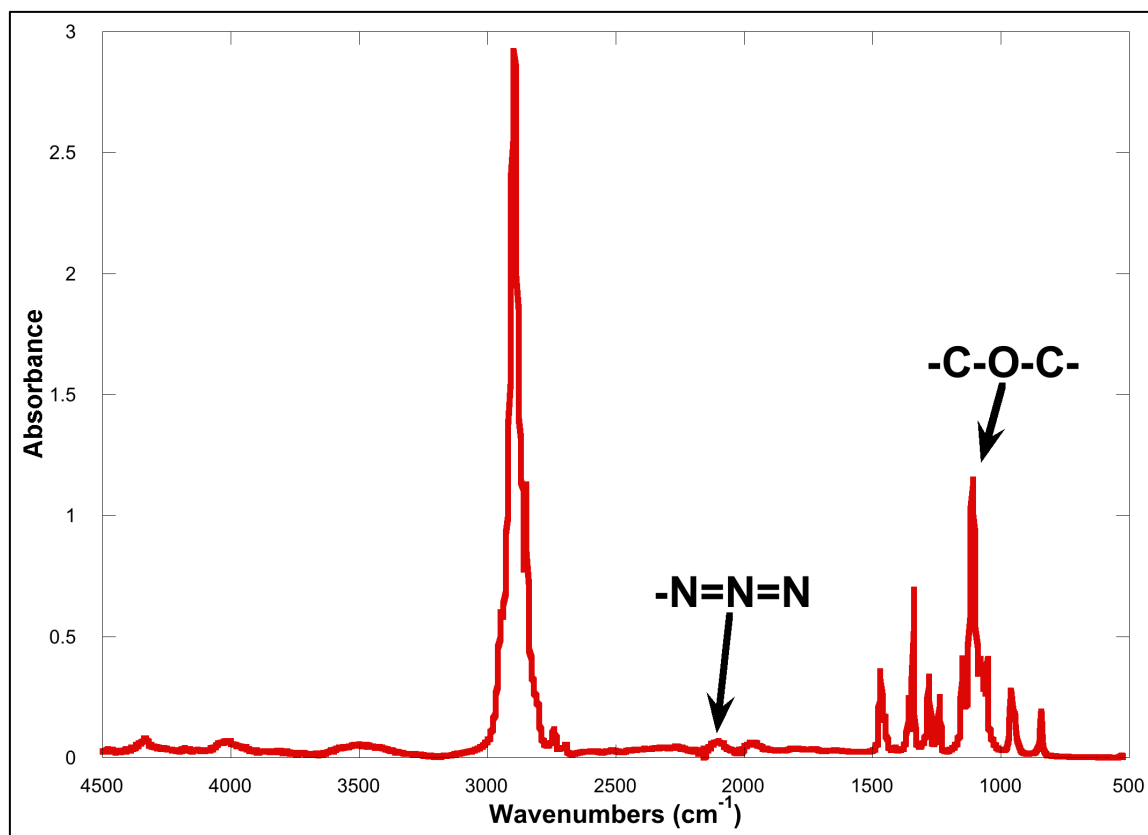


Figure 2.10. FTIR spectra of anionic ring opening polymerization of ethylene oxide using tetrabutylammonium azide and triisobutylaluminum catalyst.

2.7. ANIONIC RING OPENING POLYMERIZATION OF ETHYLENE OXIDE USING HYDROXYPROPYLTRIVINYLSILANE (HPTVS) AS INITIATOR

2.7.1. Experimental

2.7.1.1 Synthesis of 3-chloropropyltrivinylsilane

A flame dried, 500 mL round bottom flask equipped with a stir bar and purged with nitrogen was charged with 25 g (0.112 mol) of 3-chloropropyltrichlorosilane and brought to 0 °C using a sodium chloride ice bath. A 1 M solution in THF of vinylmagnesium bromide (353.81 mL, 0.336 mol) was slowly cannulated into the round bottom flask. The reaction was then brought to room temperature and reacted for 24 hours. To purify, the solution was then diluted with DCM and washed with an aqueous

ammonium chloride solution followed by three washes with a sodium chloride solution. Magnesium sulfate was then added to the organic layer to remove any residual water and then vacuum filtered. The filtrate was then reduced down using vacuum filtration and the product was distilled at 100 °C at 0.8 torr. Yield (15.69g) ¹HNMR (300 MHz, CDCl₃, δ in ppm): 0.841 (m, Si-CH₂-CH₂-CH₂-Cl), 1.825 (m, Si-CH₂-CH₂-CH₂-Cl), 3.490 (m, Si-CH₂-CH₂-CH₂-Cl), 5.782-6.201 (m, (CH₂=CH)₃-Si-).

2.7.1.2. Synthesis of 3-iodopropyltrivinylsilane

A flame dried, 500ml round bottom flask equipped with a stir bar, condenser and purged with nitrogen was charged with 15.0 g (83.0 mmol) of 3-chloropropyltrivinylsilane. Sodium iodide 24.88 g (166.0 mmol) was added to a 250 mL round bottom flask and dissolved in 160 mL of acetone. The sodium iodide solution was then syringed into the 500 mL flask and heated at 56 °C for 24 hours. The acetone was then removed under vacuum and the product was dissolved in 250ml of DCM and vacuum filtered to remove insoluble salt byproducts. The solvent was then removed by rotary evaporation and the product was distilled at 100 °C at 0.8 torr. Yield (11.65 g) ¹HNMR (300 MHz, CDCl₃, δ in ppm): 0.824 (m, Si-CH₂-CH₂-CH₂-I), 1.871 (m, Si-CH₂-CH₂-CH₂-I), 3.165 (m, Si-CH₂-CH₂-CH₂-I), 5.721-6.106 (m, (CH₂=CH)₃-Si-).

2.7.1.3. Synthesis of 3-hydroxypropyltrivinylsilane

Hexamethylphosphoramide (HMPA) (50 mL) was added to a 250 mL flame dried round bottom flask equipped with a condenser, stir bar, and purge with nitrogen. Sodium bicarbonate (3.40 g, 40.4 mmol) was added, followed by 11.0 g (40.4 mmol) of 3-iodopropyltrivinylsilane. Water (6.54 mL, 363.0 mmol) was then added via syringe and

stirred at 100 °C for 24 hours. 3-hydroxypropyltrivinylsilane was then extracted twice with chloroform and distilled at 90 °C at 0.8 torr to receive pure product. Yield (8.95 g) ¹HNMR (300 MHz, CDCl₃, δ in ppm): 0.713 (m, Si-CH₂-CH₂-CH₂-OH), 1.616 (m, Si-CH₂-CH₂-CH₂-OH), 3.590 (m, Si-CH₂-CH₂-CH₂-OH), 5.700-6.198 (m, (CH₂=CH)₃-Si-).

2.7.1.4. Anionic Ring Opening Polymerization of Ethylene Oxide using 3-hydroxypropyltrivinylsilane

Ethylene oxide, 9.27 g (0.210 mmol), was distilled into 300 mL stainless steel Parr Reactor cooled to -40 °C using an acetone dry ice bath, followed by 100 mL of THF. In a separate 50 mL flame dried, round bottom flask with stir bar and under nitrogen purge, 0.56 g (3.33 mmol) of 3-hydroxypropyltrivinylsilane was dissolved in 10 mL of THF. Via syringe, 3.31 mL of potassium naphthalenide solution (0.9 M) was added and stirred until solution turned from a cloudy yellow to pink. The initiator solution was then charged to the reactor via syringe, and followed by 50 mL of THF. The reactor was brought to room temperature and held for 24 hours. Polymerization was terminated with 1.32 mL of 2.5 M acetic acid solution in THF. The reactor was then purged with nitrogen for 1hr. Solvent was removed by rotary evaporation, and dissolved in 200 mL of chloroform. The solution was then washed with 150 mL of deionized water. The organic layer was then concentrated down and precipitated using cold DEE and the polymer was retrieved by filtration. The remaining polymer was dried in vacuum oven at 25°C (yield: 7.970 g). ¹HNMR (300 MHz, CDCl₃, δ in ppm): 0.73 (m, Si-CH₂-CH₂-CH₂-I), 1.63 (m, Si-CH₂-CH₂-CH₂-I), 3.41 (m, Si-CH₂-CH₂-CH₂-I), 5.71-6.19 (m, (CH₂=CH)₃-Si-), 3.65 (m, (CH₂-CH₂-O)_n).

2.7.2. Results and Discussion

The polymer described in this section was synthesized to create a heterobifunctional PEO that has multiple functional groups at one end that could be modified with anchoring groups to increase the interaction with magnetic nanoparticles.⁵⁴ To create the tri-functional PEO, an initiator was synthesized with three vinyl groups and an alcohol that was utilized in creating the needed alkoxide to ring open ethylene oxide, Figure 2.11.

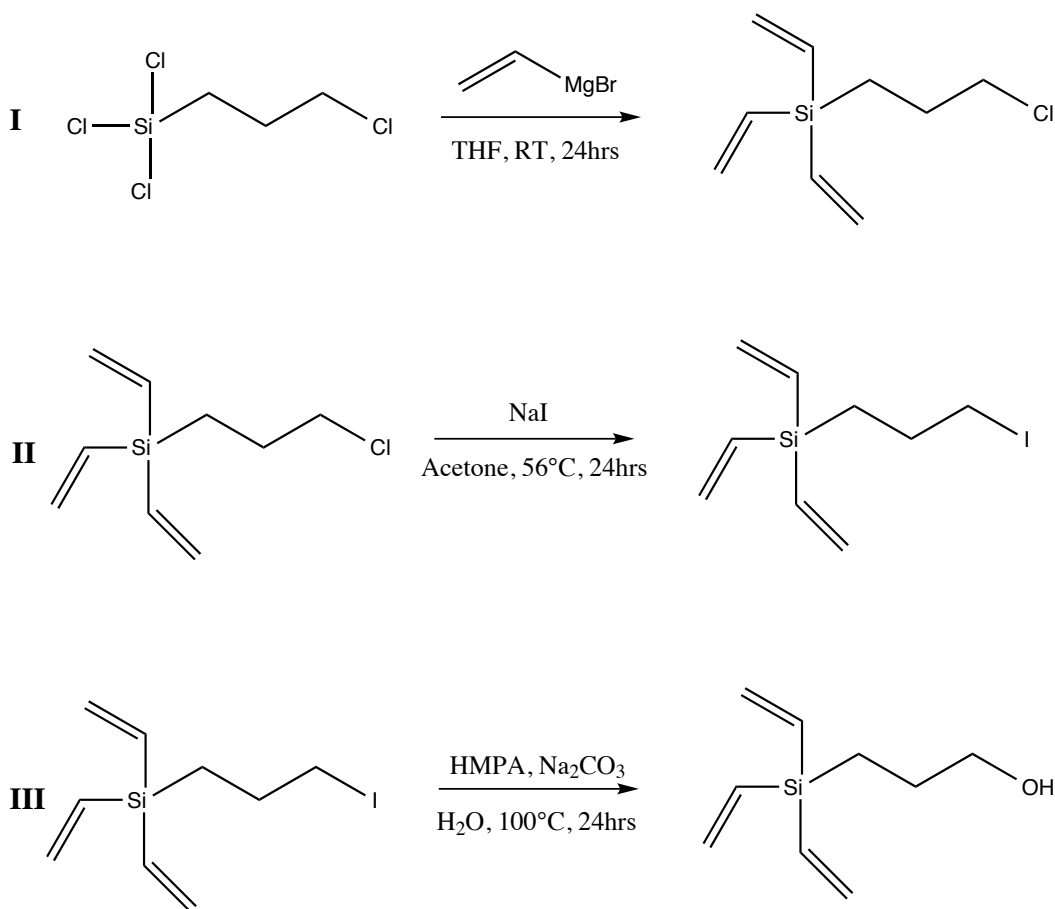


Figure 2.11. I) Synthesis of 3-chloropropyltrivinylsilane (CPTVS), II) 3-iodopropyltrivinylsilane (IPTVS), III) 3-hydroxypropyltrivinylsilane (HPTVS)

The first step in synthesizing the initiator involves the modification of 3-chloropropyltrichlorosilane (CPTCS) with vinyl magnesium bromide via a Grignard reaction, Figure 2.11 (I). Excess Grignard reagent was not used to limit the reaction with the 3-chloropropyl end group and ensure the reaction was mainly with the silyl chlorides. Using ^1H NMR, the resonance peaks of the silyl vinyl groups appeared at 5.73 and 6.30 ppm (9H). These shifts for the silyl vinyl groups are found further downfield than observed with the allyl-PEO-OH (Figure 2.6) due to the close proximity of the hydrogens in the trivinyl groups that has caused deshielding of the protons to occur. The methylene peaks of the 3-chloropropyl appeared at 3.49 (2H), 1.83 (2H), and 0.84 ppm (2H), shown in Figure 2.12.

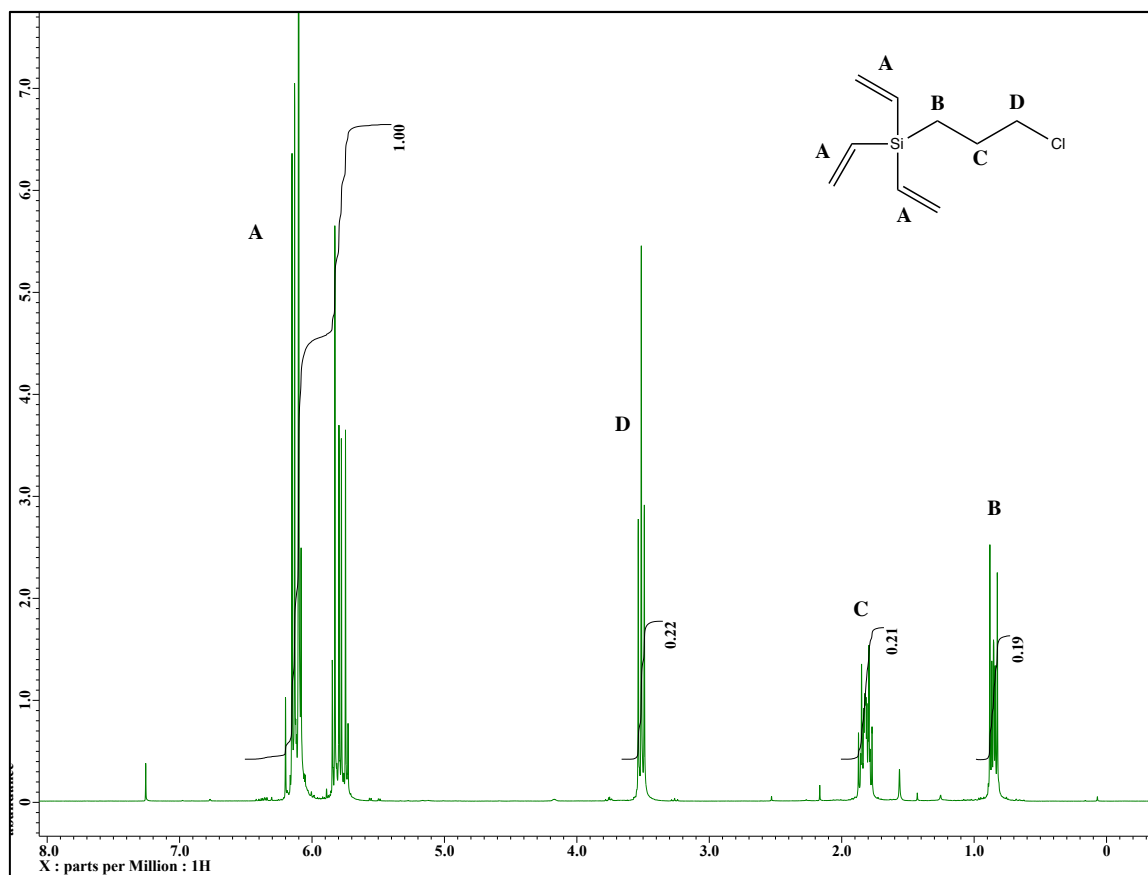


Figure 2.12. ¹H NMR spectrum of chloropropyltrivinylsilane

The second step taken was to synthesize 3-iodopropyltrivinylsilane (3-IPTVS), which involved replacing the chloride with an iodide via an S_N2 nucleophilic substitution, Figure 2.11 (II). Chloride is a much stronger nucleophile than iodide, making iodine a better leaving group. The substitution was confirmed by ¹H NMR, Figure 2.13, by seeing a small shift in the resonance of the methylene peaks adjacent to the iodine at 3.17 (2H). The other methylene peaks were observed at 1.87 (2H) and 0.82 ppm (2H). The vinyl silyl shifts were observed at 5.27 and 6.11 ppm (9H), indicating the vinyl groups are still present following the reaction. There is a shift at 2.15 ppm due to some that was not removed during purification.

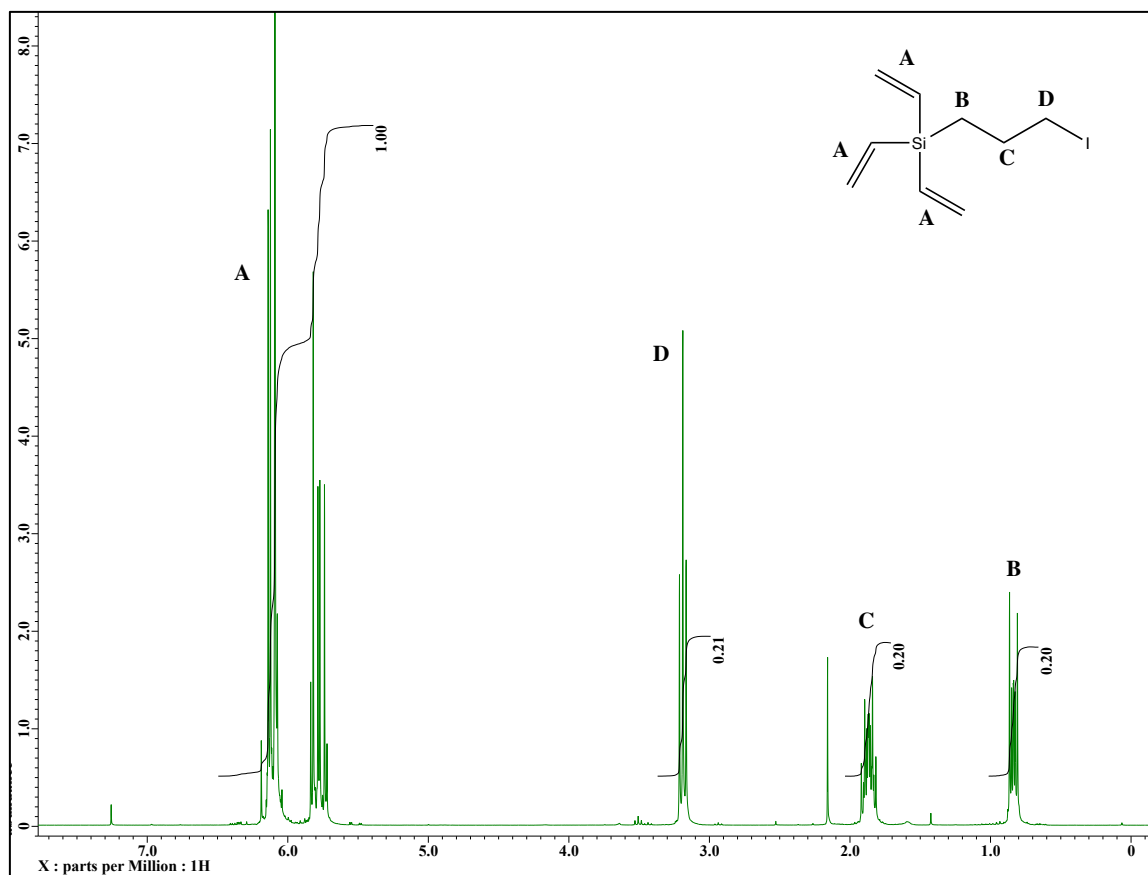


Figure 2.13. ^1H NMR spectrum of iodopropyltrivinylsilane.

The final step, Figure 2.11 (III), in the synthesis of the trivinyl initiator involves the transformation of the alkyl iodide to an alcohol via a $\text{S}_{\text{N}}2$ reaction using a polar aprotic solvent, HMPA. Conversion to alcohol was confirmed with ^1H NMR by observing a shift in the methylene peak from 3.17 ppm to 3.59 ppm. The chemical shifts were still visible at 6.20 and 5.70 ppm and the proton ratios matched the predicted; 9:2:2:2, Figure 2.14. There was a singlet at 1.69 ppm due to water in the sample.

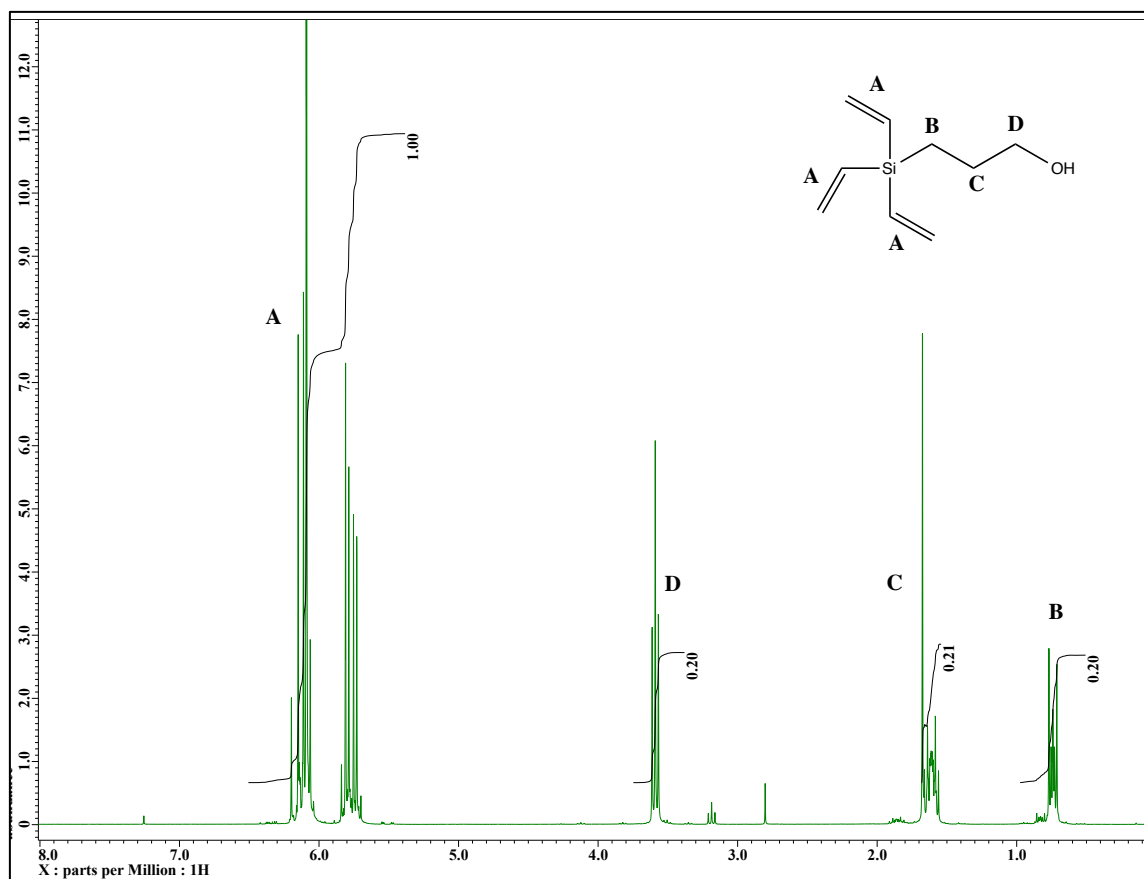


Figure 2.14. ^1H NMR spectrum of hydroxypropyltrivinylsilane.

Once the initiator was synthesized and characterized, it was used in the anionic ring opening polymerization of ethylene oxide, shown in Figure 2.15. Using potassium naphthalenide, the HPTVS was transformed into an alkoxide that will attack and open up the ethylene oxide ring. The reaction was performed at room temperature at 40 psi for 24 hours. The pressure decreased about 10 psi, indicating most of the ethylene oxide had been consumed in the reaction.

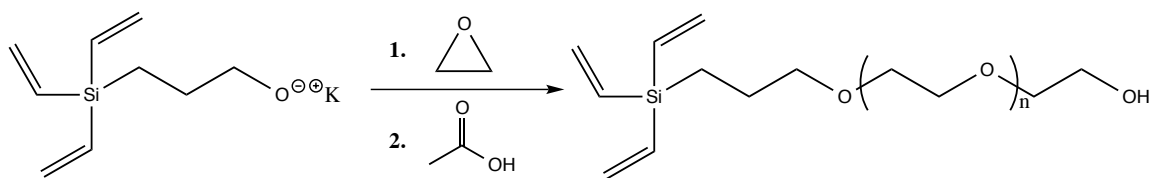


Figure 2.15. Anionic ring opening polymerization of ethylene oxide using HPTVS

The resulting polymer was characterized by $^1\text{H NMR}$, Figure 2.16, showing chemical shifts from the vinyl groups at 6.19 and 5.71 ppm. The methylene shift of PEO was a 3.67 ppm and the methylene shifts close to the tri vinyl silyl group were at 3.41, 1.63, and 0.71 ppm. Number average molecular weight was calculated by comparing the peak areas and was determined to be 6400 g mol^{-1} . The number average molecular weight determined from GPC was 6300 g mol^{-1} with a PDI of 2.1.

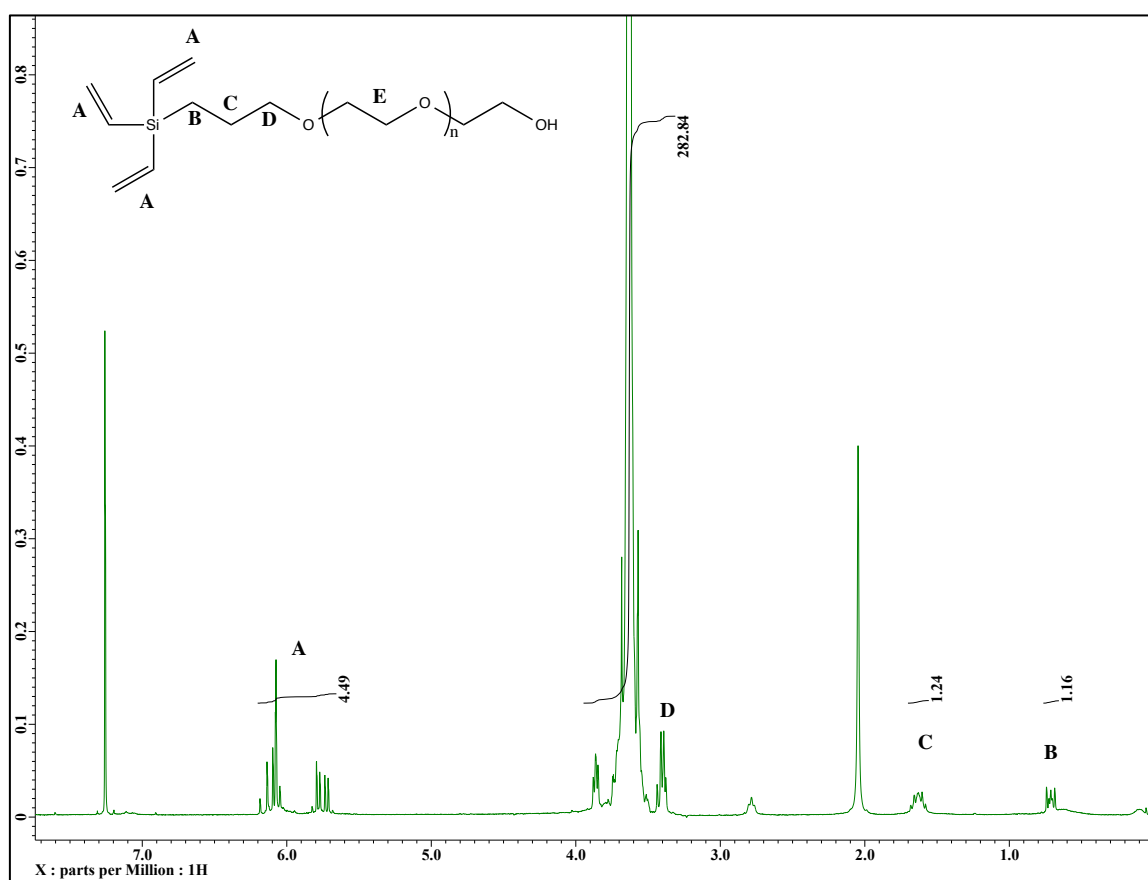


Figure 2.16. $^1\text{H NMR}$ of the anionic polymerization of ethylene oxide initiated by HPTVS.

2.8. ANIONIC RING OPENING POLYMERIZATION OF ETHYLENE OXIDE USING 2-(TETRAHYDRO-2H-PYRAN-2-YLOXY)ETHANOL (THP) AS INITIATOR

2.8.1. Experimental

Ethylene oxide, 13.3 g (0.302 mmol), was distilled into 300 mL stainless steel reactor cooled to -40°C using an acetone dry ice bath, followed by 100 mL of THF. In a separate 50 mL flame dried, round bottom flask with stir bar and under nitrogen purge, 0.64 mL (4.72 mmol) of 2-(tetrahydro-2H-pyran-2-yloxy)ethanol was dissolved in 10 mL of THF. Via syringe, 4.75 mL of a potassium naphthalenide solution (0.9 M) was added and stirred for 10 minutes. The initiator solution was then charged to the reactor via syringe, and followed by 50 mL of THF. The reactor was brought to room temperature and stirred for 72 hours. The polymerization was terminated with 1.90 mL of a 2.5 M acetic acid solution in THF. The reactor was then purged with nitrogen for one hour to remove any unreacted monomer. The solvent was then removed by rotary evaporation, and the product was dissolved in 200 mL of chloroform. The polymer solution was then washed with 150 mL of deionized water. The organic layer was then concentrated down and precipitated using cold DEE and polymer was retrieved by filtration. The remaining polymer was dried in vacuum oven at 25°C (yield: 12.20 g). ^1H NMR (300 MHz, CDCl_3 , δ in ppm): THP: 1.475-1.812 (-CH-(CH_2)₃-CH₂-), 3.852 (m, CH-(CH₂)₃- CH_2 -O-), 4.761 (t, -O- CH -O-). PEO: 3.630 (m, -(CH₂-CH₂-O)_n-).

2.7.2. Results and Discussion

When synthesizing heterobifunctional polymers, protecting groups are necessary to ensure only one end is functionalized without disturbing the other. Tetrahydropyranol (THP) is a common hydroxyl-protecting group that is stable under non acidic

conditions.¹²⁷ It can be easily cleaved by using an acid to produce a hydroxyl terminus that can be modified further.¹¹⁹ 2-(tetrahydro-2H-pyran-2-yloxy)ethanol was used as an anionic initiator to grow ethylene oxide, Figure 2.17. The reaction was performed at room temperature at 40 psi for 72 hours. The reaction was terminated after the pressure decreased about 10 psi, indicating all of the ethylene oxide has been used.

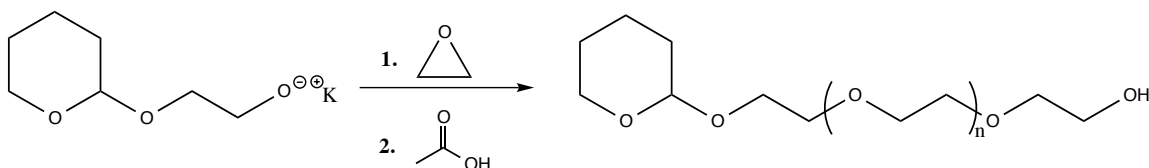


Figure 2.17. Anionic ring opening polymerization of ethylene oxide using 2

The polymer end group functionality and molecular weight was determined by ¹HNMR, Figure 2.18. The signals for the hydrogen in the THP protective group were observed at 4.76 (1H), 3.85 (2H) and 1.81-1.48 ppm (6H). The characteristic methylene peak of PEO was found at 3.63 ppm (328H). The number average molecular weight was calculated by comparing the ratio of the integration of the signals of the THP to the methylene signals of PEO; 2500 g mol⁻¹. The GPC result, calculated from a series of PEO standards, was determined to be 2150 g mol⁻¹.

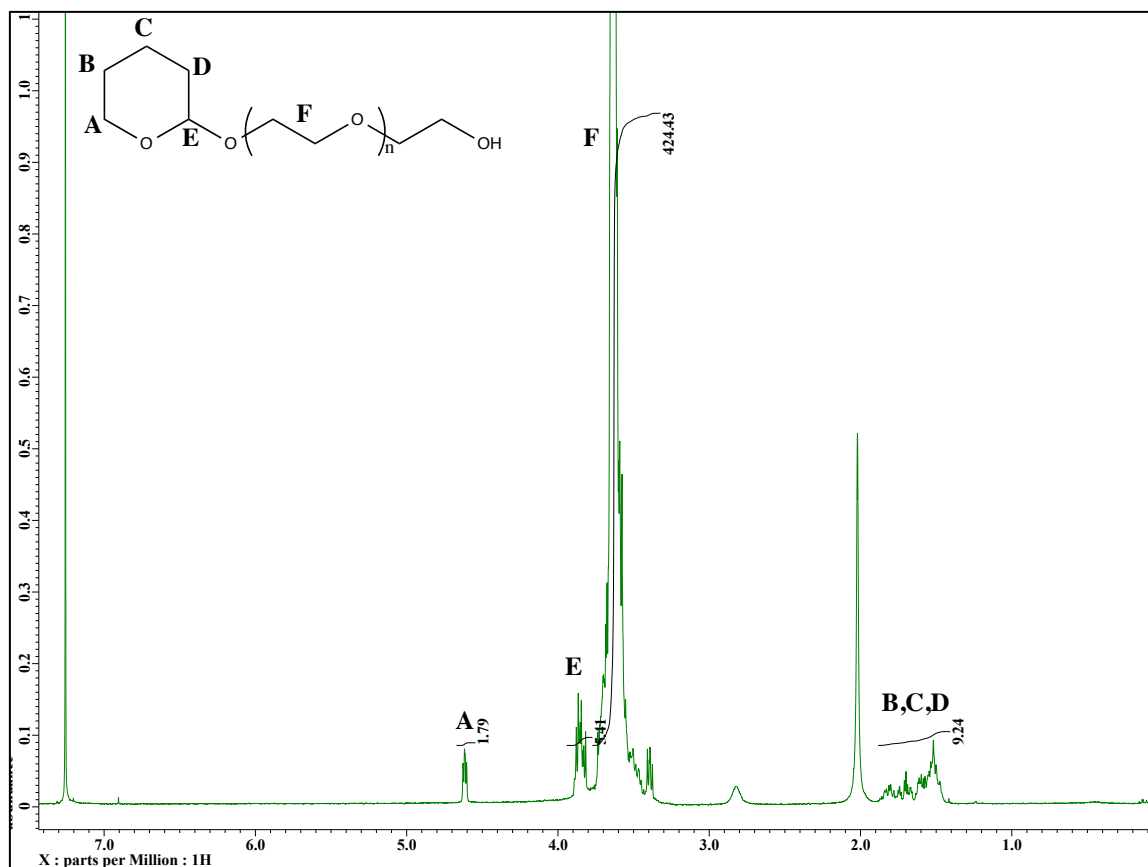


Figure 2.18. ^1H NMR spectrum of anionic ring opening polymerization of ethylene oxide using 2-(tetrahydro-2H-pyran-2-yloxy)ethanoxide

2.9. ANIONIC RING OPENING POLYMERIZATION OF ETHYLENE OXIDE USING POTASSIUM BIS(TRIMETHYLSILYL) AMIDE AS INITIATOR

2.9.1. Experimental

Ethylene oxide, 9.03 g (0.205 mol), was distilled into 300 mL stainless steel Parr Reactor cooled to -40°C using an acetone dry ice bath, followed by 100 mL of THF. At -35°C , 1.80 mL (8.26 mmol) of potassium bis(trimethylsilyl)amide solution was charge to the reactor followed by 10 mL of THF. The reactor was brought to room temperature and reacted for 36 hours. The reactor was then purged with nitrogen for 1 hour. Solvent was removed by rotary evaporation, and the polymer was dissolved in 200 mL of

chloroform. The solution was then filtered and the filtrate was then concentrated down and precipitated using cold DEE and polymer was retrieved by filtration. The remaining polymer was dried in vacuum oven at 25 °C (yield: 7.74 g). Removal of the trimethylsilyl groups was accomplished by dissolving the polymer in methanol and then slowly adding 20 drops of 1N HCl and stirred for 24 hours at room temperature. The polymer was precipitated with DEE and polymer was collected by filtration and dried in a vacuum oven at 25 °C. ¹HNMR (300 MHz, CDCl₃, δ in ppm): 2.81 (t, NH₂-CH₂-), 2.754 (s, NH₂-CH₂-), 3.635 (m, -(CH₂-CH₂-O)_n).

2.9.2. Results and Discussion

Potassium bis(trimethylsilyl)amide is a commercially available compound that can be used as an initiator to polymerize ethylene oxide with a primary amine on one end and a hydroxyl group on the other after acid treatment, Figure 2.19.¹²⁸ The polymerization was done at room temperature for 36 hours at 40 psi and was terminated when the pressure in the reaction vessel dropped 7 psi. After purification via precipitation, the collected polymer was characterized with ¹HNMR and GPC to confirm end groups and determine molecular weight.

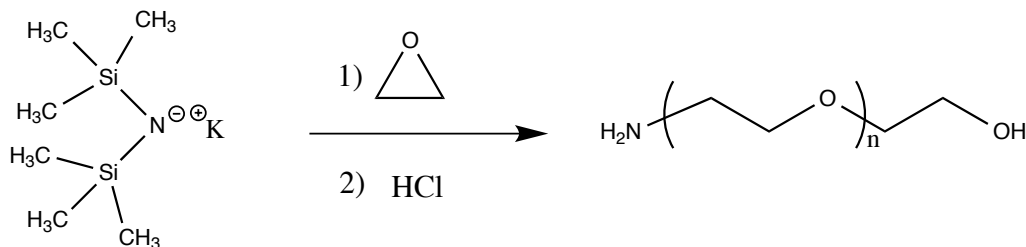


Figure 2.19. Anionic ring opening polymerizaion of ethylene oxide using potassium bis(trimethylsilyl)amide.

Figure 2.20 shows the broad primary amine signal and the adjacent methylene triplet signal overlap at 2.81 and 2.75 ppm respectively. The methylene signal was observed at 3.64, confirming polyethylene oxide was formed. The molecular weight was determined to be 4978 g mol^{-1} by comparing the ratio of the signal areas from the primary amine end group and the methylene shifts of PEO. Using polystyrene standards, GPC was used to determine the molecular weight to be 19776 g mol^{-1} with a PDI of 4.724.

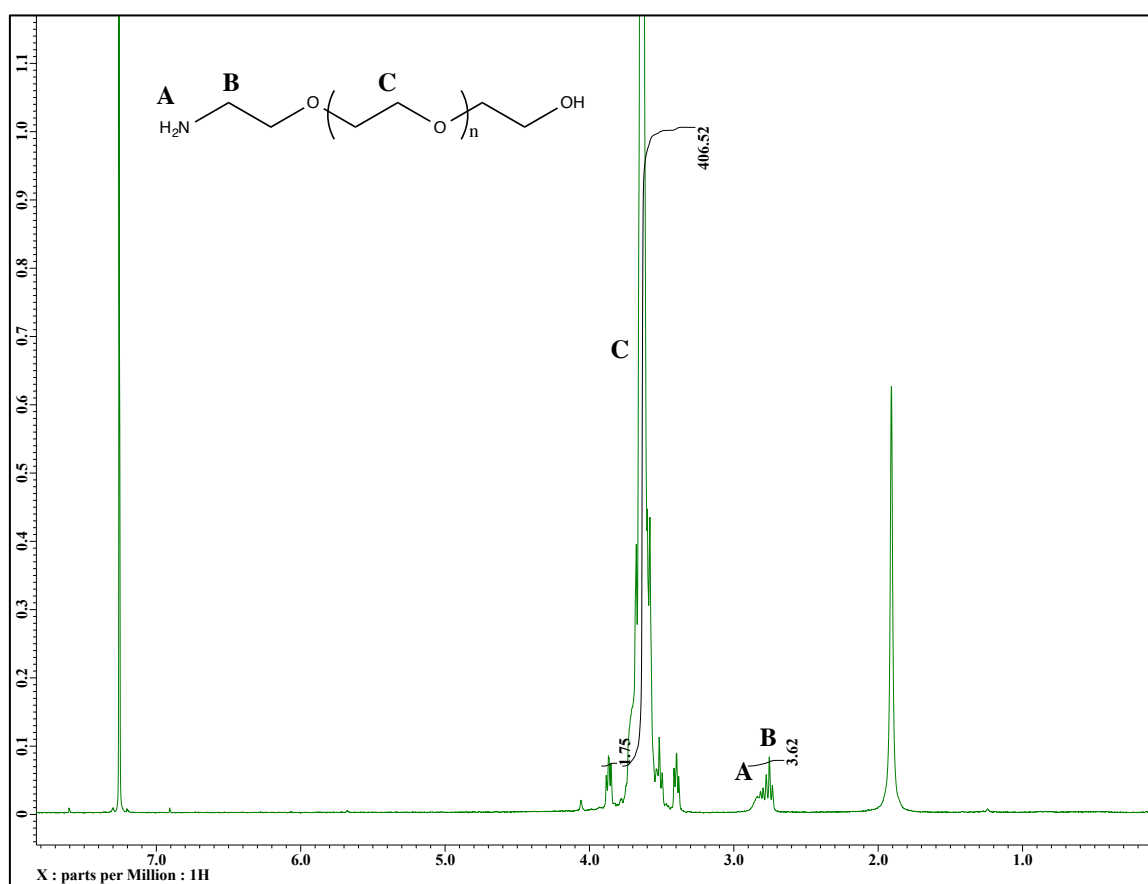


Figure 2.20. ^1H NMR spectrum of the anionic ring opening polymerization of ethylene oxide using potassium bis(trimethylsilyl)amide as an initiator.

2.10. CREATING HETEROBIFUNCTIONALITY THROUGH END GROUP MODIFICATION

This section describes multiple methods used to create a desired functionality through the modification of an alcohol terminus. These synthetic techniques will prove useful in creating a variety of heterobifunctional polymers for almost any application.

2.10.1 Modification of an alcohol terminus to a carboxylic acid

2.10.1.1. Experimental

THP-PEO-OH used in this modification was synthesized as described in section 2.7. THP-PEO-OH (2 g, 0.627 mmol), succinic anhydride (0.105 g, 1.05 mmol), and DMAP (0.009g, 0.07 mmol) was added to a flame dried 50 mL flask equipped with a stir bar and dissolved in 20 mL of anhydrous THF. The flask was capped and purged with nitrogen. The reaction was done at room temperature for 12 hours and then precipitated with cold DEE. The collected polymer was then dissolved in chloroform and precipitated again with cold DEE, this precipitation was repeated, and the polymer collected was dried in a vacuum with no heat. (Yield 1.89 g) ^1H NMR (300 MHz, CDCl_3 , δ in ppm): 2.72 (m, $-\text{OOC}-\underline{\text{CH}_2}-\underline{\text{CH}_2}-\text{COOH}$), 3.61 (m, $-(\text{CH}_2-\text{CH}_2-\text{O})_n$), and 3.87, m($-\text{CH}_2-\underline{\text{CH}_2}-\text{O}-\text{COO}-$).

2.10.1.1. Results/Discussion

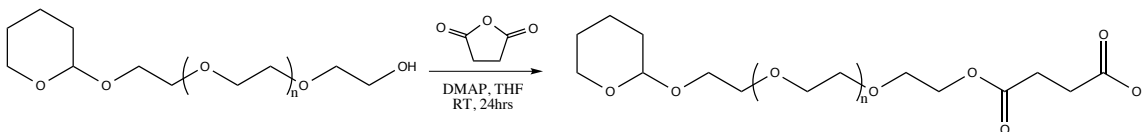


Figure 2.21. End group modification of THP-PEO-OH with carboxylic acid using succinic anhydride.

The esterification of the alcohol terminus with succinic anhydride, shown in Figure 2.21, is a common reaction that can be a very useful intermediate for synthesizing different heterobifunctional polymers¹²⁹ as well as react with certain proteins.¹²⁰ The end group functionalization was confirmed by ¹HNMR, showing characteristic shift at 3.61 ppm (2H) indicating ester linkage of the PEO to the succinic anhydride. The shift of the hydrogen of the two methylene groups located between the carbonyl groups of the succinic anhydride were found at 3.87 ppm (4H).

2.10.2. Modification of Alcohol Terminus with NitroDOPA

2.10.2.1. Experimental

The polymer used in this section was modified with a carboxylic acid using the method described in section 2.9.3. PEO-COOH (1.8g , 0.5 5mmol) was added to a flame dried flask equipped with a stir bar, along with NHS (0.063 g, 0.55 mmol) and DCC (0.141 g, 0.684 mmol) and dissolved in anhydrous THF. The flask was sealed and was reacted for 8 hours at room temperature under a nitrogen head.

The reaction was then vacuum filtered to remove any insoluble N,N'-dicyclohexylurea and then precipitated with cold DEE and the white precipitant was collected. The white precipitant was then dissolved in chloroform and precipitated with cold DEE two more times. The white precipitate was collected and dried under vacuum. (Yield 1.55 g) ¹HNMR (300 MHz, CDCl₃, δ in ppm): 2.804 (m, -OOC-CH₂-CH₂-COO-), 2.690 (s, -CH₂-CH₂- of NHS), 3.631 (m, -(CH₂-CH₂-O)_n).

NitroDOPA, a catechol amine, is a desirable end group for many polymers because of its strong binding affinity to metal oxides.¹³⁰ The PEO was now equipped

with an end group that would easily react with amines, Figure 2.22. This was taken advantage of by reacting it with the amine of nitroDOPA, shown in Figure 2.23. The resulting polymer was then precipitated with cold DEE to remove the byproduct of NHS. The precipitate was then dissolved in chloroform and vacuum filtered to remove any unreacted nitroDOPA. The filtrate was then precipitated with cold DEE and the resulting polymer was collected and stored in chloroform. ^1H NMR (300 MHz, CDCl_3), δ (ppm): 3.64 (m, $\text{CH}_2\text{-CH}_2\text{-O}$), NitroDOPA: 6.12 and 6.90 (s, CH in ring).

2.10.2.2. Results and Discussion

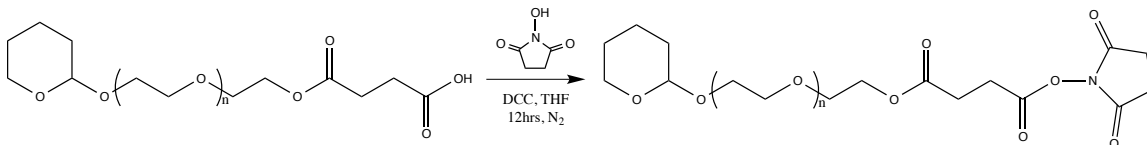


Figure 2.22. End group modification of THP-PEO-COOH with NHS intermediate.

NHS is commonly used as an intermediate to react with primary amines.^{120,131} It is also a popular synthetic technique used in linking bioconjugates to polymers.¹³²⁻¹³⁴ A PEO previously modified with a carboxylic acid was activated with NHS in preparation to react with the amine of nitroDOPA, Figure 2.22. The reaction was performed in anhydrous THF for 12 hours with DCC. Precipitation of insoluble N,N'-dicyclohexylurea indicated the reaction took place and it was removed by filtration. ^1H NMR was used to confirm NHS-ester linkage. The methylene shift of the NHS end group was indicated by a singlet at 2.69 ppm (4H).

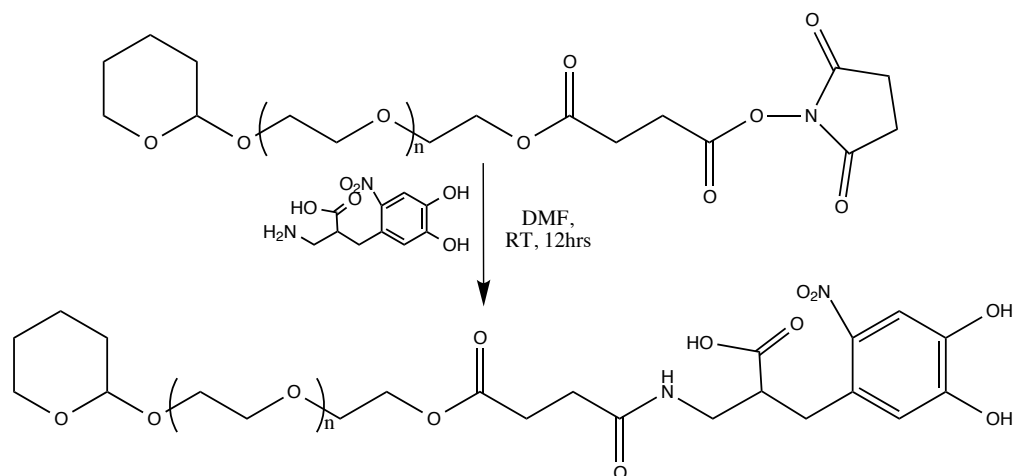


Figure 2.23. End group modification of THP-PEO-NHS with nitroDOPA.

Once the PEO-NHS intermediate (0.2 g, 0.059 mmol) was synthesized and characterized, it was then reacted with nitroDOPA (0.017 g, 0.071 mmol), a catechol amine, in anhydrous DMF for 12 hours, Figure 2.23. The reaction was purified by precipitation with DEE. It was then dissolved in chloroform and filtered to remove any unreacted nitroDOPA that is insoluble. The modification was confirmed by ^1H NMR with the appearance of shifts at 6.05 and 6.90 ppm, which are the proton resonance of the benzene ring of the nitroDOPA.

2.10.3. Modification of the Alcohol Terminus to an Alkyne

2.10.3.1 Experimental

A THP-PEO-OH, synthesized as describe in section 2.7, was used and was modified with an alkyne, shown in Figure 2.24, using the following procedure. THP-PEO-OH (1.5 g, 0.35 mmol) and sodium hydride (0.03 g, 1.3 mmol) were charged to a flame dried round bottom flask equipped with a stir bar and dissolved in 40 mL of THF. The reaction was brought to 0 °C using a salt ice bath and 120 μL of propargyl bromide solution (1.4 mmol) was slowly added over 30 minutes at 0 °C. Once all the propargyl

bromide was added, the reaction was stirred for another 30 minutes at 0 °C and then removed from ice bath to warm to room temperature and react for 24 hours. The resulting polymer was precipitated with cold DEE three times and solid was collected and dried under vacuum. The polymer was then dissolved in 20 mL of methanol and 20 drops of one molar HCl solution was slowly added. The reaction was stirred for 24 hours at room temperature to remove the protecting group. The polymer was the precipitated with cold DEE. The collected polymer was then dissolved in chloroform and precipitated again with cold DEE. The resulting solid was collected and dried under vacuum. Yield: 0.91 g. ¹HNMR (300 MHz, CDCl₃, δ in ppm): 2.43 (m, $\underline{C}H\equiv C-CH_2-$), 4.19 (m, $CH\equiv C-\underline{C}H_2-$), 3.65 (m, $-(CH_2-CH_2-O)_n$).

2.10.3.2. Results and Discussion

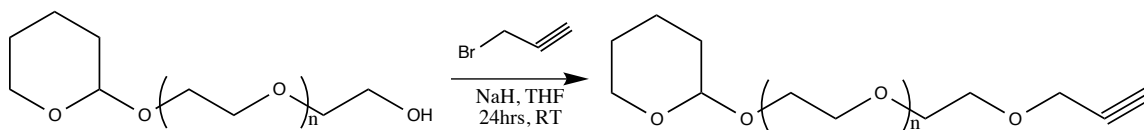


Figure 2.24. End group modification of THP-PEO-OH with propargyl bromide to give alkyne functionality.

Modification of a hydroxyl-terminated PEO with an alkyne group was completed using a substitution reaction with propargyl bromide, shown in Figure 2.22. The functionalization of PEO with an alkyne will allow for further derivation with azide-functionalized molecules via a 1,3 dipolar cycloaddition between the two functionalities to form a triazole linkage, which is a reaction that is synonymous with “click chemistry.”^{119,135} The reaction took place under room temperature conditions in anhydrous THF for 24 hours. Sodium hydride was used to catalyze the S_N2 reaction, producing an ether linkage connecting the propargyl group to the hydroxyl group of the PEO. ¹HNMR

confirmed the modification with an alkyne. The chemical shifts for the single proton of the on the alkyne was observed at 2.43 ppm (1H) and the methylene peak two carbons over showed proton resonance at 4.19 ppm (2H).

2.10.4. Modification of the Alcohol Terminus to a Methacrylate

2.10.4.1. Experimental

A (TMS)₂-N-PEO-OH, was synthesized as describe in section 2.8 was used and was modified with an alkyne using the following procedure. (TMS)₂-N-PEO-OH (1.0 g, 0.2 mmol) and sodium hydride (0.03 g, 0.8 mmol) were charged to a flame dried round bottom flask equipped with a stir bar and dissolved in 40 mL of THF. The reaction was brought to 0 °C using a salt ice bath and 80 µL of methacryloyl chloride solution (0.8 mmol) was slowly added over 30 minutes at 0 °C. Once all the methacryloyl chloride was added, the reaction was stirred for another 30 minutes at 0 °C and then removed from ice bath to warm to room temperature and react for 24 hours. The polymer was then dissolved in 20 mL of methanol and 20 drops of 1M HCl solution was slowly added. The reaction was stirred for 24 hours at room temperature to remove the TMS protecting groups. The polymer was the precipitated with cold DEE. The collected polymer was then dissolved in chloroform and precipitated again with cold DEE. The resulting solid was collected and dried under vacuum. Yield: 0.711 g. ¹HNMR (300 MHz, CDCl₃, δ in ppm): 6.13 and 5.57(t, $\text{CH}_2=\text{C}(\text{CH}_3)\text{-CH}_2\text{-}$), 4.19 (t, $\text{-C(=O)-O-CH}_2\text{-}$), 3.64 (m, $\text{-(CH}_2\text{-CH}_2\text{-O)}_n\text{)$, 1.95(s, $\text{CH}_2=\text{C}(\text{CH}_3)\text{-CH}_2\text{-}$).

2.10.4.2. Results and Discussion

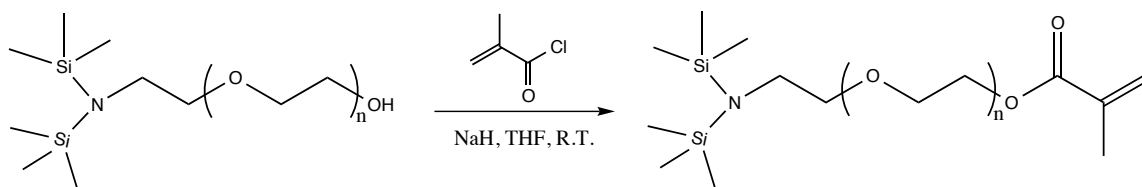


Figure 2.25. End group modification of PEO-OH with methacryloyl chloride.

Hydroxyl terminated PEO was modified with methacryloyl chloride using a S_N2 reaction, catalyzed with NaH. The polymer was characterized with ^1H NMR and modification was easily confirmed by the appearance of shifts at 6.13 and 5.57 ppm(2H) for the hydrogen of the terminal vinyl group. The methyl group on the methacrylate end group appeared at 1.95 ppm and the methylene hydrogens of the ethylene oxide repeat unit with a multiplet at 3.64 ppm. PEO with a methacrylate end group can be very useful in creating star graft copolymers,¹³⁶ drug modification using thiol-ene chemistry,¹⁰³ and crosslinking of magnetic nanoparticles to increase magnetic response.¹³⁷

2.11. CONCLUSION

Polyethylene oxide is very versatile polymer that can be used in a variety of applications. Developing skills of polymer synthesis and endgroup modification will allow for an arsenal of heterobifunctional polyethers that can be used for surface coatings that will provide functionality. These synthetic techniques are not limited to PEO oxide; they are well-studied techniques that can be applied to other polymer systems. The polymers described in this chapter were synthesized and modified with relative ease and the techniques were used in later chapters to synthesize specialized polymers that will be

used to modify magnetic nanoparticles for biomedical applications, described in later chapters.

CHAPTER 3. SYNTHESIS AND CHARACTERIZATION OF HETEROBIFUNCTIONAL POLY(ETHYLENE OXIDE) PLATFORM FOR BIOMEDICAL MAGNETIC NANOPARTICLES

3.1. ABSTRACT

Contemporary magnetic nanoparticle composites are individually designed for a specific application: magnetic hyperthermia, cell separation, and MRI contrasts agents. The work that is described here involves the synthesis of a single magnetic nanoparticle composite with a surface that can be customized for any application. The discussion of the syntheses and characterization of a heterobifunctional polyethylene oxide (PEO) using nitroDOPA as a robust anchoring group on one end and an alkyne as the reactive surface for additional application specific modification. The potential for these scaffolds allows them to be utilized in a variety of research fields because of the efficiency and ease of modification that is inherit in the Huisgen 1,3-dipolar cycloaddition between an azide and alkyne, commonly known as “click chemistry.” Synthesis of this specialized polymer-particle complex exhibited biological stability and modifiable surface by attaching a fluorescent dye using “click chemistry.”

3.2. INTRODUCTION

Magnetic nanoparticles are ideal materials for bioimaging,¹³⁸ therapy and delivery.¹³⁹ These blossoming technologies are not possible without designing and synthesizing specialized materials to stabilize the magnetic nanoparticles in biological environments. For the stabilizing layer, the material must be biologically inert and have sufficient steric hindrance to provide a long circulation time in the body.¹⁴⁰ To increase efficiency of materials used in biological imaging, therapy and delivery, the surface must

be enhanced with biological targeting and labeling molecules to both increase the concentration of the particles in the desired location of the body and to monitor the particles' fate.¹⁴¹

When designing polymer-particle systems for biomedical applications, it is very important to have a robust anchor to ensure particle stability in protein rich environments. Some traditional anchor groups studied for iron oxide nanoparticles are carboxylic acids,⁵⁴ alcohols,⁵⁵ amines,⁵⁶ silanes,¹⁴² ammonium,¹⁴³ and phosphates.⁵⁸ Another molecule being heavily researched as a robust anchor for iron oxide nanoparticles are catechols, which were inspired from a protein adhesive featured in mussels.¹⁴⁴ Catechol-derived ligands have been found to displace other binding groups on the surface of iron oxide¹⁴⁵ as well as create stable particles in physiological conditions.^{66,146} The catechol groups used for anchoring to iron oxide are generally found in dopamine-derived molecules that can be attached to polymers through the terminal amine using a common crosslinking chemistry that utilizes N-hydroxysuccinimide (NHS) esters to activate carboxylic acid for reactions with amines.¹³¹

In this chapter, a heterobifunctional polyethylene oxide (PEO) ligand was synthesized for the stabilization and functionalization of magnetic nanoparticles. Utilizing ordinary chemistry, a synthetic route was developed that produces a heterobifunctional PEO ligand with a robust anchoring group and a reactive surface. PEO is ideal for theranostic systems, term used to describe particles that can be used for both therapeutic and diagnostic applications, not only because of how inert the backbone is to

protein absorption,¹⁴⁷ but this relatively unreactive polymer chain allows for modification of the end groups with relative ease.¹¹⁴

3.3. EXPERIMENTAL

3.3.1. Synthesis of nitroDOPA

In a 50 mL round bottom flask, equipped with a stir bar, 30 mL of DI water was cooled in a brine salt bath to 0 °C before adding sodium nitrite (1.52 g, 17.88 mmol) and L-3,4-dihydroxyphenylalanine (L-DOPA) was added (1.97 g, 9.99 mmol) and allowed to cooled. While stirring, 0.92 mL (90.23 mmol) of sulfuric acid was added dropwise to form an orange precipitate. Once all of the acid was added, the solution was stirred overnight. The product was collected by vacuum filtration, washed with methanol, and dried in a vacuum oven (30% yield).

¹HNMR (300 MHz, DMSO-D₆), δ (ppm): 7.46 and 6.84 ppm (s, CH, ring, nitroDOPA), 3.54-3.49 ppm (t, J=15, -CH₂-CH-N-), 3.31-2.98 ppm (m, -CH₂-CH-N-),
¹³CNMR (300 MHz, DMSO-D₆) δ (ppm): 170.7, 153.4, 145.2, 139.2, 126.9, 119.9, 112.6, 54.8, 40.0, 35.4.

3.3.2. Synthesis of THP-PEO-OH

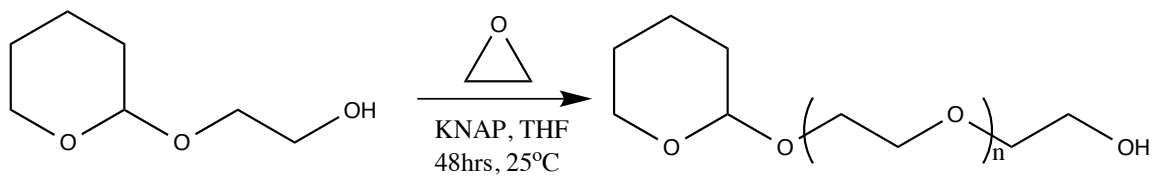


Figure 3.1. Anionic ring opening polymerization of ethylene oxide using THP initiator.

EO (13.3g, 0.30 mol) was distilled into 300 mL stainless steel reactor cooled to -40 °C using an acetone dry ice bath, followed by 100 mL of THF. In a separate 50 mL

flame dried, round bottom flask with stir bar and under nitrogen purge, dissolved 2-(tetrahydro-2H-pyran-2-yloxy)ethanol (0.65 mL, 4.72 mmol) in 10 mL of THF. Via syringe, 4.75 mL of potassium naphthalenide (0.9 M) was added and stirred for 10 minutes. The initiator solution was then charged to the reactor via syringe, and followed by 50ml of THF. The reactor was brought to room temperature and held for 72 hours. Polymerization was terminated with 1.90 mL of 2.5 M acetic acid solution in THF. The reactor was then purged with nitrogen for 1hr. Solvent was removed by rotary evaporation, and then dissolved in 200 mL of chloroform. The solution was then washed with 150 mL of deionized water. The organic layer was then concentrated down and precipitated using cold DEE and polymer was retrieved by filtration. The remaining polymer was dried in vacuum oven at 25 °C and characterized by ¹HNMR. Molecular weight was calculated by comparing the ratio of the area of THP to the polyethylene backbone and was found to have a molecular weight of 6300 g mol⁻¹.

¹HNMR (300 MHz, CDCl₃), δ (ppm): THP: 1.47-1.88 (m, CH-(CH₂)₃-CH₂), 3.87 (m, CH-(CH₂)₃-CH₂-O), 4.61 (t, J=6.9, O-CH-O). PEO: 3.64 (m, CH₂-CH₂-O).

3.3.3. Synthesis of THP-PEO-Alkyne

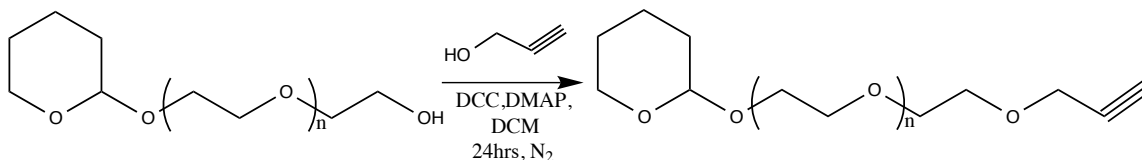


Figure 3.2. End group modification of THP-PEO-OH with propargyl bromide.

A 100ml round bottom flask was equipped with a stir bar and flame dried. The flask was then charged with THP-PEO-OH (2.0g, 0.33 mmol) and sodium hydride (0.024

g, 1.0 mmol) and finally sealed and purged with nitrogen. THF (20 mL) was then added via syringe to dissolve reactants and was brought to 0 °C using a NaCl ice bath for 30 minutes. Propargyl bromide (0.09 mL, 1.0 mmol) was added slowly via syringe over 30 minutes, followed by 30 minutes of stirring at 0 °C. The reaction was removed from ice bath and warmed to room temperature and stirred for 24 hours. The final solution was filtered via vacuum filtration and subsequently precipitated twice with DEE. The final product was dried in vacuum overnight.

$^1\text{HNMR}$ (300 MHz, CDCl_3), δ (ppm): 1.47-1.88 (m, $\text{CH}(\text{CH}_2)_3\text{-CH}_2$), 4.63-4.61 (t, O-CH-O), 3.64 (m, $\text{CH}_2\text{-CH}_2\text{-O}$), 2.43-2.44 (t, $\text{-O-CH}_2\text{-C}\equiv\text{CH}$), 4.198-4.190 (d, $\text{-O-CH}_2\text{-C}\equiv\text{CH}$)

3.3.4. Deprotection of THP-PEO-Alkyne

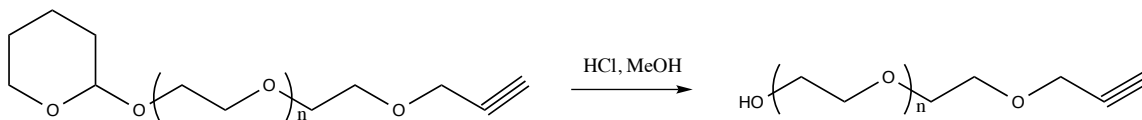


Figure 3.3. Cleavage of tetrahydropyranol to yield alkyne-PEO-OH

THP-PEO-alkyne (0.8 g, 0.17 mmol) was dissolved in 10 mL of methanol. Three drops of 1 M HCl solution were added and the solution and stirred for 4 hours. The product was recovered by crashing into DEE, and solid was collected using vacuum filtration. The product was characterized by $^1\text{HNMR}$.

$^1\text{HNMR}$ (300 MHz, CDCl_3), δ (ppm): 3.64 (m, $\text{CH}_2\text{-CH}_2\text{-O}$), 2.42-2.44 (t, $\text{-O-CH}_2\text{-C}\equiv\text{CH}$), 4.187-4.195 (d, $\text{-O-CH}_2\text{-C}\equiv\text{CH}$)

3.3.5. Synthesis of Alkyne-PEO-COOH

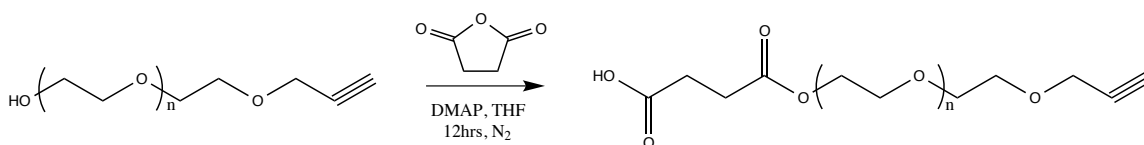


Figure 3.4. Modification of alcohol terminus with carboxylic acid using succinic anhydride.

A round bottom flask equipped with a stir bar was flame dried and charged with alkyne-PEO-OH (0.8 g, 0.17 mmol) and placed in a vacuum oven for 30 minutes at 80 °C. SA (0.03 g, 0.27 mmol) and DMAP (0.002 g, 0.02 mmol) were added to round bottom flask and then it was purged with nitrogen. Finally, anhydrous THF (20 mL) was then added to the flask via syringe and stirred for 8 hours. The reaction was then precipitated with cold DEE. The precipitant was collected and dissolved in 5 mL of DCM and precipitated again with cold DEE (2X). The final precipitant was collected and dried in a vacuum oven overnight. The polymer was characterized using ¹HNMR.

¹HNMR (300 MHz, CDCl₃), δ (ppm): 3.64 (m, CH₂-CH₂-O), 2.58 (m, -CH₂-CH₂-C(O)-O-), 2.42-2.44 (t, -O-CH₂-C≡CH), 4.187-4.195 (d, -O-CH₂-C≡CH)

3.3.6. Synthesis of Alkyne-PEO-NHS

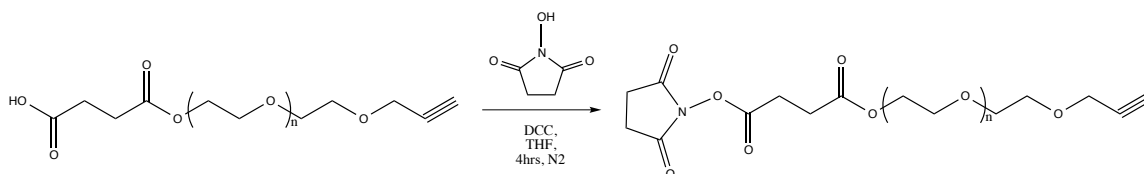


Figure 3.5. PEO-alkyne modified with NHS intermediate

In a flame dried, 25 mL round bottom flask with a stir bar, alkyne-PEO-COOH (0.73 g, 0.15 mmol), NHS (0.02 g, 0.18 mmol), and DCC (0.04 g, 0.18 mmol) were added, capped and purged with nitrogen. THF (20 mL) was added via syringe and was

reacted for 4 hours at room temperature. The solution was then vacuum filtered to remove any dicyclohexylurea that precipitated during the reaction. Using rotary evaporation, the THF was removed from the filtrate and the product was dissolved in 5 mL of DCM and precipitated with DEE (2x). The precipitate was collected and dried in a vacuum oven (83% yield). The product was characterized by ¹HNMR.

¹HNMR (300 MHz, CDCl₃), δ (ppm): 3.64 (m, CH₂-CH₂-O), 4.22 (m, -CH₂-O-C(O)-), 2.72 (m, -CH₂-CH₂-C(O)-O-), 2.42-2.44 (t, -O-CH₂-C≡CH), 4.19-4.20 (d, -O-CH₂-C≡CH), 2.80 (s, -C(O)-CH₂-CH₂-C(O)-).

3.3.7. Synthesis of Alkyne-PEO-NitroDOPA

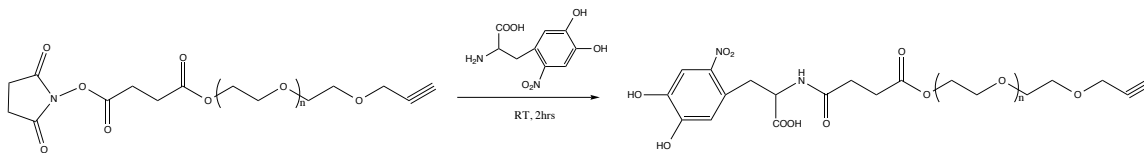


Figure 3.6. Modification of PEO with nitroDOPA

A flame dried, 50 mL Erlenmeyer flask equipped with a stir bar was charged with alkyne-PEO-NHS (0.69 g, 0.14 mmol) and nitroDOPA (0.04 g, 0.17 mmol), capped, and purged with nitrogen. Next, 10 mL of DMSO was added via syringe and stirred for 4 hours at room temperature. Finally, the resulting reaction was precipitated with DEE and the product was dissolved in chloroform and filtered to remove any excess nitroDOPA. The final polymer was precipitated with cold DEE, collected, and dried in vacuum oven (87% yield). The final product was characterized using ¹HNMR.

^1H NMR (300 MHz, CDCl_3), δ (ppm): 3.64 (m, $\text{CH}_2\text{-CH}_2\text{-O}$), 2.72 (m, $-\text{CH}_2\text{-CH}_2\text{-C(O)-O-}$), 2.42 (s, $-\text{O-CH}_2\text{-C}\equiv\text{CH}$), 4.20 (d, $-\text{O-CH}_2\text{-C}\equiv\text{CH}$). NitroDOPA: 6.12 and 6.70 (s, CH in ring).

3.3.8. Synthesis of magnetite nanoparticles

The 7.2 nm magnetic nanoparticles, synthesized using thermal decomposition of iron(III) acetylacetonate (2 mmol), 1,2-hexadecanediol (10 mmol), oleylamine (4 mmol), benzyl ether (20 mL), and 6 nm iron oxide seeds were added and stirred under a nitrogen flow and brought to 200 °C for one hour to remove any moisture. Finally the reaction was brought to reflux for 30 minutes under a nitrogen head. The particles were purified by precipitation of ethanol and characterized using TEM and DLS.

3.3.9. Modification of magnetite nanoparticles

The magnetic nanoparticles were modified by first dissolving alkyne-PEO-nitroDOPA (200 mg, 0.04 mmol) into 10ml of chloroform followed by the slow addition of 1ml (2 mg of $\text{Fe}_3\text{O}_4 \text{ mL}^{-1}$) of magnetic nanoparticles, which were also dispersed in chloroform, while sonicating over 30 minutes. The solution was allowed to stir overnight. The particles were then purified by precipitation with hexane, centrifuged to separate particles from solvent. They were then dispersed in ethanol and subsequently precipitated using hexane and separated via centrifugation to collect particles. Finally, the particles were dispersed in deionized water and dialyzed for 3 days.

3.3.10. Functionalization of alkyne-PEO-nitroDOPA coated magnetic nanoparticles with azido-functionalized dyes

Modification with azido-fluorescein dye

To 10ml of DI water, 0.2 mL of modified particles (0.7 mg of modified particles mL⁻¹) was added. The azido-fluorescein dye (0.003 mmol) was added to solution followed by CuSO₄ (0.013 mmol) and sodium ascorbate (0.003 mmol). The reaction was then covered with foil and stirred at 32 °C for 24 hours. The particles were then removed from heat and dialyzed for 2 days against DI water.

Modification with azido-fluorescein and carbazole dye

To 50ml of THF, 1ml of modified particles (4.11mg/mL) was added. Azido-fluorescein (0.67mg, 0.001mmol) and azido-carbazole (0.21mg, 0.001mmol) was then added to the solution. While stirring, 121 μL aqueous solution of CuSO₄ (15mM) and 54μL aqueous of sodium ascorbate (11.1mM) was added to the solution and reacted for 24 hours at 32 °C. The particles were removed for heat and the THF was then removed by rotary evaporation. The particles were then dispersed in 5ml of DI water and dialyzed for 3 days against DI water.

3.4. RESULTS AND DISCUSSION

The synthetic design begins with the anionic ring opening polymerization of ethylene oxide using 2-(tetrahydro-2H-pyran-2-yloxy)ethanol (THP) as the alkoxide initiator (Figure 3.1), based on previous work by Hiki et al.¹¹⁹ This synthetic approach is ideal for creating narrow molecular weights and is more efficient than partial derivation of diols.¹¹⁴ Beginning with one protected end group allows for precise and efficient modification for desired heterobifunctionality. With one of the end groups protected, the

free alcohol was modified with propargyl bromide via a substitution reaction to produce the alkyne functionality needed (Figure 3.2). After cleaving the tetrahydropyranol protecting group with an acid (Figure 3.3), the other alcohol was free to be modified. Through a series of reactions, which included modification with succinic anhydride (SA) (Figure 3.4) and the N-hydroxysuccinimide (NHS) (Figure 3.5), the polymer was primed to be modified through the amine of nitroDOPA (Figure 3.6).

NitroDOPA was synthesized using a procedure by Yang et al¹⁴⁸ and used as our anchoring system based on a study by Amsted et al that compared the stability of a variety of catechol complexes in which they found nitroDOPA having one of the higher binding affinities.⁶² Using ¹³CNMR (Figure 3.7) and FT-IR (Figure 3.8), nitration of the DOPA was confirmed by the symmetric and asymmetric stretching peaks at 1330 and 1532 cm⁻¹, respectively.

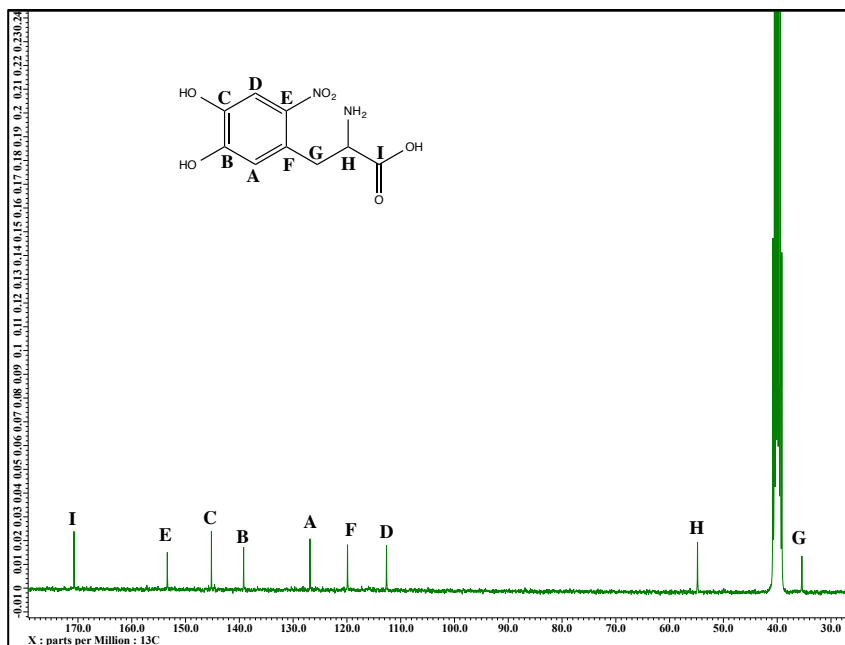


Figure 3.7. ¹³CNMR spectra of nitroDOPA in D₂O

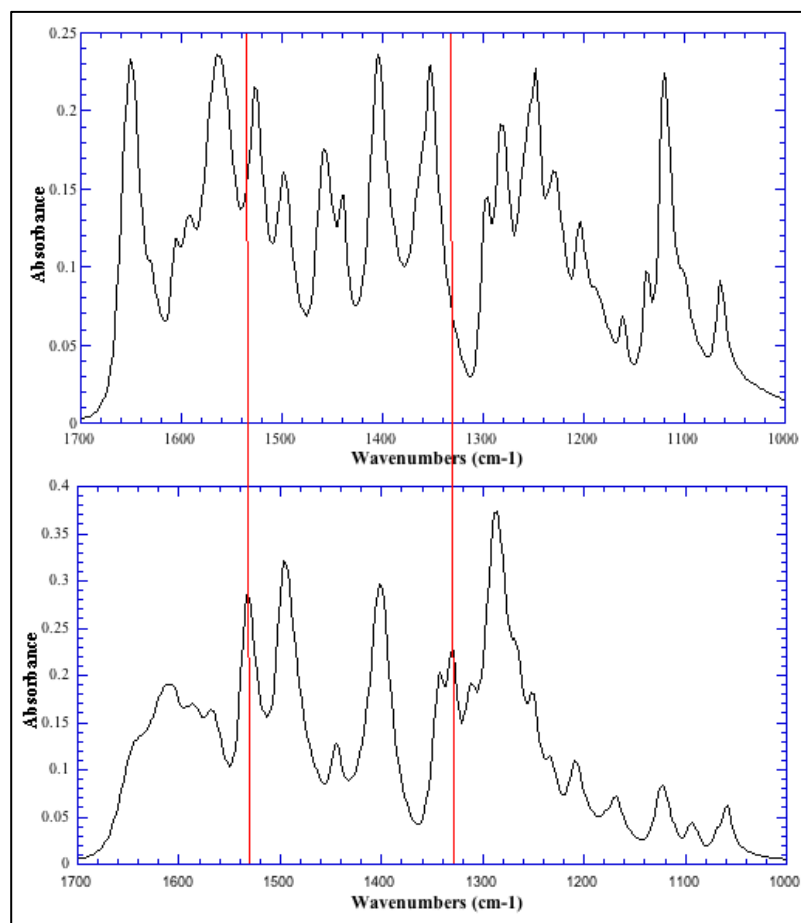


Figure 3.8. Interferogram of DOPA (top) and nitroDOPA (bottom). Symmetric and asymmetric stretching peaks at 1330 and 1532 cm^{-1} confirm nitration.

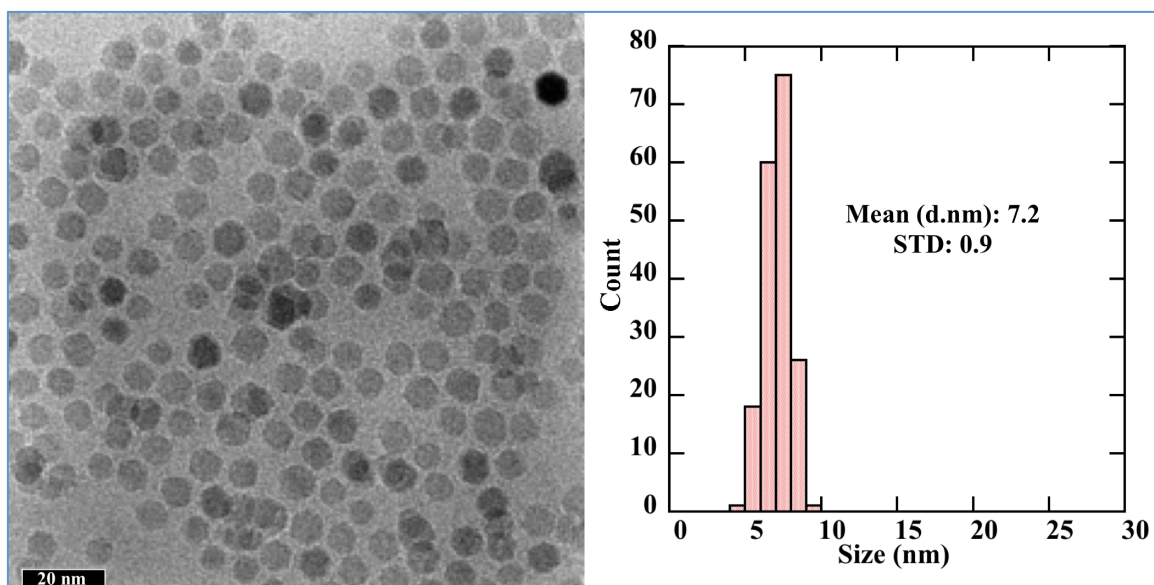


Figure 3.9. TEM micrograph of iron oxide nanoparticles synthesized via thermal decomposition with a mean size of $7.2\text{nm} \pm 0.9$.

Monodispersed iron oxide nanoparticles in hexane were synthesized using a method from Sun et al.¹⁴⁹ The particles core size was found to be $7.2\text{ nm} \pm 0.9\text{ nm}$ in diameter by TEM (Figure 3.9) and the hydrodynamic diameter was found to be $29.2 \pm 17.1\text{ nm}$ (Table 3.1). The particles were then modified via ligand exchange using PEO modified with nitroDOPA. Sonication and stirring overnight aided in the replacement of the oleylamine, a hydrophobic ligand, with the polymer ligand in chloroform. The particles were then precipitated with an anti-solvent and finally dispersed into DI water. PEO with a molecular weight of 6000 g mol^{-1} was used to modify the particles because it provides sufficient steric hindrance to avoid agglomeration due to the magnetic nature of the particles. Because the human circulatory system is sensitive to objects with a size greater than 200 nm , the brush sized used will provide a small enough platform for modification with large functional moieties to stay below the size range that can be

filtered out. The particles dispersed in DI water was a great indicator that the particles were successfully modified with PEO (Figure 3.10), and TEM micrograph (Figure 3.10) shows a halo from the less dense polymer around the dense magnetic nanoparticles. If the polymer chains were fully extended, the chain length is about 34 nm, giving a total polymer-particle diameter of 61 nm. When analyzing the dry diameter of 10 particles, the average diameter measured was 42 nm, which is within the size range expected for the molecular weight used to modify the 7.2 nm magnetic nanoparticles.

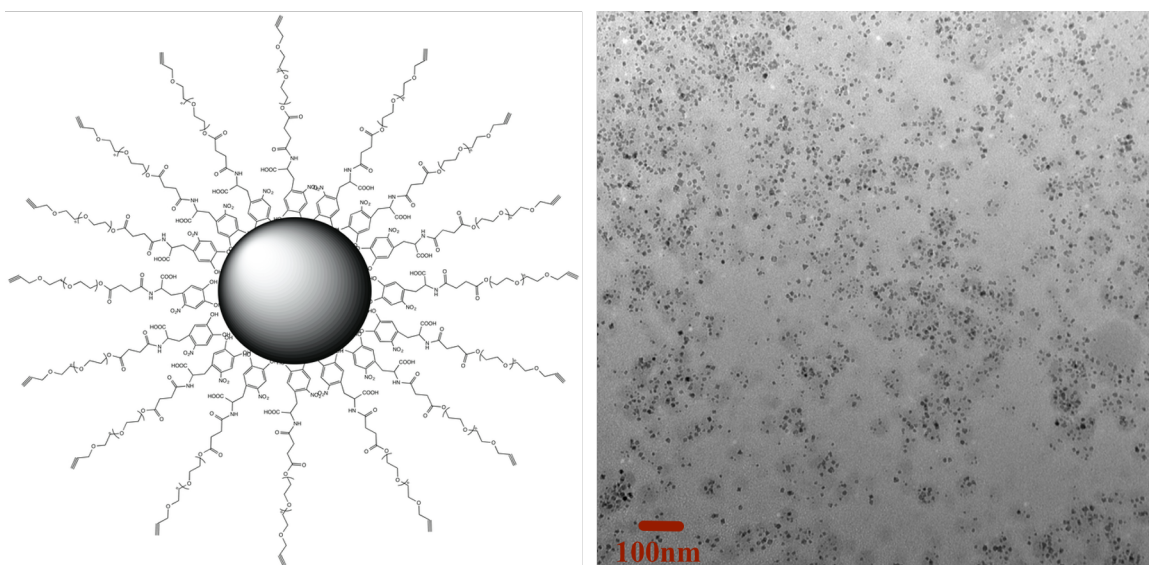


Figure 3.10. Schematic of a magnetic nanoparticle modified with alkyne-PEO-nitroDOPA (left) and TEM micrograph of particles after modified with alkyne-PEO-nitroDOPA (right).

When creating nanoparticles for biological applications, analyzing the particle-environment interaction is important.^{57,131} Characterizing these particles in ionic and protein rich solutions is a great technique for simulating stability in biological environments. Using dynamic light scattering (DLS), modification of the aforementioned 7.2 nm oleylamine coated nanoparticles with the water soluble PEO was confirmed. The

final hydrodynamic diameter was an average of 77 nm in water, as shown in Table 3.1. For drug delivery systems, this size will be able to circulate within the body without getting filtered out by the reticulo-endothelial system (RES).¹⁵⁰ The particles were further characterized with thermogravimetric analysis (TGA) (Figure 3.11) to find the surface loading of polymer on the surface of the particle. There was about a 95% weight loss of polymer, which comes out to be about 11 chains per nm², suggesting some free polymer still associated with the particles after 3 days of dialysis. Initially, it was presumed that some oleic acid, used to suspend the particles before they were modified with polymer, might have been trapped on the surface during modification. TGA analysis of the particles before they were modified with polymer showed an 87% weight loss from 179-233 °C due to the oleic acid. This feature is not observed in the TGA of the modified particles, Figure 3.11. So, the high loading of polymer on the surface could be due to crosslinking between the nitroDOPA endgroups that can create a large macromolecule that was not removed with the molecular weight cutoff used for dialysis.

Table 3.1. DLS of magnetic nanoparticles before and after modification.

	Z-Avg (d.nm)	PDI	I (% , d.nm)	V (% , d.nm)	N (% , d.nm)
OA Coated	29.24	0.295	35.42±17.14	20.06±8.93	14.57±4.51
PEO-Coated	77.31	0.138	89.49±31.65	66.83±25.72	51.52±14.73

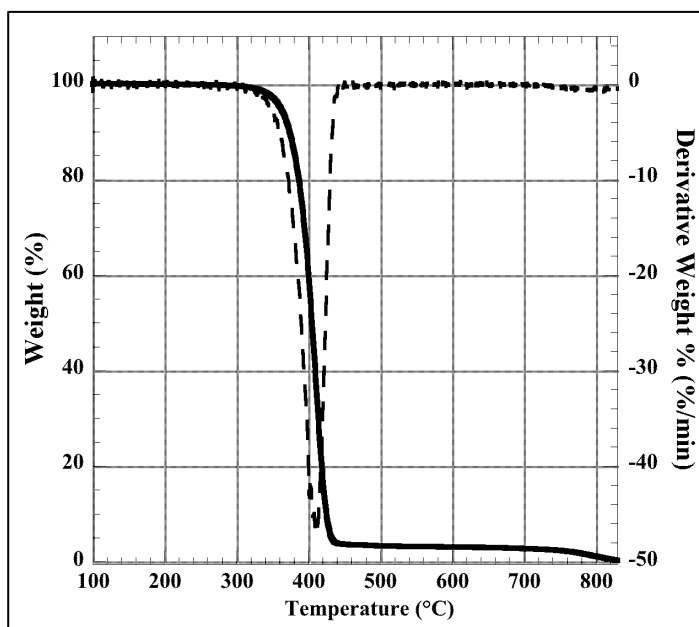


Figure 3.11. Thermograph of particles modified with alkyne-PEO-nitroDOPA

Although the particles are stable in water, this is irrelevant in the complex environment of the human body. Materials used in biological applications can be limited in their effectiveness due to absorption plasma proteins that can inhibit the circulation time in the body.¹⁵¹ Proteins can attach to the particles and provoke agglomeration rendering the particles useless. To observe how this particles system will behave in a simulated biological environment, phosphate buffer saline (PBS), fetal bovine serum (FBS), and bovine serum albumin (BSA) were added, 10% by volume (0.1 mL), to a dilute solution of the particles (0.9 mL, 0.1 mg of modified particles mL⁻¹), to see how the hydrodynamic diameter was affected, thus indicating the colloidal stability in the respected media.¹⁵² As seen in Figure 3.12, there was no significant change in hydrodynamic diameter observed when the particles were put in ionic and protein rich environments.

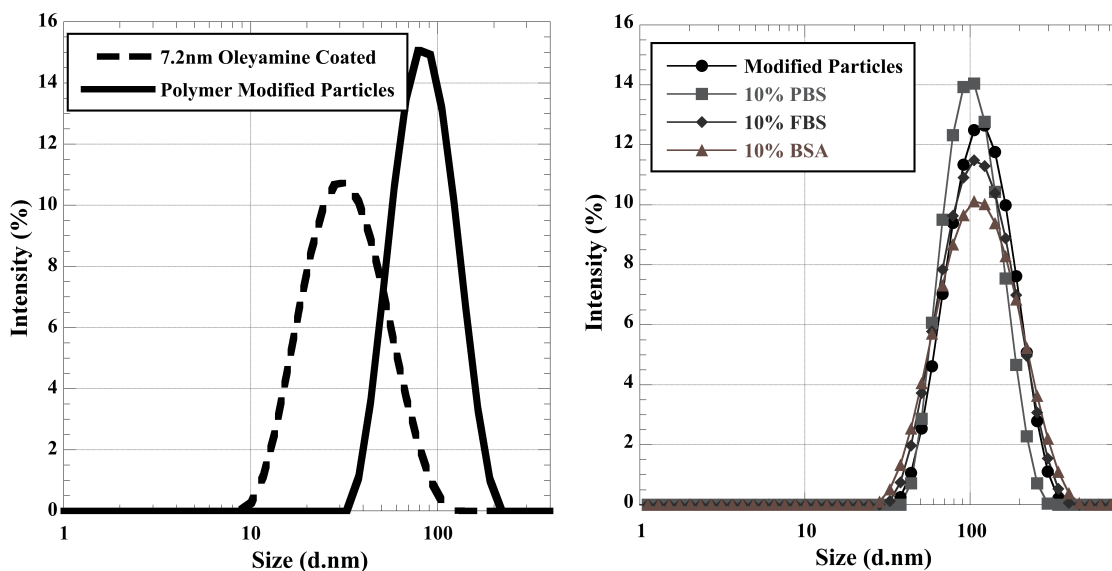


Figure 3.12. (Left) Hydrodynamic diameter by intensity of magnetic nanoparticles before and after modification with alkyne-PEO-nitroDOPA; size data chart available (Right) Hydrodynamic diameter by intensity of the particles titrated with PBS, FBS, and BSA.

Now that this polymer-particle complex has been successfully synthesized and characterized in simulated biological environments, the functional surface can be modified for biomedical targeting and imaging applications. Fluorescein-azide, Figure 3.13 (B), was then “clicked” in using a Huisgen 1,3-dipolar cycloaddition between the alkyne of the particle surface and the azide of the fluorescent dye molecule, using copper (II) sulfate and sodium ascorbate to drive the reaction.¹⁵³ These particles were dialyzed for 3 days in the absence of light to ensure removal of excess dye, catalyst and byproducts. The photoluminescence spectrum (Figure 3.14) shows a maximum emission at 517 nm for the particles modified with fluorescein and no visible emission for the particles before modification.

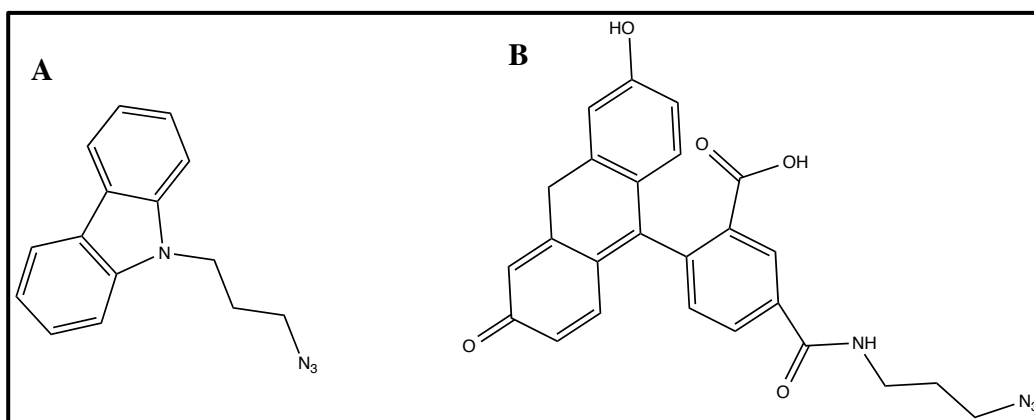


Figure 3.13. Schematic of azide modified dyes used to modify magnetic nanoparticles using “click chemistry.” A) carbazole modified with an azide and B) fluorescein modified with an azide.

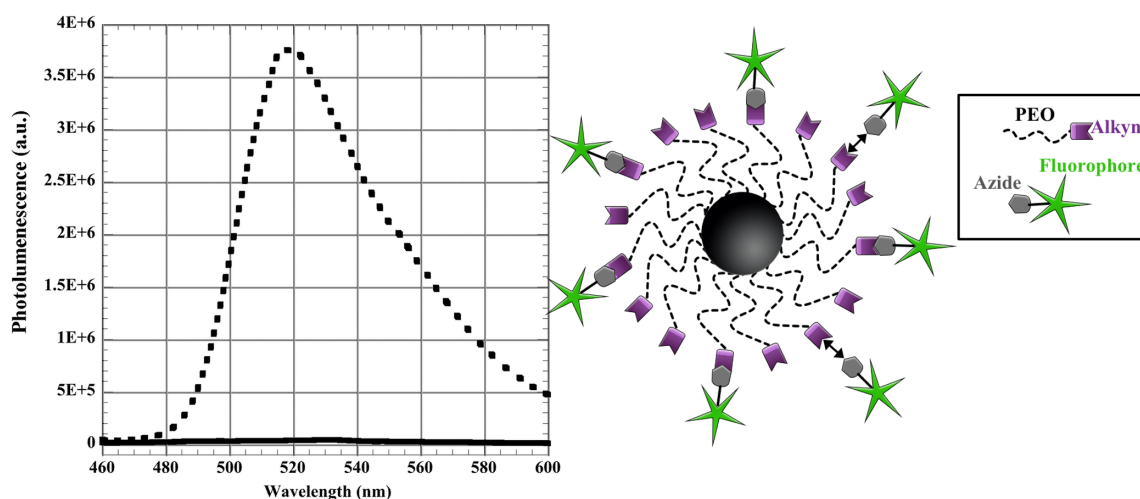


Figure 3.14. Image on the left shows a photoluminescence spectrum of particles before and after functionalization with fluorescein. Image on the right represents the final construction of magnetic nanoparticle with functional surface modified with a fluorophore.

To demonstrate the versatility of the alkyne surface, the particles were then modified with equimolar amounts of carbazole and fluorescein dye, Figure 3.13 (A) and (B) respectively. These two dyes were chosen because their emissions are at different wavelengths, carbazole at 350 and 366 nm¹⁵⁴ and fluorescein at 515 nm.¹⁵⁵ After the

particles were modified, dialysis against water was done for 3 days to ensure excess dye and catalyst was sufficiently removed. Photoluminescence was then used to conform the modification of the particles by first exciting at 290 nm to yield a broad emission peaks at 348 and 363 nm, Figure 3.15 (A). The same sample was then excited at 400 nm and an emission was observed at 417 nm, Figure 3.15 (B).

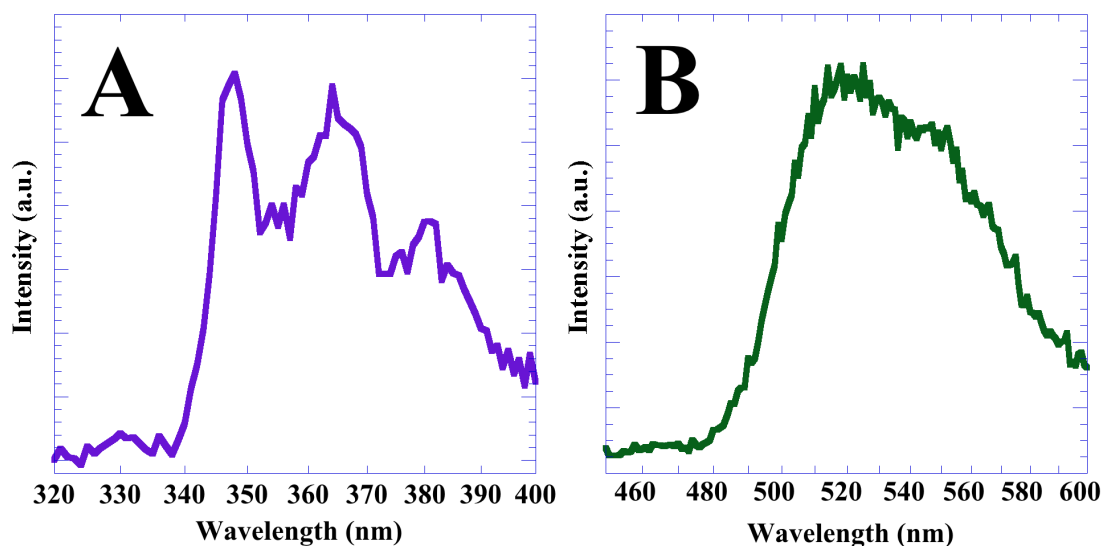


Figure 3.15. Photoluminescence of mono-anchored nanoparticles after modification with A) carbazole dye (348 and 363 nm) and B) fluorescein dye (417 nm).

3.5. CONCLUSIONS

The design and synthesis of this specialty heterobifunctional PEO provides a great platform for biomedical magnetic nanoparticle research. This uncomplicated synthesis of such a specialized material lends itself to the production of biologically stable nanoparticles with an alkyne surface that provides a customizable scaffold for a variety of biomedical applications.

Synthesis of a unique heterobifunctional PEO was accomplished by ring opening polymerization of EO using a protected initiator and sub-sequential end group modifications with relative ease. This polymer is equipped with robust anchoring to magnetite via a catechol, biological stability via PEO, and a functional surface via an alkyne. Confirmed by DLS, the once water-insoluble magnetite nanoparticles, were stabilized in water. These functionalized particles are now capable of carrying a variety targeting and imaging agents, through “click chemistry,” which is represented in the drawing in Figure 1.4. The accessibility of the surface functionality was demonstrated by adding an azido-functionalized fluorescein that was detected using photoluminescence, at a wavelength of 517 nm. The ability to add multiple functional moieties of the surface was also displayed using two different dyes (carbazole and fluorescein) that emit at different wavelengths that could easily be characterized by photoluminescence. The development of this polymer-particle complex allows for a biologically stable platform to easily and efficiently build biomedical devices for use in any theranostic application.

CHAPTER 4. SYNTHESIS AND CHARACTERIZATION OF MULTI-ANCHORED HETEROBIFUNCTIONAL POLY(ETHYLENE OXIDE) FOR ENHANCED STABILITY AND FUNCTIONALITY OF MAGNETIC NANOPARTICLES

4.1. ABSTRACT

The research and development of surface coatings for magnetic nanoparticles is important for improving colloid stability of these particles in biological conditions. For efficient delivery of the magnetic nanoparticles, they must remain stable for long enough in the harsh environment of the body to get sufficient concentration to the infected area. Improved stability can be accomplished by increasing the number of interactions between the surface coating and the magnetic nanoparticles to decrease the interactions of proteins that can interfere with colloidal stability. This chapter discusses the synthesis of a heterobifunctional polyethylene oxide (PEO), with an amine on one end and an alkyne on the other, which is chemically attached to polyacrylic acid (PAA) and subsequently modified with nitroDOPA to provide multiple anchoring groups per PEO chain. Improved stability was not only observed, by comparing it to a mono-anchored PEO in extreme ionic and protein rich environments, but there is an alkyne surface on the particle that can be modified, in water, with azide-functionalized moieties using “click chemistry.”

4.2. INTRODUCTION

Functional magnetic nanoparticles have become an important research focus for use in biomedical applications. These applications include magnetic hyperthermia,^{2,156} magnetic resonance imaging,^{20,21} and cell separation.^{22,23} The small size and manipulation of magnetic properties of these materials also have potential for non-invasive diagnostics and treatments to improve quality of life for patients.

There are a variety of ways to create functional magnetic nanoparticles, but the fundamental designs of these materials stay the same. Generally, in each individual nanoparticle, the core material is magnetic and is coated with a water-soluble material that is either physically or chemically adsorbed on to the surface. The core can be made up of an assortment of magnetic materials, including iron platinum, cobalt oxide, and iron oxides.¹³⁹ Because these materials are synthesized using thermal decomposition methods, they have hydrophobic ligands that are only dispersible in organic solvents. They must be modified with hydrophilic materials for biomedical applications. There are a variety of hydrophilic surface designs that have been researched to create magnetic nanoparticles suspended in water, including dextran, pluronics, and polyethylene oxide (PEO).¹³⁹

Magnetic nanoparticles for biomedical applications, like any pharmaceutical drug, have power in numbers. The ultimate goal is to have a high accumulation in the affected area without using high dosages that may affect the patient negatively. This can be accomplished in magnetic nanoparticle composites by designing ligands that increases the lifetime of the particles in the body,¹³¹ as well as taking advantage of the particles' surface¹³⁹ to target certain cells by exploiting over expressed receptors.

To improve circulation of the material in the body, nanoparticles must be protected from nonspecific reactions from proteins in the biological environment. Using ligands with multiple anchoring groups has been reported for stabilizing quantum dots¹⁵⁷ and gold nanoparticles¹⁵⁸ in biological conditions. Bagaria et al. found that grafting a sulfonated block copolymer onto the surface of 2-aminopropyl triethoxy silane (APTES) modified magnetic nanoparticles provided colloidal stability in brine solutions at 90 °C

over 30 days. They report this was due to the multiple grafting points provided by the number of sulfonated groups along the polymer chain to the APTES on the nanoparticle surface.^{159,160} Dr. Riffle's research group at Virginia Tech synthesized a heterobifunctional PEO with a functional anchoring group comprised of three phosphonate zwitterions. They were able to produce extended colloidal stability in phosphate buffer saline (PBS) over 24 hours, which was not seen in heterobifunctional PEO modified with a single phosphonate zwitterions.¹⁶¹ Ligands with multiple robust anchoring groups, i.e. catechols, for iron oxide nanoparticles have also shown improved colloidal stability.¹⁶² In fact, Saville et al. reported that increasing the number of nitroDOPA groups, from one to three, per PEO chain increases the colloidal stability of the magnetic nanoparticles in protein rich environments significantly.¹³¹

Designing ligands for biological targeting imaging applications can be exhaustive and the reactions can be inefficient. The synthesis of these ligands generally requires harsh solvents that must be completely removed before any biological interaction. "Click chemistry" was designed to bring two groups together to create a strong and stable linkage. Originally developed for facile protein modification, it was later used to efficiently modify polymers. The most common of the "click reactions" is the Huisgen 1,3-dipolar cycloaddition between an alkyne and an azide. Na et al. have demonstrated this by modifying polyacrylic acid (PAA) with methyl-terminated and azide-terminated PEO, using multiple catechols (~6) to provide enhanced stability at different pH and salt concentrations. The particles also provided surface functionality through the azide that was reacted with alkyne-modified rhodamine B using "click chemistry."¹⁶³

Reported is the synthesis and characterization of a magnetic nanoparticle composite comprised of an iron oxide core and a functional polyethylene oxide (PEO) scaffold with enhanced stability in biological environments that can be tailored for a variety of biomedical applications using “click chemistry.” The scaffolding was created by first linking a specially designed heterobifunctional PEO to PAA and then modifying the newly formed brush with nitroDOPA for anchoring to the magnetic nanoparticle surface. To illustrate the enhanced stability of the aforementioned particle, it was submitted to a variety of simulated biological environments at body temperature and compared to a mono-anchored particle of similar size and composition. The multi-anchored particles were also modified with different functional moieties to exhibit the flexibility and customization of the surface for a variety of theranostic applications.

4.3. EXPERIMENTAL

4.3.4. Modification of Protected amine-PEO with alkyne

The procedure used is based on previous work done by Kim et al.¹¹⁶ Protected Amine-PEO-OH(2.0 g, 0.33 mmol) and sodium hydride (32 mg, 1.32 mmol) was charged to a 100 mL round bottom flask equipped with a stir bar. The flask was sealed with a septum and purged with nitrogen for 30 seconds. THF (40 mL) was added via syringe and the reaction was brought to 0 °C using an ice bath. Propargyl bromide (0.15 g, 1.32 mmol) was slowly added via syringe over 30 minutes. All the reactants were left to stir for another 30 minutes at 0 °C. The flask was then removed from the ice bath and brought to room temperature to react for 24 hours. The final solution was filtered to remove excess sodium hydride and precipitated with DEE twice to collect polymer.

$^1\text{HNMR}$ (300 MHz, CDCl_3), δ (ppm): 3.56 (m, $\text{CH}_2\text{-CH}_2\text{-O}$), 2.43 (s, $-\text{O-CH}_2\text{-C}\equiv\text{CH}$), 4.19 (s, $-\text{O-CH}_2\text{-C}\equiv\text{CH}$), 2.75 (m, $(\text{TMS})_2\text{-N-CH}_2\text{-}$) 1.19 (m, TMS).

4.3.5. Deprotection of amine-PEO-alkyne

The deprotection of the amine was accomplished by dissolving the polymer (1.8 g, 0.30 mmol) into methanol and then slowly adding 20 drops of a 1 M HCl solution and stirring over night under a nitrogen head. The product was precipitated with DEE (2x) and the solid was collected. The cleavage of the bis(trimethylsilyl) (BTMS) group was confirmed by $^1\text{HNMR}$.

$^1\text{HNMR}$ (300 MHz, CDCl_3), δ (ppm): 3.65 (m, $\text{CH}_2\text{-CH}_2\text{-O}$), 2.44 (s, $-\text{O-CH}_2\text{-C}\equiv\text{CH}$), 4.19 (s, $-\text{O-CH}_2\text{-C}\equiv\text{CH}$)

4.3.6. Modification of poly(acrylic acid) with amine-PEO-alkyne

In a 100 mL round bottom flask equipped with a stir bar and condenser, amine-PEO-alkyne (0.8 g, 0.14 mmol) was dissolved in 40 mL of THF and brought to 0 °C. DCC (0.03 g, 0.14 mmol) was then added and stirred for 30 minutes under constant nitrogen purge. Finally PAA (0.05 g, 0.03 mmol) and DMAP (0.003 g, 0.03 mmol) was added and brought to reflux at 70 °C for 2 days. After two days, the solution was filtered to remove any undissolved reactants and precipitated with DEE. The polymer was then dissolved in DCM and precipitated with DEE (2X) and the final solid was characterized by $^1\text{HNMR}$.

$^1\text{HNMR}$ (300 MHz, CDCl_3), δ (ppm): 3.56 (m, $\text{CH}_2\text{-CH}_2\text{-O}$), 2.43 (s, $-\text{O-CH}_2\text{-C}\equiv\text{CH}$), 4.20 (s, $-\text{O-CH}_2\text{-C}\equiv\text{CH}$), (b, 1.20-2.25, PAA)

4.3.7. Modification of PAA-PEO-alkyne with NitroDOPA

To a 100 mL flame dried, round bottom flask equipped with a stir bar, PAA-PEO-alkyne (0.4 g, 0.0015 mmol) was dissolved in DMF and brought to 0 °C using an ice bath. EDC (0.002 g, 0.013 mmol) and TEA (2.0 μ L, 0.015 mmol) were both added while purging with nitrogen and stirred at 0 °C for 30 minutes. The final reactants, nitroDOPA (3.0 mg, 0.012 mmol) and DMAP (0.3 mg, 0.003 mmol), were added under a constant nitrogen purge and stirred for another 30 minutes. Finally, the reaction was removed from the ice bath and brought to 80 °C for 5 days. The purification was accomplished by bringing the reaction to room temperature and filtering out any solids. The polymer was then precipitated with DEE and the solid was dissolved in chloroform. Vacuum filtration was then used to remove any excess nitroDOPA. The filtrate was collected and polymer was collected by precipitation in DEE (2x). The polymer was then dissolved in DI water and dialyzed using 1000 g mol⁻¹ MWCO dialysis membrane. Product was confirmed by ¹HNMR and FTIR.

¹HNMR (300 MHz, CDCl₃), δ (ppm): 3.62 (m, $\underline{CH}_2\text{-}\underline{CH}_2\text{-O}$), 2.43 (s, $\text{-O-CH}_2\text{-C}\equiv\text{CH}$), 4.19 (s, $\text{-O-CH}_2\text{-C}\equiv\text{CH}$), (b, 1.20-2.25, PAA). nitroDOPA: 6.12 and 6.70 (s, CH in ring).

4.3.8. Modification of Magnetic Nanoparticles with Polymer

NitroDOPA-PAA-PEO-alkyne (0.2 g, 0.0007 mmol) was dissolved in 10 mL of chloroform. 7.2 nm particles in hexane (1 mL, 2 mg of Fe₃O₄ mL⁻¹) were slowly added over 30 minutes while using sonication. Once all the particles were added, the solution was stirred overnight. The particles were then precipitated with hexane and dispersed in 5

mL of ethanol to dissolve any of the displaced oleylamine and precipitated with hexane to collect the polymer-modified particles. The particles were then dispersed in DI water and dialyzed for 2 days.

4.3.9. Cell Viability Studies

Materials used for cell viability were as follows: 96 well plate was purchased from BD biosciences, CCD18-Co cells, L929 cells (ATCC[®] CCL-1[™]) and EMEM (30-2003[™]) were purchased from ATCC and used as received, phosphate buffer solution from Sigma Aldrich was autoclaved prior to usage, trypsin-EDTA (25-053-CI) and trypsin Blue (25900-CI) were purchased from Cellgro and used as received.

The cytotoxicity of the modified magnetic nanoparticles particles was done by adding 200 μ l of L929 cells (4.5×10^5 cells per well)/ CCD18-Co (2×10^4 cells per well) into a two 96 well plate and incubated for 24 hours at 37 °C, 5% CO₂ atmosphere. The particles were then plated, in quadruplicate by adding 1, 2, 3, 4, 5, 6, 8 μ l and a control with no particles. One plate was incubated with particles for 24 hours and the other was incubated for 48 hours before analyzing. MTS assays were performed using a modified protocol suggested by Promega. The plates were washed with PBS twice followed by the addition 100 μ l of media before 20 μ l of CellTiter 96[®] AQueous One Solution Reagent was added to each well. The plates were then incubated at 37 °C at 5% CO₂ atmosphere for 4 hours before absorbance at 490 nm was read using 96-well plate reader.

4.3.10. Modification of particles with Azido-Cy5.5 Dye

To 10ml of DI water, 0.5 mL of modified particles (0.7 mg of modified particles mL⁻¹) was added. The azido-Cy5.5 (0.003 mmol) was added to solution followed by

CuSO₄ (0.013 mmol) and sodium ascorbate (0.003 mmol). The reaction was then covered with foil and stirred at 28 °C for 12 hours. The particles were then removed from heat and dialyzed for 3 days against DI water.

4.4. RESULTS AND DISCUSSION

A heterobifunctional PEO was synthesized using a combination of ring opening polymerization and end group modification, as portrayed in Figure 4.1. Using potassium bis(trimethylsilyl)amide solution has been used as an anionic initiator, to ring open ethylene oxide to produce PEO with a protected amine at one end and a free alcohol at the other.¹⁶⁴ NMR displayed methylene shifts of PEO at 3.56 ppm and the adjacent hydrogen to the protected amide group at 2.75 ppm. Using propargyl bromide in the presence of NaH, the free alcohol on the PEO was substituted with propargyl end group, indicated by peaks 2.43 and 4.19 ppm in the ¹HNMR. Then using a 1M HCl solution, the TMS that was protecting the amine was removed, which was seen from the absence of the shift at 1.19 ppm.

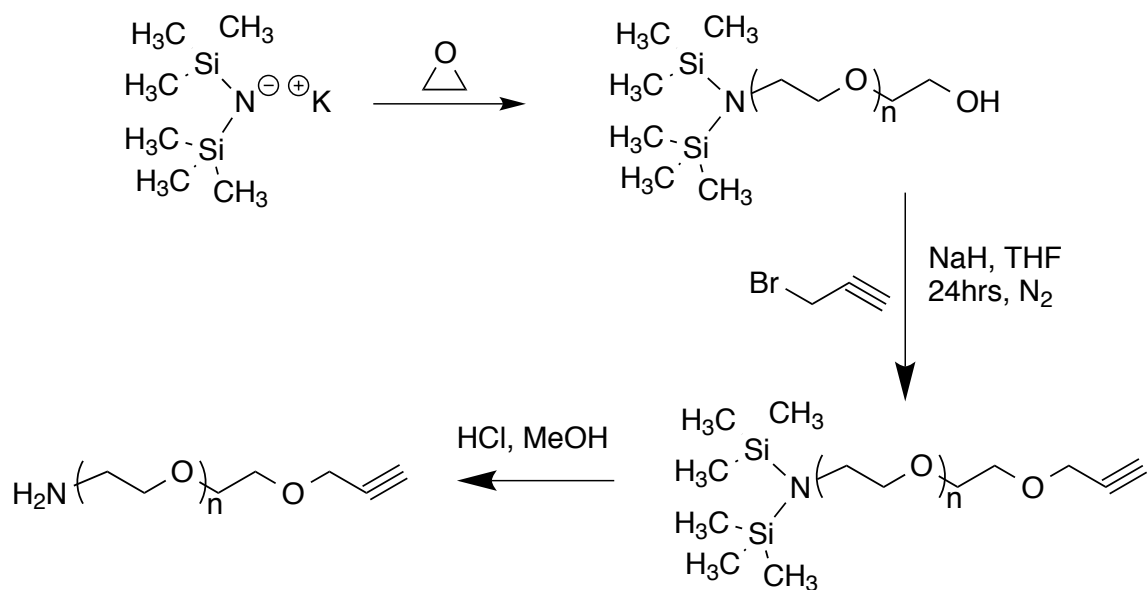


Figure 4.1. Schematic of synthesis and end group modification to yield heterobifunctional PEO (amine-PEO-alkyne)

The heterobifunctional PEO prepared was now primed to react with the carboxylic acids of PAA, as presented in Figure 4.2. Using DCC coupling, the amine-PEO-alkyne was reacted with the carboxylic acids of PAA, targeting a 5:1 ratio of PEO to PAA chain.¹⁶³ A broad peak at 1.20-2.25 ppm confirmed the presence of PAA after the reaction. The peaks of the propargyl end group were still present at 2.43 and 4.20 ppm. Using the ratio of integrals between the α hydrogen of the PAA (25H) and the single proton on the alkyne terminus of the PEO (1H) the grafting density on the PAA was found to be approximately 6 chains of PEO per PAA. The FTIR spectrum in Figure 4.3 also confirms the presence of the alkyne at 3237 cm^{-1} , the carboxyl stretch at 1648 cm^{-1} and the amide stretch at 1531 cm^{-1} .

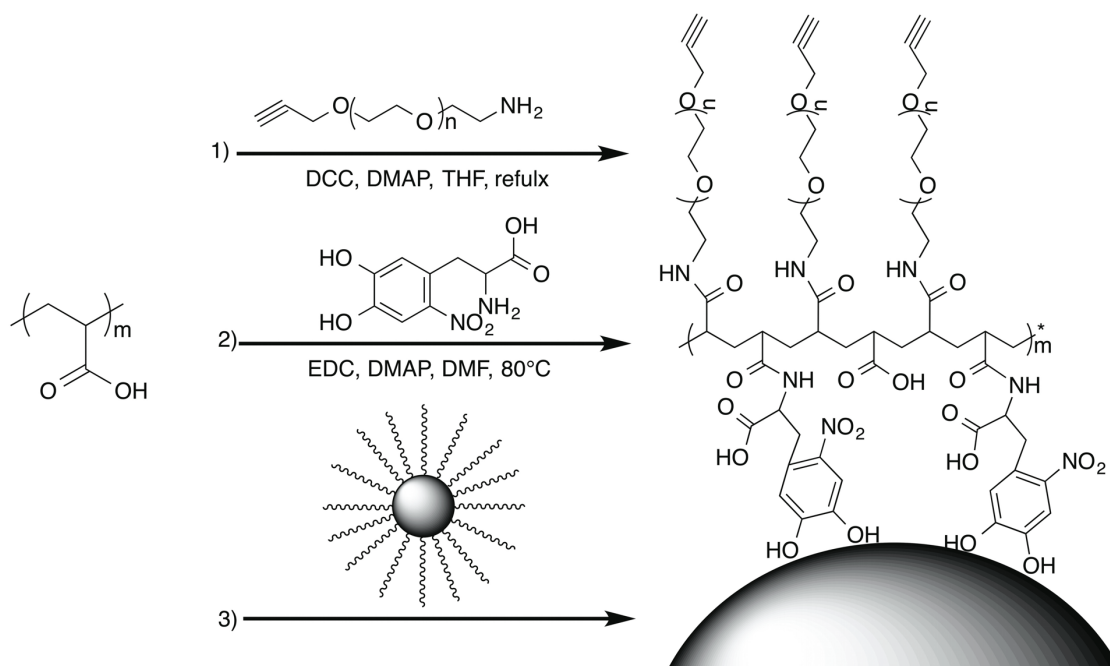


Figure 4.2. Schematic of step taken to synthesize multi-anchored particles. 1) Modification of PAA with amine-PEO-alkyne. 2) Modification of PAA-PEO-alkyne with nitroDOPA. 3) Particle modification with multi-anchored particles

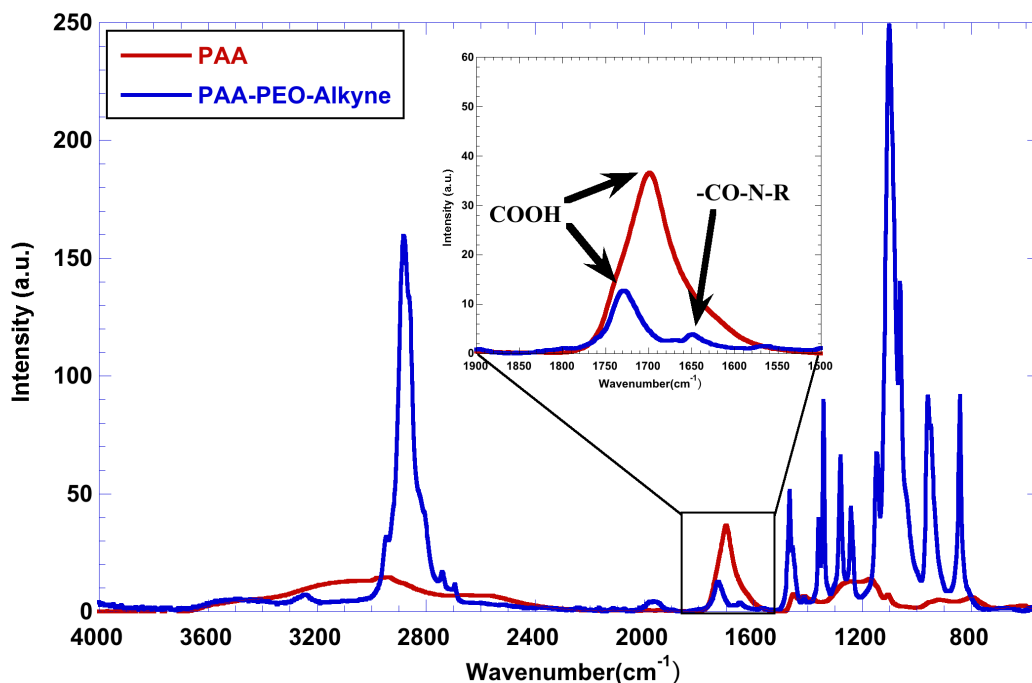


Figure 4.3. FTIR spectra of PAA (red) and PAA-PEO-alkyne (blue). Peak at 1728 cm^{-1} is attributed to carboxyl from PAA, and the peaks at 1648 and 1531 cm^{-1} are attributed to the carboxyl amide bond between amine-PEO-alkyne.

Using EDC coupling, PAA-PEO-alkyne was modified with nitroDOPA, in a 10:1 ratio. An excess of nitroDOPA was used to ensure there is increased anchoring when modifying the iron oxide nanoparticles. NitroDOPA-PAA-PEO-alkyne, after purification, was immediately dissolved in chloroform and used in the modification of nanoparticles. Using sonication while slowly adding particles to the polymer solution helps facilitate the ligand exchange and ensure maximum surface coverage. The transfer of particles to water was a good indication of a successful modification. Using DLS and TEM, surface modification was confirmed by an increase in hydrodynamic radius and polymer halo around the dense magnetic nanoparticle, Figure 4.4. The surface coverage of polymer on

the particle was determined by TGA, Figure 4.5. There was an 81.3% weight loss, from 372 °C to 415 °C, from the nitroDOPA-PAA-PEO-Alkyne (9.49 mg).

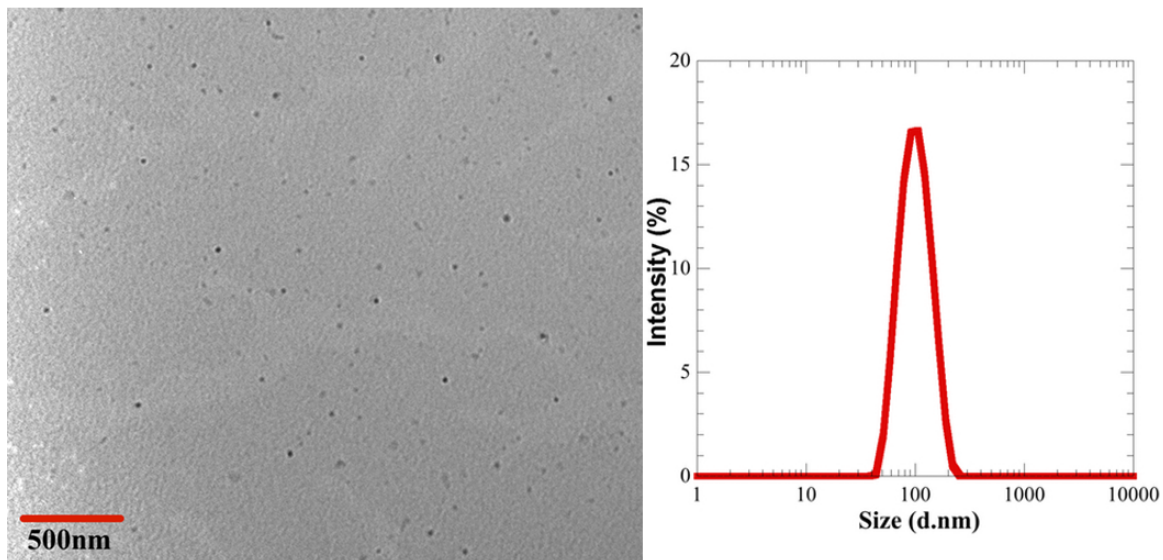


Figure 4.4. TEM micrograph (left) of multi-anchored particles and DLS (right) of the modified particles in DI water.

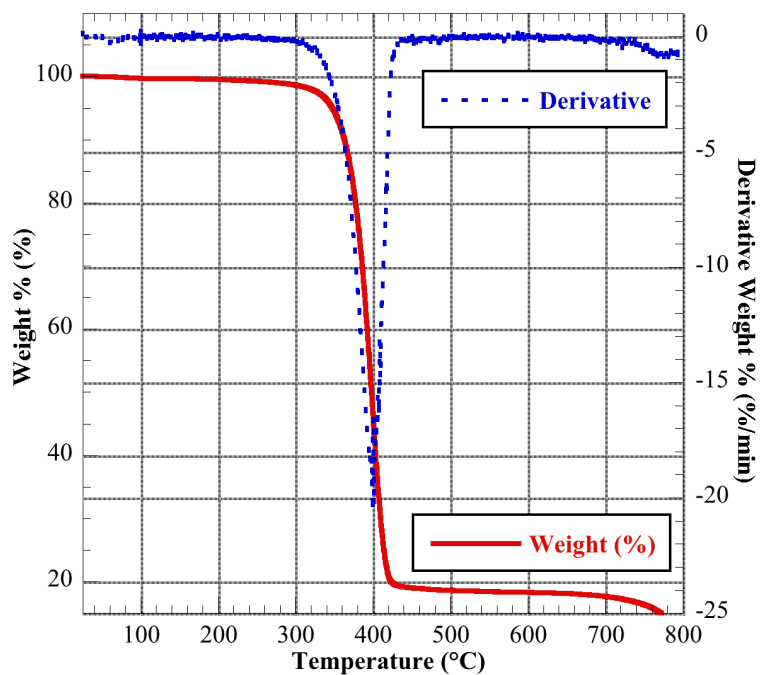


Figure 4.5. TGA thermogram of multi-anchored magnetic nanoparticles, 81.3% weight loss.

The particles were analyzed with FTIR to corroborate the DLS and make sure it had the desired surface functionality. As seen in Figure 4.6, the peak at 3237 cm^{-1} confirms the presence of the alkyne¹⁶⁵ as well as the presence of carboxylic acids from PAA (1711 cm^{-1}) and amide linkages (1643 and 1561 cm^{-1}) from the nitroDOPA and/or PEO to the PAA.

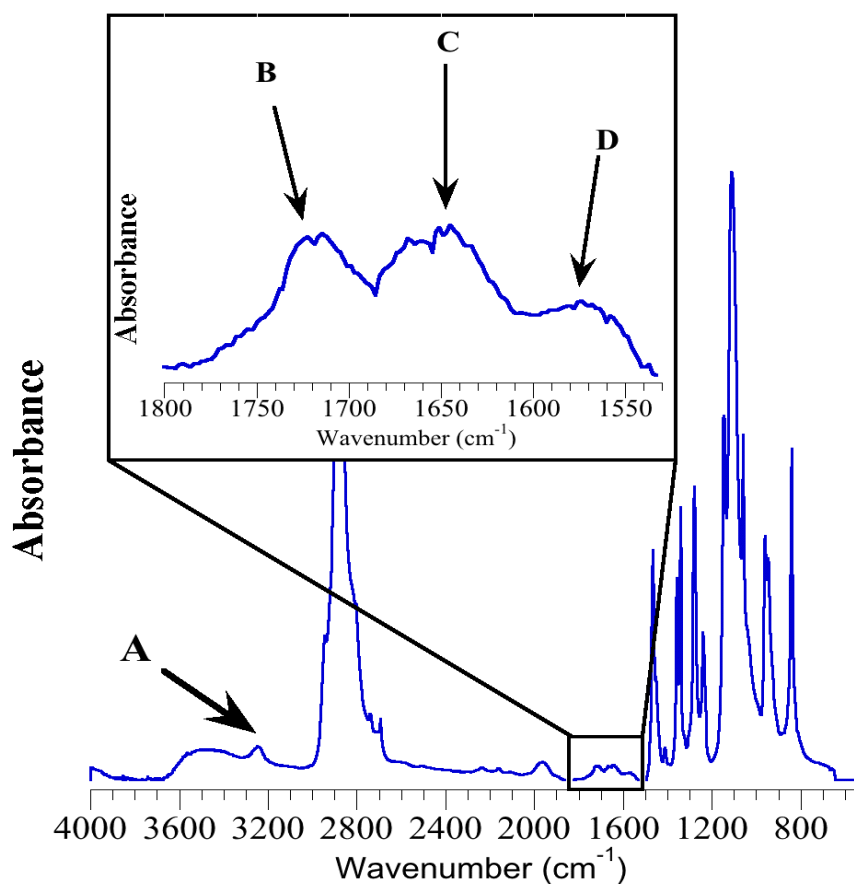


Figure 4.6. FTIR spectrum of multi-anchored particles. A) Alkyne group on the surface of the particle. B) Carbonyl stretching of PAA (1711 cm⁻¹). C and D) Amide-carbonyl stretch (1643 and 1561 cm⁻¹) indicating modification of PAA.

The particles were then subjected to a series of biological simulations to establish if the multi-anchoring enhances the stability compared to mono-anchored modified particles, which are previously reported. PBS is a buffer solution that matches the ionic strength of the human body and is commonly used in biological research. Each particles solution (0.1 mg/mL) was titrated with 10, 30, 50 and 100% by volume of 1 N PBS solution and the hydrodynamic diameter was observed using DLS. The results shown in Figure 4.7 show the enhanced stability of the multi-anchored particles compared to the

mono-anchored. At 100% by volume of PBS with the mono-anchored particles there is an obvious decrease in original particles size and the formation of large clusters greater than 1000 nm. No visible effect on size was observed for the multi-anchored particles.

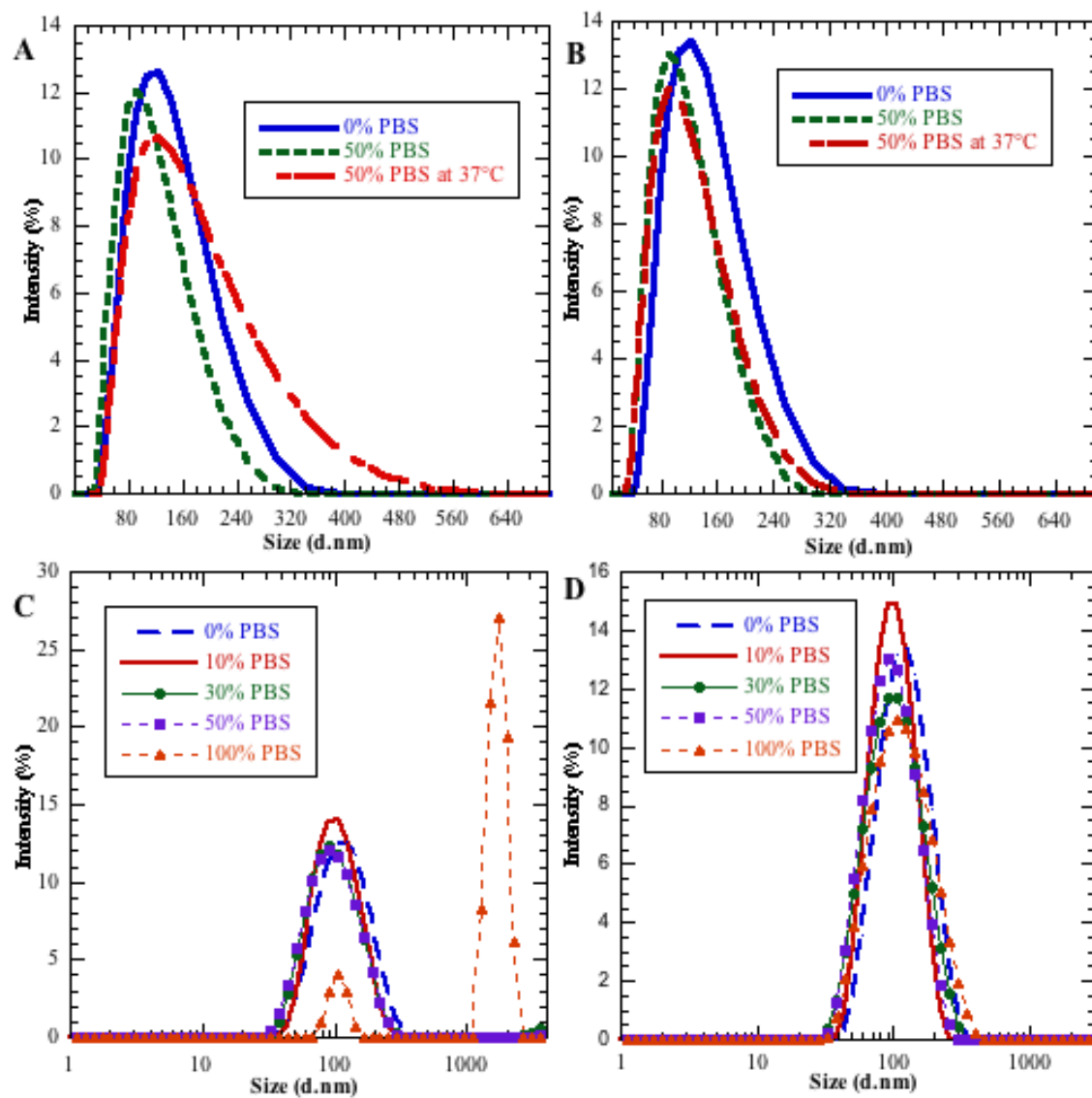


Figure 4.7. Stability studies comparing mono and multi-anchored particles. A) DLS of mono-functional particles in 50% by volume PBS at 37 °C; B) DLS of multi-functional particles in 50% by volume PBS at 37 °C; C) DLS of mono-anchored particles titrated with PBS from 0-100% by volume; D) DLS of multi-anchored particles titrated with PBS from 0-100% by volume;

The human body operates at temperatures greater than room temperature, so using DLS, the hydrodynamic diameter of the particles was measured in a 50% by volume of PBS (1N) at the average human body temperature, 37 °C, for 5 minutes. In Figure 4.7, the multi-anchored particles show no change in hydrodynamic diameter in this simulated environment. The mono-anchored size distribution, although stable in the same ionic environment, broadens with an increase in temperature. The multiple nitroDOPA groups increase the amount of interactions with the surface of the iron oxide nanoparticles keeping the steric interactions intact that are involved in keeping the particles discrete and stable.¹³¹

Table 4.1 Presents the results of the time dependence studies done in a 50% FBS in magnetic nanoparticles solution (v/v).

	Mono-anchored (d.nm)	Multi-anchored (d.nm)
DI Water	118.90	105.71
50% FBS	121.00	100.79
50% FBS at 70 °C	122.40	107.80
50% FBS over 24hrs*	203.65±30.14	95.73±21.85

*average hydrodynamic diameter over 24 hours; measurements taken every 12 minutes

Time dependence studies, Table 4.1 were done in FBS, fetal bovine serum, on both the mono and multi-anchored particles to see how their stability compares to each other in a high temperature, protein rich environment. One milliliter of each particle system, each with a concentration of about 1 mg of multi-anchored particles mL⁻¹ in DI water, was added to a cuvette and 500 µL of FBS (0.125m mg of hemoglobin) was titrated into the cuvette and vortexed for 20 seconds. The particles were first measured at room temperature and the mono-anchored particles had approximately a 3nm increase in diameter. The multi-anchored particles had a slight decrease in hydrodynamic diameter of

about 5 nm. The hydrodynamic diameter of the particles was measured at 70 °C and only a slight increase in particles size was observed; 1.4 nm for the mono-anchored and 7.1 nm for the multi-anchored. The samples were then measured again at 70 °C every 12 minutes for 24 hours. The mono-anchored particles' average hydrodynamic diameter over the 24 hours almost doubled in size from 122.4 nm to 203.56 nm. The size increase is indicative of clustering that can occur when ligands are displaced by proteins in the environment, decreasing the steric hindrance. This phenomenon was not observed for the multi-anchored particles, the average size over 24 hours was measured to be 95.73 nm. Statistical analysis, using one way ANOVA, showed there was a statistically significant difference between the average sizes measured for the mono and multi-anchored particles ($p < 0.0001$, $n = 108$). This data shows how crucial multiple anchoring groups are for stability in harsh biological environments.

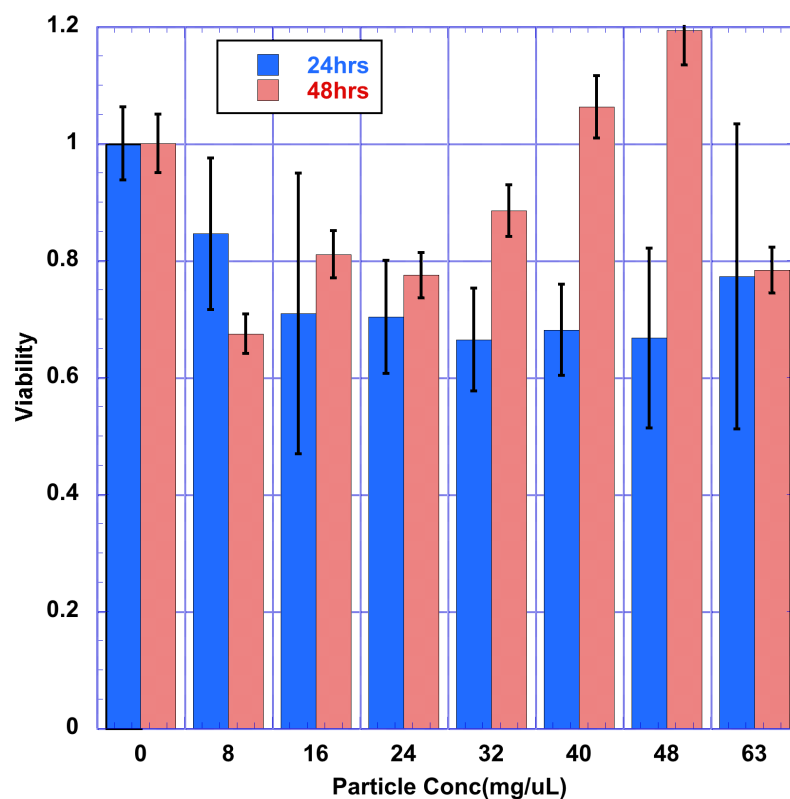


Figure 4.8. Cell viability of L929 cells after exposure with multi-anchored particles for 24 and 48 hours at different concentration of iron. (mean \pm standard dev.; n=3)

When synthesizing materials for biomedical applications, evaluating of its toxicity is very important.^{166,167} An MTS assay was done on the multi-anchored particles to determine if there is a negative cytotoxic effect. MTS assay utilizes (3-[4,5-dimethylthiazol-2-yl]-2,5 diphenyl tetrazolium bromide) dye that is processed into formazan by living cells that has an absorbance at 490nm that can be quantified.¹⁶⁸ The viability is determined by counting the live cells incubated with the particles and comparing them to the number of proliferated cells in the control, cells that have not been exposed to the multi-anchored magnetic nanoparticles. L929 mouse fibroblast cells are used in many publications to test the cytotoxicity of magnetic nanomaterials.¹⁶⁹⁻¹⁷³

Figure 4.8 shows the cell viability results of incubated multi-anchored particles over 24 and 48 hours at different concentrations of iron in media with L929 cells, ranging from 8 to 63 mg mL⁻¹ and MTS assay was done to quantify the live cells. The particles that were incubated for 24 hours showed a decrease in viability compared to the control, of approximately 25% on average, for all concentrations. Statistical analysis using a one-way ANOVA showed that there was no statistically significance difference between the mean of the control and all the concentrations tested ($p=0.18$). This indicates that there is no significant effect of concentration on the cytotoxicity of the multi-anchored magnetic nanoparticles. The L929 cells were also exposed to the multi-anchored nanoparticles for 48 hours to see if there may be a time dependence toxicity that could not be seen in the 24 hours study. Statistically, ANOVA analysis showed that there was no statistically significant difference between the means of the control and the different concentrations over 48 hours ($p=0.42$). In fact, cell growth was observed after 48 hours of incubation. Below, in Figure 4.9, micrographs of the L929 cells with different concentrations of multi-anchored nanoparticles were taken after 24 hours of treatment. In Figure 4.9, optical micrographs of the cells showing the control and the cells incubated with 63 mg mL⁻¹ of Fe₃O₄ nanoparticles particles after 24 hours. Healthy cells, circled in green in Figure 4.9 (A), are extended and attached to the bottom of the cell well plate. Dead cells are detached from the cell well plate and ball up; an example of a dead cell is circled with a red circle in Figure 4.9 (B). Optical micrographs of the cells after incubated for 48 hours are displayed in Figure 4.10 to show there was no visible difference between the control and cells exposed to 63 mg mL⁻¹ Fe₃O₄ nanoparticles.

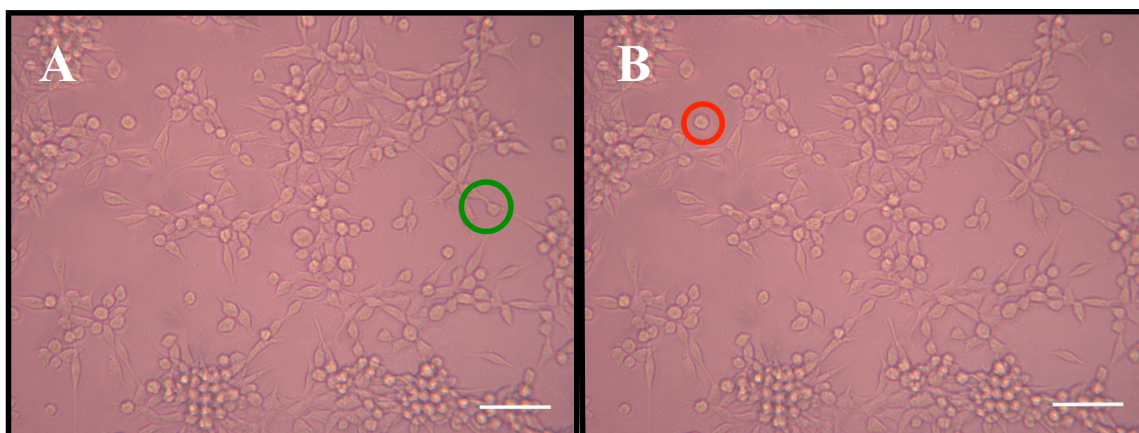


Figure 4.9. Micrographs of cells incubated with multi-anchored magnetic nanoparticles after 24 hours. A) Control, B) 63 mg of $\text{Fe}_3\text{O}_4 \text{ mL}^{-1}$, respectively. All scale bars are 100 micrometers. Green circle shows an example of a living cell and red circle shows a dead cell.

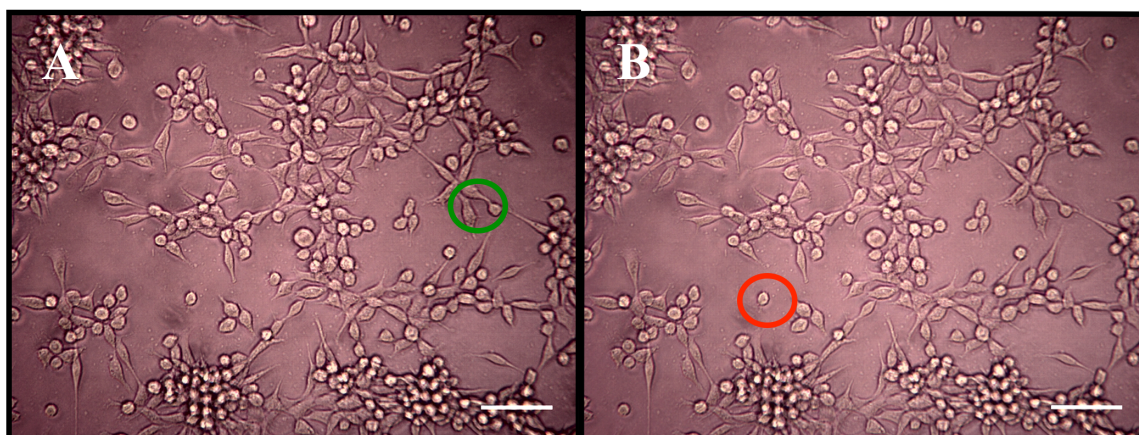


Figure 4.10. Micrographs of cells incubated with multi-anchored magnetic nanoparticles after 48 hours. A) Control, B) 63 mg of $\text{Fe}_3\text{O}_4 \text{ mL}^{-1}$, respectively. All scale bars are 100 micrometers. All scale bars are 100 micrometers. Green circle shows an example of a living cell and red circle shows a dead cell.

To demonstrate the availability of the surface to be functionalized with an azido-conjugated molecule, an azido-Cy5.5 was “clicked” on to the surface of the polymer-magnetic nanoparticle complex in water at 28 °C for 12 hours in the absence of light. Sodium ascorbate was used to reduce copper (II) sulfate in solution to catalyze the

reaction and yield the 1,4 conformation of the 1,2,3, triazole.¹⁰⁹ Cy5.5 is an example of a near infrared (NIR) dye that has an emission range of (700-1000 nm).¹⁷⁴ After dialysis for 3 days, the modified particles were analyzed using photoluminescence by exciting at 650 nm and observing an emission peak at 705 nm, Figure 4.11. The multi-anchored particles, not modified with Cy5.5, were also excited at the same wavelength, but no emission was observed. A NIR dye was chosen to modify the particles because it can easily be detected with photoluminescence and it shows that these particles can be modified with a molecule that is used.

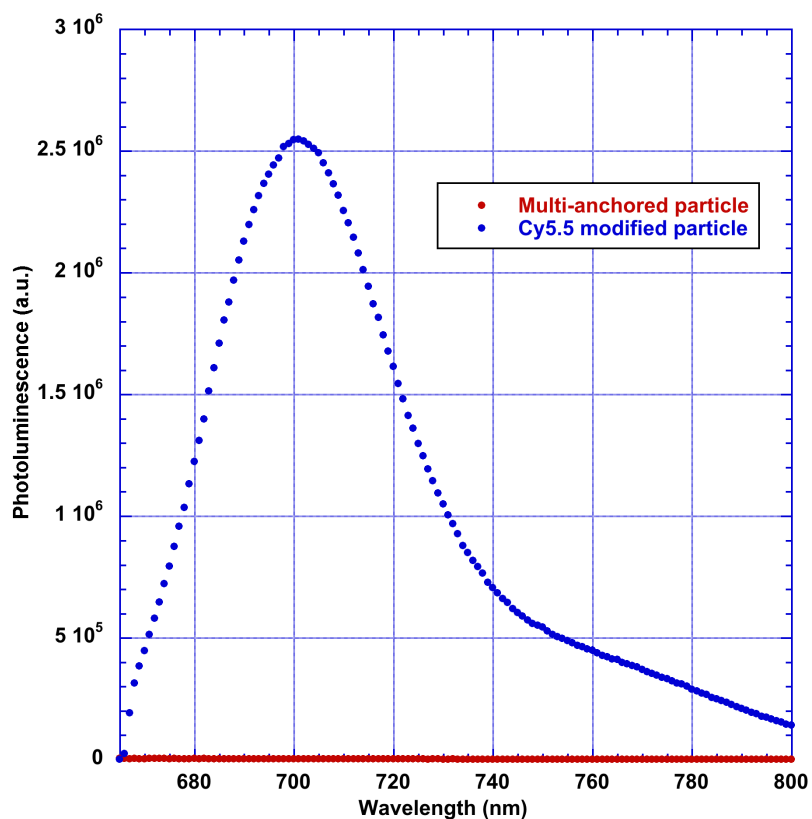


Figure 4.11. Photoluminescence of multi-anchored particles before and after being modified with Cy5.5 using “click chemistry.”

4.5. CONCLUSIONS

The goal of this work was to produce a PEO ligand to improve the stability of magnetic nanoparticles for biomedical applications. This was accomplished by using poly(acrylic acid) as the spine to hold multiple anchoring groups per PEO chain. Using anionic polymerization of ethylene oxide, initiated by potassium bis(trimethylsilyl)amide solution, and end group modification a heterobifunctional PEO was synthesized with an alkyne on one end that can easily be functionalized using “click chemistry” and an amine that could be reacted with the carboxylic pendants of poly(acrylic acid). The use of nitroDOPA gave a stable anchor to the iron oxide surface. Increased stability in extreme biological environments was demonstrated by comparing it to mono-anchored particles of a similar nature in ionic and protein rich solutions. Not only is this polymer-magnetic nanoparticle complex stable in harsh biological environments, but toxicity studies on these particles show statistically insignificant decrease in viability as a function of concentration and incubation time, up to 48 hours. The functionality of the surface incorporated in the design of this stabilizing ligand was displayed by successfully modifying with a near-IR dye (Cy5.5), commonly used for biological imaging, by “click chemistry.”

CHAPTER 5. VERSATILITY OF A MULTI-ANCHORED HETEROBIFUNCTIONAL POLY(ETHYLENE OXIDE) MODIFIED MAGNETIC NANOPARTICLES

INTRODUCTION

When designing the polymer-magnetic nanoparticle complex described in Chapters 3 and 4, the initial application in mind was targeted magnetic hyperthermia for the treatment of cancer. When discussions arose with different research groups in fields of biology and bioengineering, the desire for magnetic nanoparticles suspended in aqueous media that can be tailored to their specific applications was a problem they were not equipped to solve. The particles synthesized in the aforementioned in Chapters 3 and 4, originally designed for targeted magnetic hyperthermia of cancer, were now needed for other studies, Figure 5.1, involving alternative antibiotics,¹⁷⁵ effects of nanoparticles on biofilms,¹⁷⁶ and a new approach of thermostics for cancer early detection and treatment.¹⁷⁷

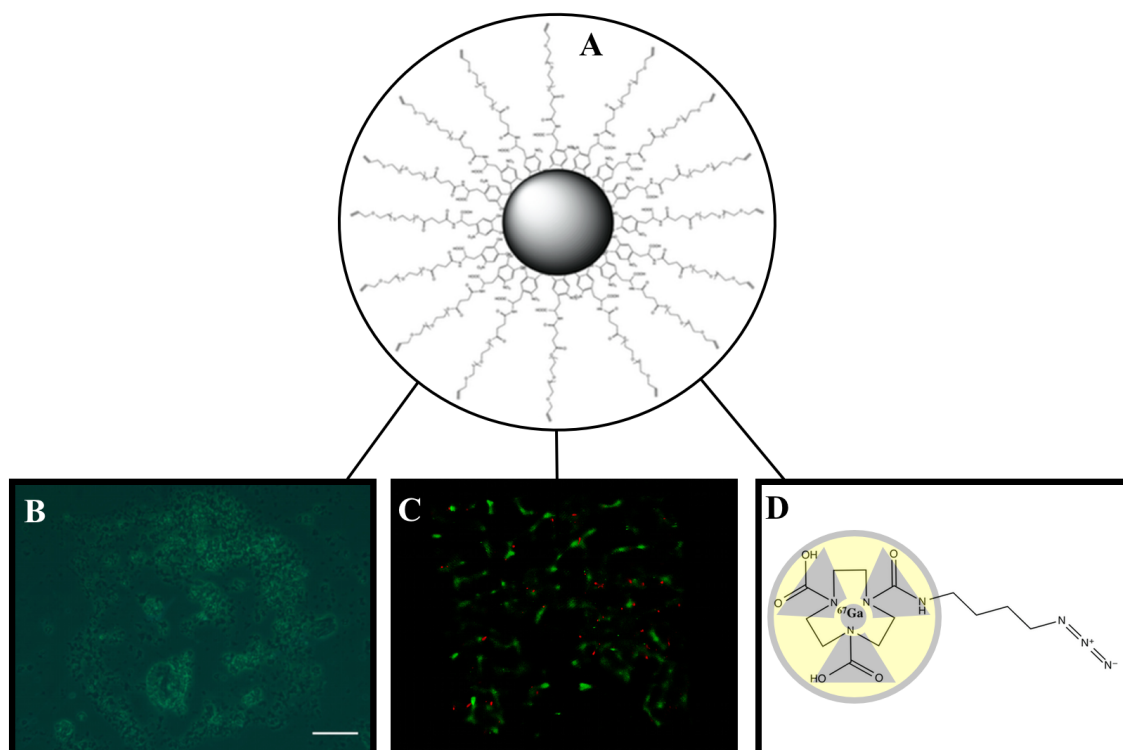


Figure 5.1. Schematic summarizing the flexibility of the heterobifunctional PEO scaffolding used to modify magnetic nanoparticles. A) magnetic nanoparticle modified with alkyne-PEO-nitroDOPA, B) micrograph of clustered *E. coli* using magnetic nanoparticles functionalized with Tr-32, C) 3D fluorescent imaging of biofilms treated with magnetic nanoparticles with Cy5.5 dye, and D) Chelated ^{64}Ga ligand used to modify magnetic nanoparticles for SPECT/MR imaging.

BACTERIAL AGGREGATION AND TREATMENT USING MAGNETIC HYPERTHERMIA

Dr. Tzeng's group in the biology department at Clemson University were working on clustering different types of dangerous bacteria that is commonly found in an infected colon and applying an alternating magnetic field to disrupt their growth. They needed magnetic nanoparticles coated with a tri-carbohydrate that will actively target the bacteria's surface. Carbohydrates, linked to nanoparticles, have been found to bind to bacterial surface receptors, called adhesins, for use in detection and treatment of bacterial

infections.¹²¹ The mono-anchored magnetic nanoparticles with an alkyne surface, described in Chapter 3, was modified with an azido tri-saccharide using “click chemistry.” The solution was then dialyzed for 3 days before given to Dr. Tzeng’s research group where they then used them to cluster *E. coli* K99 bacterial cells.

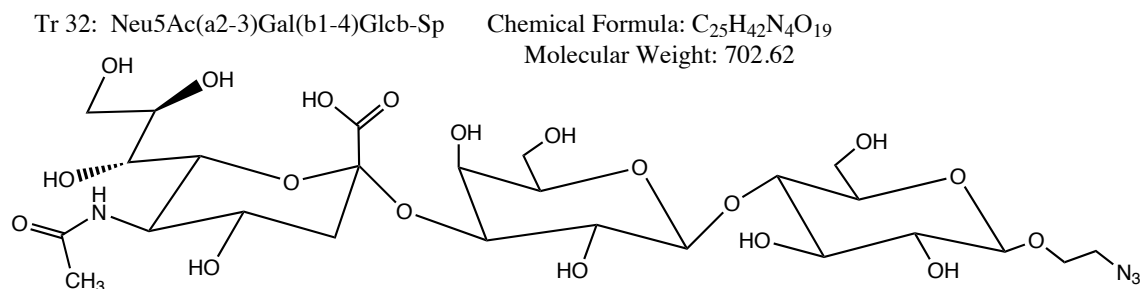


Figure 5.2. Structure of Tr32 tri-saccharides that was used to target *E. coli* K99 bacteria.

Aggregation studies were done on both the mono-anchored nanoparticles and the particles modified with Tr-32, Figure 5.2. Both of the particles complexes were added to *E. coli* K99 bacterial cells and mixed for 30 minutes at room temperature. The Tr-32 nanoparticles were also added to *E. coli* O157:H7, as a negative control. An aliquot was then taken and observed under an optical microscope, fluorescent and phase contrast micrographs are displayed in Figure 5.3. As expected visible aggregation did not occur, Figure 5.3 (A) and (B), with the mono-anchored particles with the *E. coli* K99 because of the lack of Tr-32 on the surface of the particles. To study the specificity of the binding of Tr-32 to *E. coli* K99, the modified particles were added to a different bacterial cell, *E. coli* O157:H7. As seen in Figure 5.3 (C), there was no aggregation observed. When the Tr-32 modified particles were added to *E. coli* K99 the bacterial cells were aggregated to structures over 100 μm larger, Figure 5.3 (D). A colony forming unit (CFU) assay was used to quantify the bacterial cells before and after treatment with nanoparticles.¹⁷⁵ The

data was conclusive, Figure 5.3, showing no significant reduction of CFU for the mono-anchored particles and a one-log reduction of CFU when the *E. coli* K99 cells were targeted and agglomerated.

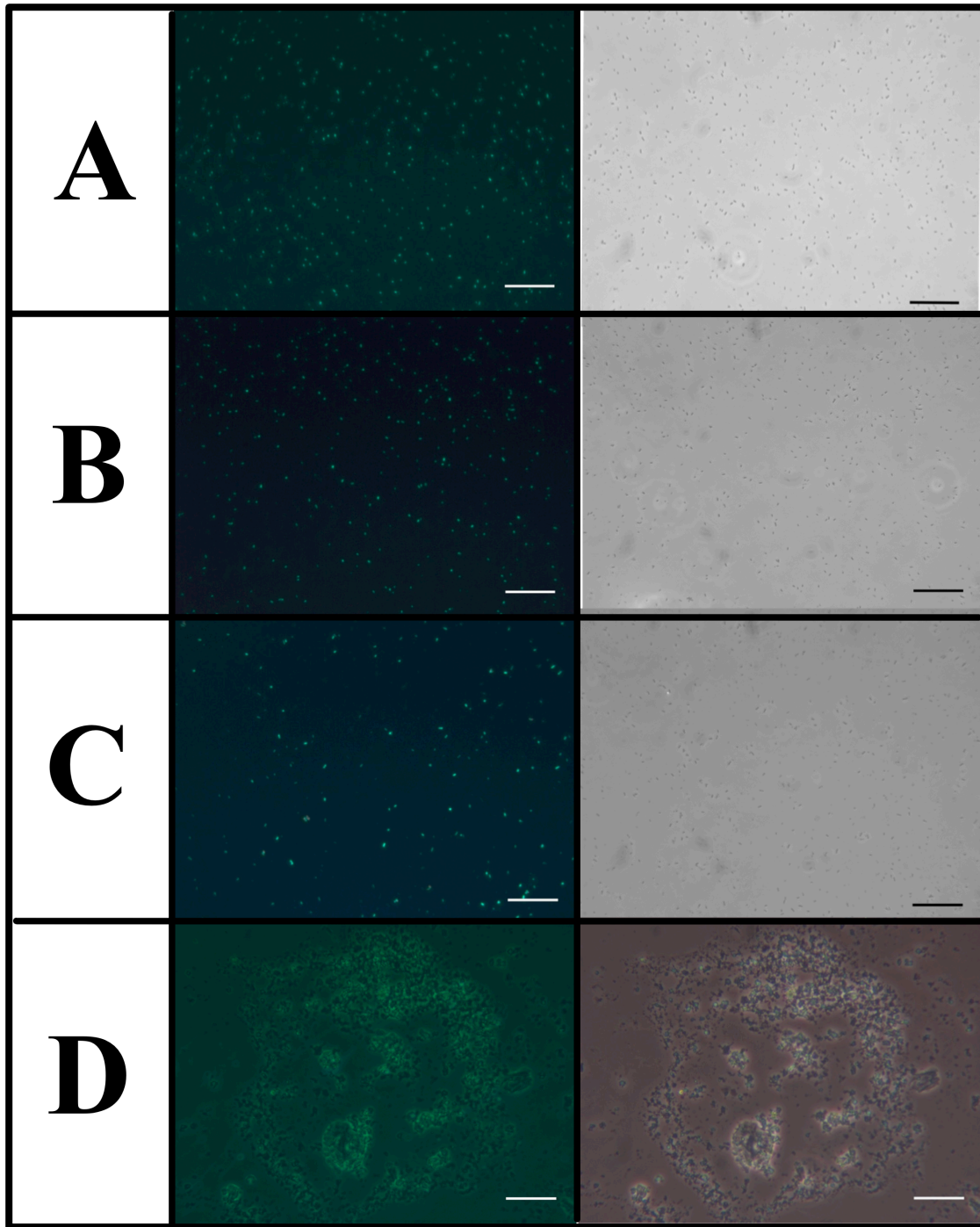


Figure 5.3. Fluorescence (left column) and phase-contrast (right column) microscopy of A) *E. coli* K99 in PBS, B) *E. coli* K99 with mono-anchored particles (unmodified), C) *E. coli* O157:H7 with Tr-32 modified particles, D) *E. coli* K99 with Tr-32 modified particles. All scale bars are 100 μ m.

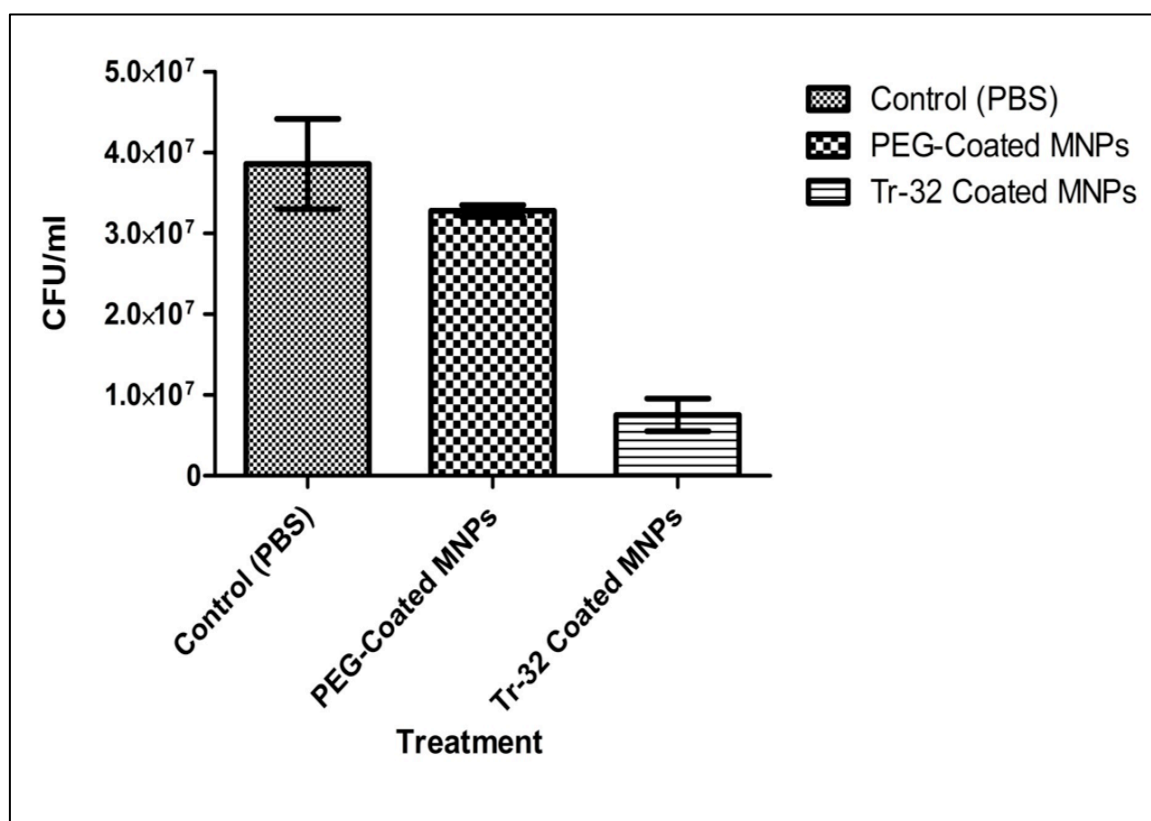


Figure 5.4. *E. coli* treatment with mono-anchored particles (unmodified) and Tr-32 modified particles. Data represented as Mean ± SD (n=3)

The *E. coli* K99 bacteria treated with the Tr-32 modified magnetic nanoparticles were characterized in an alternating current (AC) calorimeter to use magnetic hyperthermia to destroy the bacterial cells. Each sample was placed inside a temperature controlled water bath (45 °C) inside of a 5-turn, 2" in diameter copper coil. At 207 KHz and 480 A, we were able to produce an alternating magnetic field of 32.4 to 38.8 KAm^{-1} . Initial experiments were done at 37 °C to emulate body temperature but because the concentration of magnetic nanoparticles was low, for the max field and frequency, the water dissipated the energy and temperature at which the bacteria will die could not be

reached. The temperature was then increased to 45 °C for all measurements so the amount of energy needed to increase the temperature for the hyperthermia treatment of the bacterial cells, at 47°C, could be accomplished. The samples were put in the alternating magnetic field for 5, 10, 15, 30 and 60 minutes. CFU assay was then used to quantify and compare the treatments of different lengths. In Figure 5.4, the histogram shows that there was no significant change was observed in the control in all experiments. The mono-anchored particles exposed to a field for up to 15 minutes showed no significant loss of colony forming units. Thirty and sixty minute treatments yielded a one-log reduction in CFUs. All the samples were equilibrated to 45 °C before the magnetic field was applied, so the magnetic nanoparticles had to increase the temperature of the environment above temperature set by the water bath to have significant cell death. The particles modified with Tr-32 after 5 and 10 minutes in the magnetic field doubled the CFUs, which is hypothesized to the particles breaking up the aggregates from the motion of the particles in the field. After 15 minutes of treatment, there was a one log reduction and a two log reduction after 30 and 60 minutes which is a statistically significant decrease in CFUs,($p < 0.0001$). The two log reduction of CFUs for *E coli* K99 are on the same order of a many disinfectants that claim to kill 99.999% of bacteria. The efficiency of targeting and killing bacteria, shown with these initial hyperthermia results, is proof that these polymer-magnetic nanoparticle complexes are a viable alternative to antibiotics.

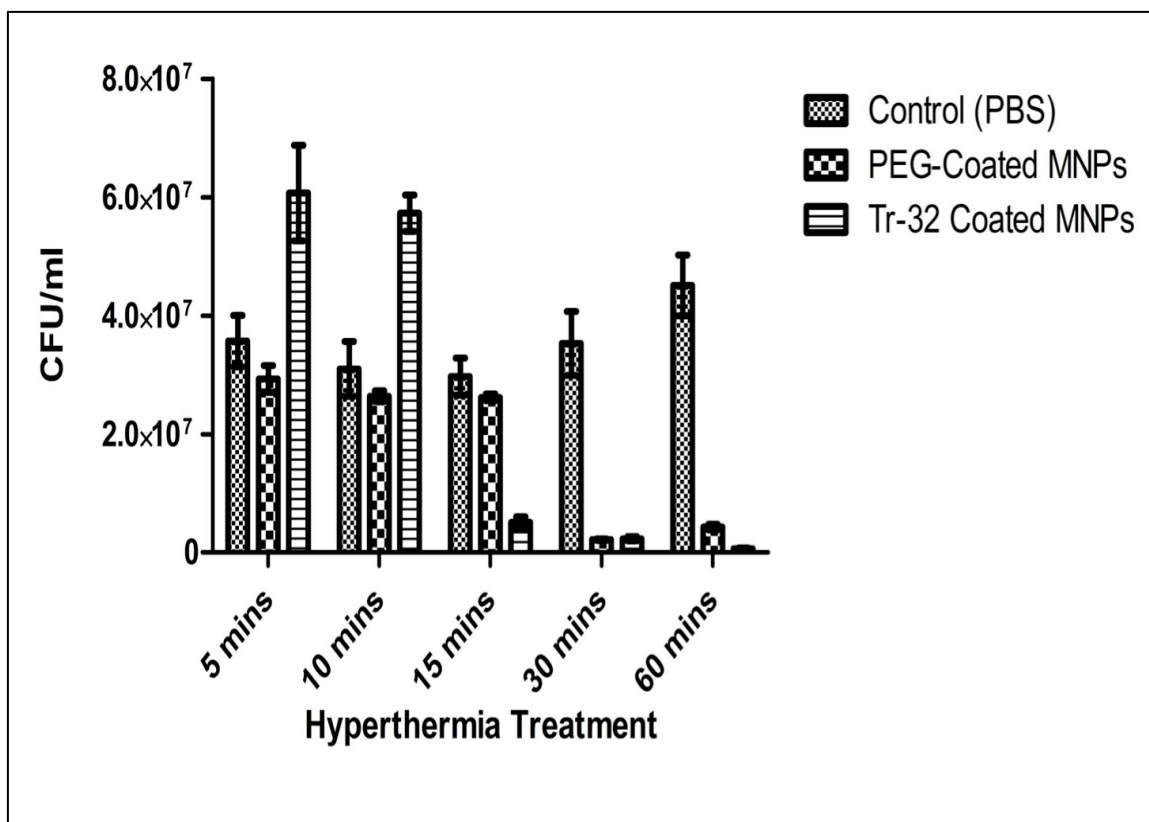


Figure 5.5. Hyperthermia treatment of *E. coli* with mono-anchored particles (unmodified) and Tr-32 modified particles. Data represented as mean \pm SD (n=3) ($p < 0.001$)

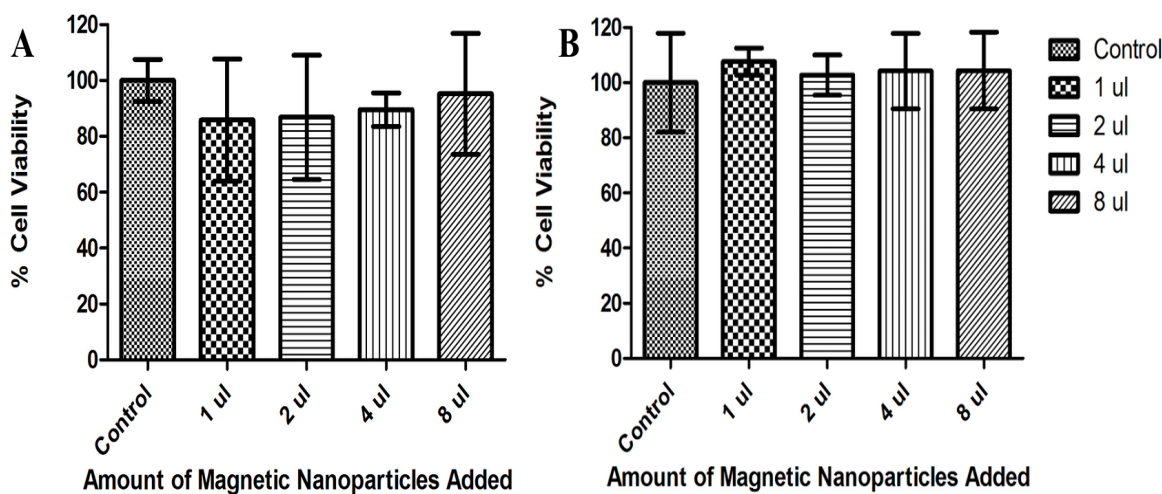


Figure 5.6. A) MTS assay of mono-anchored nanoparticles in human colon cells (CCD18-Co). B) MTS assay of Tr-32 modified nanoparticles in human colon cells (CCD18-Co).

MTS assays were performed on the mono-anchored magnetic nanoparticles and Tr-32 modified nanoparticles in human colon cells (CCD18-Co). This specific cell line was chosen because of where the targeted bacteria are located. In Figure 5.6 (A), there were no significant cytotoxic effects of the unmodified particles to the colon cells. After the particles were modified with Tr-32, there were still no significant cytotoxic effects observed of the nanoparticles, Figure 5.6 (B).

The initial work reported in this section shows that targeting, clustering, and hyperthermia of a specific type of *E. coli* is possible if time in the magnetic field is long enough. This can be improved by increasing the concentration and/or the size of the magnetic particles to increase the size of the clustering of the bacterial cells and the amount of heat generated to induce cell death. In the future work it will also be important to determine the ideal number of tri-saccharides per particle, not only for Tr-32 but other

tri-saccharides used for targeting specific bacteria, that is needed for clustering for more efficient particle design.

INTERACTIONS OF MAGNETIC NANOPARTICLES IN BACTERIAL BIOFILM

Nanoparticle research is important for the advancement in biomedical applications but there is also a concern on the impact of these materials on the environment. Biofilms are an important source of nutrients for ecosystems and is the base food supply for a lot of organisms.¹⁷⁸ Biofilms can contain *Legionella* bacteria found in industrial settings that is very harmful to humans because of potential outbreak of Legionnaires' disease, so prevention and treatment of biofilms is very important.¹⁷⁹ Legionnaires' disease is a combination of diseases involving pneumonia and flu-like illness that makes it difficult to diagnose without microbiological testing.¹⁸⁰ In fact, it is such a problem in some areas of the world that statistical and impact research is being published this year for incidences that occurred in Glasgow, UK and Christchurch, New Zealand.¹⁸¹

Dr. Tamara McNealy's research group at Clemson University is currently studying the effects of different types of metal nanoparticles on *Legionella pneumophila* biofilms that are found in natural and man-made environments.¹⁸² Raftery et al. characterized *Legionelle pneumophila* biofilms after they have been subjected to gold, platinum, silver and iron oxide nanoparticles. They discovered that the platinum and iron oxide nanoparticles had the largest reduction in the biofilm after 48 hours of exposure by analyzing and comparing the surface roughness of the metal nanoparticle treated and a control.¹⁷⁶

They were able to conclude that there was an adverse effect, but they were not able to visualize where and how the particles interact with the biofilms. Their group approached needed a water-soluble magnetic nanoparticles with a fluorescent dye so a Leica GSD microscope could be used to observe where polymer-magnetic nanoparticles settle in a biofilm. Polymer-magnetic nanoparticle complexes synthesized in Chapter 4 was modified with and azido Cy5.5, as described in section 4.3.10. Cy5.5 is a near IR dye that emits at 707 nm, which was far enough down the visible light spectrum from the Syto11 green fluorescent nucleic acid stain used for observing the biofilm that emits at 527 nm.

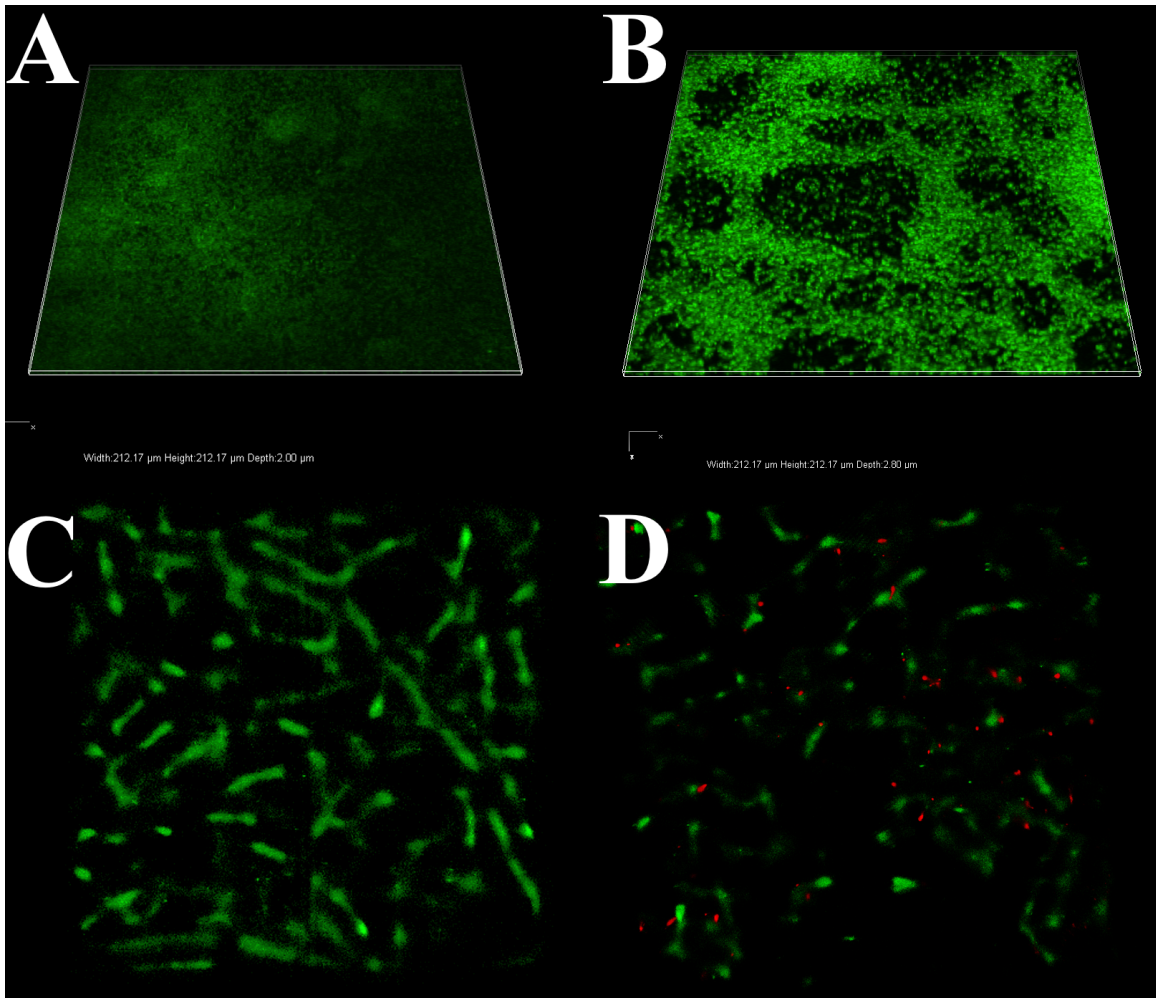


Figure 5.7. 3D Micrographs of *L. pneumophila* before and after treated with nanoparticles. A) Confocal micrograph of biofilm control. B) Confocal micrograph of biofilm treated with 1 µg of Fe/L of Cy5.5 modified magnetic nanoparticles. C) GSD micrograph of control. D) GSD micrograph of biofilm treated with 1 µg of Fe/L of Cy5.5 modified magnetic nanoparticles.

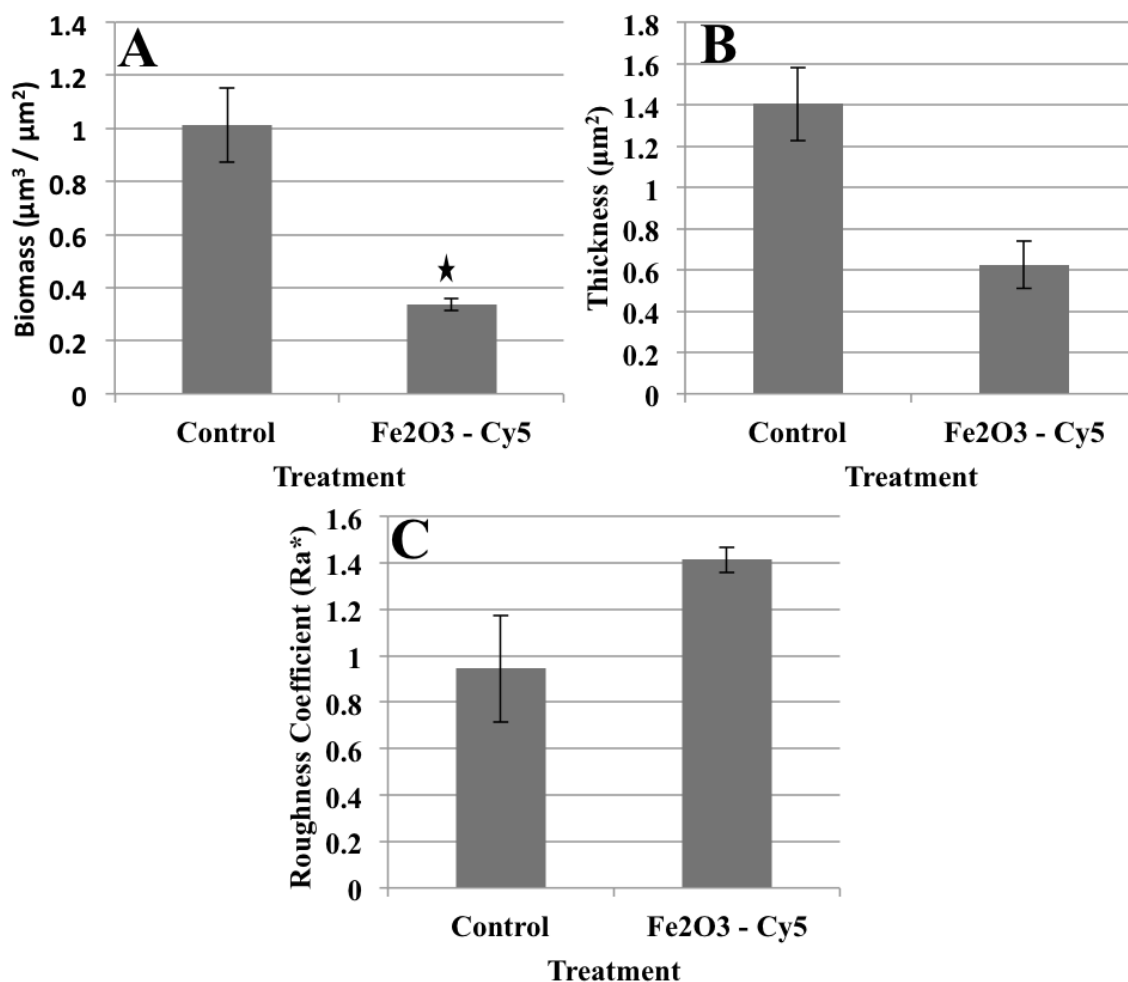


Figure 5.8. A) Biomass, B) Thickness, and C) Roughness analysis of biofilms before and after Cy5.5 particles were added. Data represented as Mean \pm SD (n=3)

There is definite disruption in the biofilm, as seen in Figure 5.7 (B), as compared to the control, Figure 5.7 (A). There is a visible decrease in the bio-volume after treatment with the Cy5.5 modified magnetic nanoparticles. Characterization of the control biofilm and the biofilm treated with particles was analyzed for change in biomass, thickness, and roughness. There was a statistically significant decrease in biomass after the addition of nanoparticles, (Figure. 5.8 (A), $p=0.008$, t-test). There was also a significant decrease in the thickness of the film, Figure 5.8 (B), confirming the loss of

height of biofilm due to the magnetic nanoparticles ($p=0.021$, t-test). Finally roughness was quantified, Figure 5.8 (C), and the results show an almost 40% increase compared to the control. Figure 5.8 (C) and (D) are before and after particle addition, respectively. The image for the control was taken after being exposed to specific wavelength and then scanned to read the excitation. Figure 5.9 is an overlaid 3D image that was excited at about 508 nm to image the biofilm (green) and then was excited at about 673 nm to image the Cy5.5 modified magnetic nanoparticles (red). The magnetic nanoparticles are being internalized and dispersed into the biofilm; because they are discrete magnetic nanoparticles modified a water-soluble ligand. The structure allowed the nanoparticles to enter gaps in the biofilms and destabilize the structure of the matrix. This phenomenon is difficult to observe with fluorescent confocal microscopy. This initial work will be able to give more information about how these nanoparticles are interacting once inside of the matrix that will help understand the mechanism used for biofilm reduction and can help develop new materials that will remove contaminating biofilms.¹⁷⁶

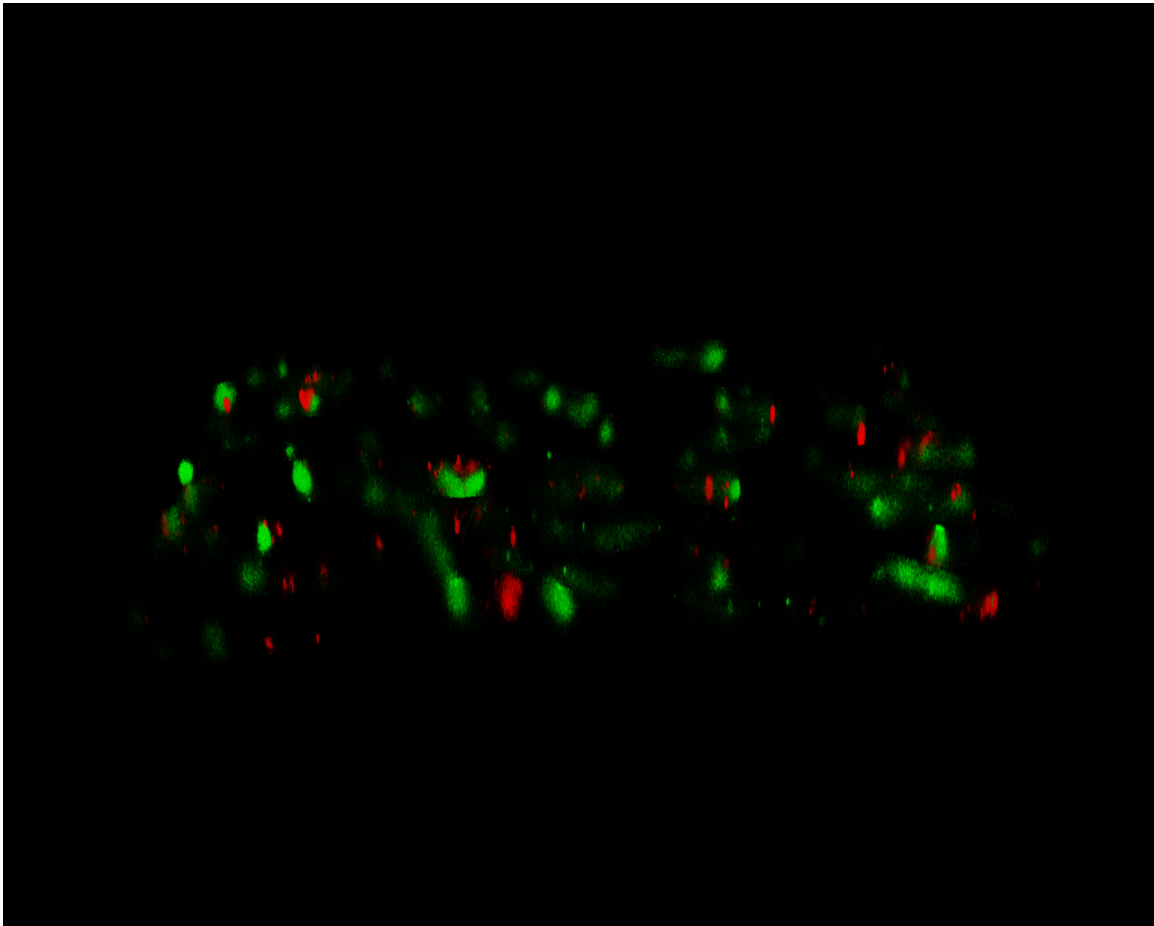


Figure 5.9. Side profile of GSD image of biofilm (green) modified with Cy5.5 magnetic nanoparticles (red)

MULTIFUNCTIONAL DIAGNOSTIC PROBE FOR SPECT/MR IMAGING

Improving the efficiency of materials used for theranostics is very important for early detection and treatment, especially for many types of cancers that can metastasize rapidly. Dr. Urs Häfeli from the University of British Columbia proposed that combining multiple imaging techniques, magnetic resonance imaging (MRI) and single-photon emission computed tomography (SPECT), can give provide more information to medical practitioners to better diagnose their patients.¹⁷⁷ SPECT requires radiotracers (radioactive iodine, indium and technetium) in very low concentrations for a measureable signal, but

cannot provide anatomic information because of its poor spatial resolution. To detect the locations of abnormalities, MRI is a much better tool for examining tissue because it uses contrast agents, such as magnetic nanoparticles, that magnetically relax as a function of its molecular environment.¹⁸³ So combining these two great techniques will require a material that can facilitate radiotracers for high sensitivity and superparamagnetic nanoparticles for high spatial resolution.

The polymer-magnetic nanoparticles that have been described in Chapter 4 were the perfect solution for creating a multifunctional diagnostic probe. Some of the multi-anchored magnetic nanoparticles, Chapter 4, was shipped to their laboratories in Vancouver and they were able to successfully modify the particles with ⁶⁷Ga.

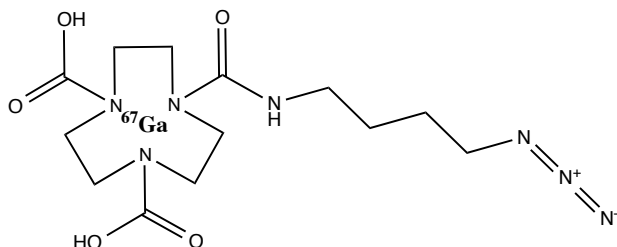


Figure 5.10. Schematic 1,4,7-triazacyclononane-1,4,7-triacetate (NOTA) ligand that is commonly used to chelate ⁶⁷Ga radiotracer.

The functionalization of the multi-anchored magnetic nanoparticles with a radio tracer was accomplished by first modifying the particles with an azide ligand,^{184,185} Figure 5.8, using copper(II) sulfate and sodium ascorbate to create copper(I) catalyst in situ, that has the ability to chelate rare earth metals. After the particles were modified, they were dialyzed against water for 2 days and then lyophilized. The particles were then dispersed in water and mixed with ⁶⁷GaCl₃, shaken for twenty minutes, centrifuged with a 30 kDa MWCO filter, washed, and then collected. Based on the number of the ⁶⁷Ga

present, there was an average of 68% labeling efficiency. This is very new data and repetition of modification should be done to ensure labeling of ^{67}Ga . Once these materials have been thoroughly characterized, their biodistribution and ability to monitor biomolecular processes should be studied to see how well these particles survive in situ using mice models.

CHAPTER 6. FUTURE WORK

Magnetic nanoparticles are one of the most fascinating materials to study because their applications are limitless. Designing different polymer surfaces for magnetic nanoparticles can provide a very useful tool for therapeutics and diagnostics that can be tailored to individual patient's need. The original frustration of creating made to order heterobifunctional PEO for magnetic nanoparticles, with different surface chemistries to further research in different research groups brought about the need for creating a functional scaffolding that could create a batch of universal biologically stable magnetic nanoparticles. This universal particles design using PEO has great potential for fundamental research in magnetic nanoparticles in biomedical applications. The control of molecular weight and end group functionality inherent in anionic ring opening polymerization of ethylene oxide will allow researchers to study the effect of molecular weight and surface chemistry on biological phenomena, i.e. targeting, heating efficiency, and biodistribution.

It has been shown that the design and synthesis of a universal ligand is possible on small scales because of limitations of reaction times and cost of materials. For these universal magnetic nanoparticle complexes to become a viable alternative to synthetic drugs already on the market, scaling up is necessary. So, designing new initiators that can efficiently polymerize ethylene oxide to provide the desired functionality and molecular weight will improve yields because there will be a decrease the number of end group modifications. One possible idea is to synthesize an initiator from propargyl alcohol, or amine, where the terminal carbon-hydrogen bond (C-H) of the alkyne is protected. This

can be done using a trimethylsilyl group, to protect the acidic proton of the alkyne from the caustic environment generally needed to create the anion that initiates the ring opening of ethylene oxide, Figure 6.1. Anionic ring opening polymerization of ethylene oxide using this method will allow for the production of various molecular weights with narrow distributions.

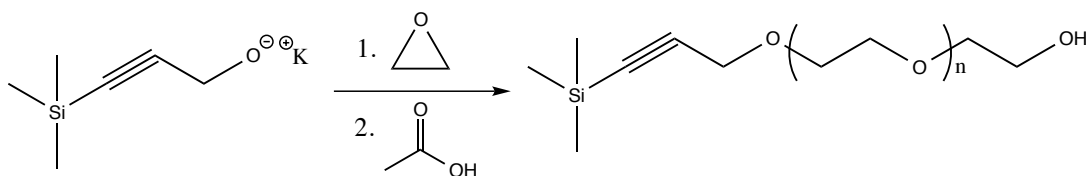


Figure 6.1. Proposed anionic ring opening polymerization of ethylene oxide using a protected propargyl alcohol as an initiator.

Once the process of synthesizing specialized heterobifunctional PEO with an alkyne on one end for easy functionalization and a catechol on the other end for strong binding to metal nanoparticles is streamlined, a large library of polymer-magnetic nanoparticle complexes of various molecular weights and metal core diameters is possible in the foreseeable future. Aliquots from this library could then be easily modified due to the alkyne surface, using “click chemistry,” with a variety of functional moieties specific to the desired application. Some examples of functional moieties that can be used are fluorescent dyes for imaging,¹⁵⁵ rare earth metals for temperature sensing,¹⁸⁶ active targeting drug delivery,¹⁸⁷ radiotracers to improve diagnostic techniques,¹⁴⁸ and/or a combination of them to create a multifunctional device, a schematic of this multifunctional device is shown in Figure 6.2.¹⁰⁸

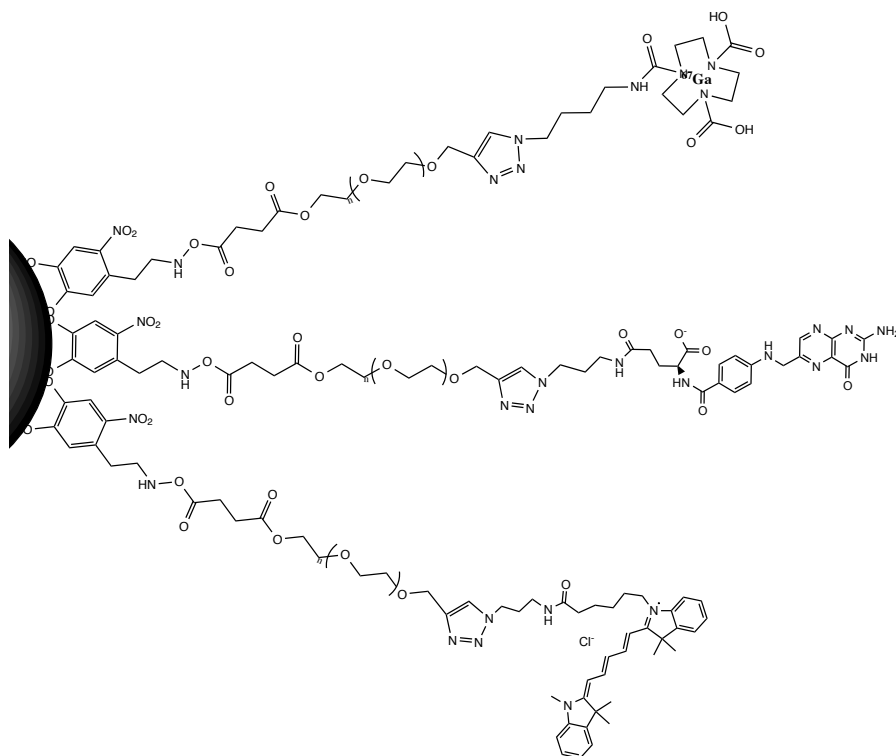


Figure 6.2. Magnetic nanoparticle functionalized with a variety of functionalities on the same nanoparticle. From top to bottom: moiety that can chelate different metals, folic acid to target overexpressed folate receptors, and Cy5 NIR dye that can be used for imaging through human tissue.

Magnetic nanoparticles that are modified with multiple binding groups per polymer chain have been shown to increase the steric stability in biological environments. They have been synthesized in a variety of ways using multi-functional initiators or modification of PAA to make brushes.^{131,163} Atom transfer radical polymerization (ATRP) could be used to copolymerize a heterobifunctional PEO analogue with an alkyne on one end and a methacrylate on the other with a catechol methacrylate. This approach can synthesize a block copolymer that is water-soluble, has a surface that can be functionalized using click chemistry, and has a catechol that can strongly interact with

metal oxide surfaces, schematic in Figure 6.3. The heterobifunctional analogue would be synthesized by anionic ring opening polymerization of ethylene oxide using a protected propargyl alcohol. Then through end group modification, it will be modified with a methacrylate using methods discussed in section 2.10.4. The dopamine analog would first be protected as an acetonide¹⁸⁸ and then reacted with methacroyl chloride via a substitution reaction. Once the analogs are synthesized, using copper(I) chloride and 2,2' bipyridyl (Bipy) to radically polymerize them together and then the catechol could be deprotected with acid and then magnetic nanoparticles could be modified. This is another example of a type living polymerization that can yield narrow molecular weight polymers with control of each block length¹⁸⁹ that can be used to study the optimal ratio of PEO to catechol needed for creating biologically stable magnetic nanoparticles.

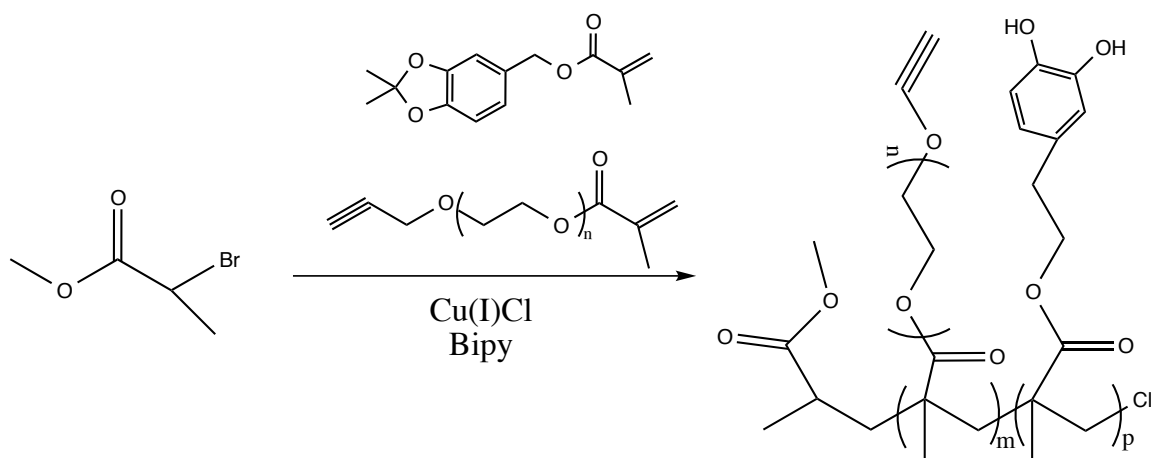


Figure 6.3. Schematic of ATRP polymerization of PEO-alkyne and catechol-methacrylate block copolymer.

Well characterized materials for biomedical applications is important for creating efficient therapeutic devices for magnetic hyperthermia to ensure positive results for

patients. This same library can be used for fundamental research in understanding how particles interactions (determined by molecular weight, magnetic core size, concentration and surface chemistry) affect the SAR in an alternating magnetic field.¹⁹⁰

The surface functionality of an alkyne on the magnetic nanoparticles also facilitates crosslinking the particles using “click chemistry” to form clusters of magnetic nanoparticles, Figure 6.4, which can offer improved magnetic properties. Using a short chain molecule with an azide on both sides can be used to link the alkyne surface of the magnetic nanoparticles together. The controlled clustering of the particles will create a different anisotropy and interaction that will increase the saturation magnetization of the particles.¹⁹¹ This approach to clustering magnetic nanoparticles will still have an alkyne functional surface that can be modified further with targeting and imaging moieties using “click chemistry.”

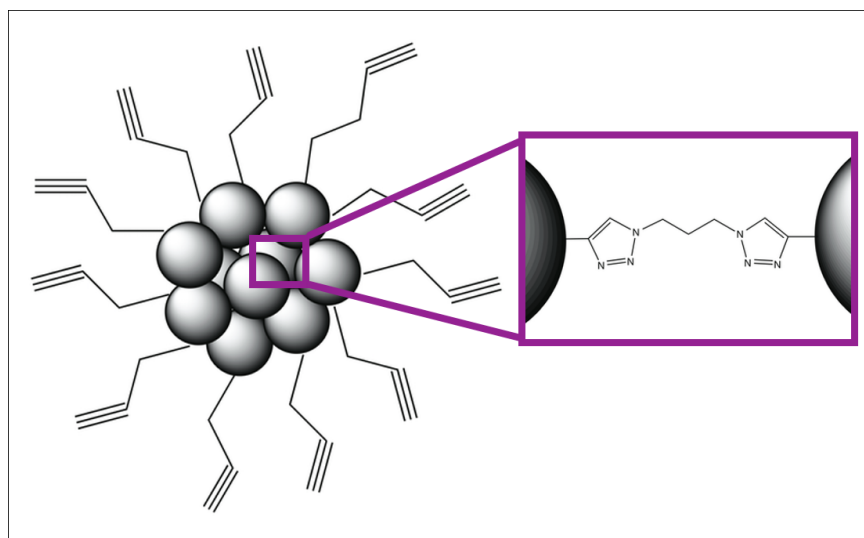


Figure 6.4. Schematic of clustered nanoparticles via “click chemistry” using a bis-azide to link the alkyne surface of the magnetic nanoparticles.

Using targeting agents for delivering the magnetic nanoparticles to infected areas is very useful for increasing the efficiency of the treatment because of the increase concentration at the site to initiate endocytosis.¹⁹² Unfortunately, this usually only happens at the surface where the receptors are over-expressed and are not internalized, and will require multiple treatments to completely remove tumor. One way to facilitate the internalization of nanoparticles into infected cells is by combining different charges and targeting moieties onto the surface,¹⁹³ represented by Figure 6.5. Different functional groups that can provide a variety of surface chemistry when dispersed in water (i.e. amine, carboxylic acid, thiol, alcohol, and methyl groups) can be used for studying how different surfaces can affect the biodistribution and cell uptake of nanoparticles in the human body. Their location and concentration can be visualized and quantified using fluorescent magnetic resonance imaging.

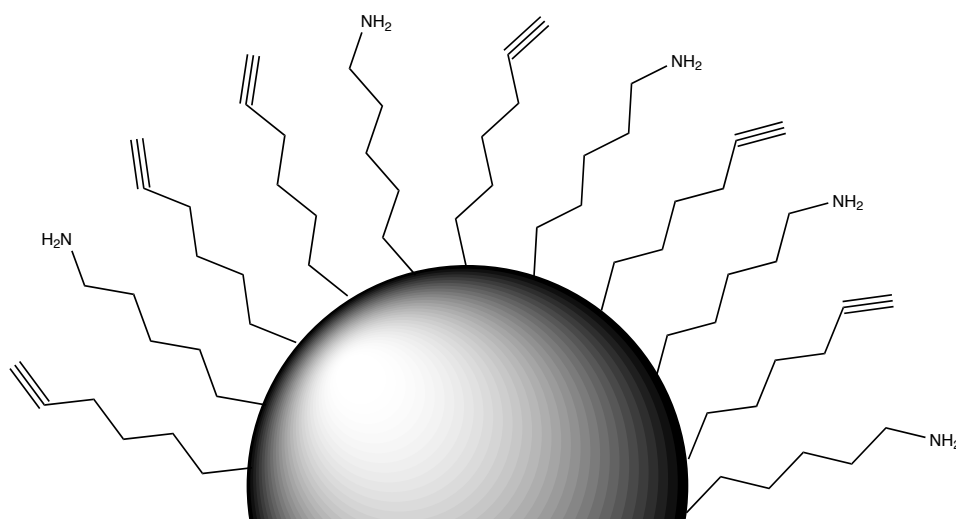


Figure 6.5. Magnetic nanoparticle displaying a surface with a combination of alkyne for functionalization with a targeting or fluorescent moiety and amines for aiding in internalization.

The materials designed and synthesized in this work have great potential for fundamental research on materials used for magnetic hyperthermia that is necessary if they are to be a viable alternative to current treatments on the market. A water-dispersible nanoparticle that can be easily functionalized for a variety of applications, which has been presented in Chapter 5, is very important for biological research but material development must continue to optimize the number of steps to synthesize these specialized materials for them to be a realistic option.

CHAPTER 7. CONCLUSIONS

This work has presented the synthesis of a variety of heterobifunctional PEOs that were prepared by the anionic ring opening polymerization of ethylene oxide and end group modification. The variety of polymers synthesized in Chapter 1 were the motivation to develop a specialized heterobifunctional PEO that can be utilized for building a water-soluble magnetic nanoparticle complex with functional scaffolding for use in an assortment of biological applications. To confirm the versatility of the functional scaffolding, it was modified with a variety of fluorescent dyes that could be easily observed using photoluminescence. The particles were also modified with two dyes simultaneously to demonstrate the multifunctional capabilities that can be very useful for targeted therapeutics and diagnostics.

To improve the biological stability of the magnetic nanoparticles that is needed for increased circulation and efficient drug delivery, a specialized heterobifunctional PEO and nitroDOPA was attached to a PAA backbone to increase the number of anchoring groups that can interact with the iron oxide surface. The increase in biological stability of the multi-anchored nanoparticles compared to mono-anchored nanoparticles was demonstrated by submitting them to protein and ionic rich environments at elevated temperatures while measuring the change in hydrodynamic diameter.

The ease of customization of these particles was attractive to other research areas outside of magnetic hyperthermia of cancer. They were modified with: a tri-saccharide to target and cluster *E. coli* K99; a fluorescent dye to image them in biofilms; and a radiotracer that can be used as in vivo biomedical diagnostic probes. These polymer-

magnetic nanoparticle complexes show great potential for offering an alternative to current theranostics and fundamental magnetic hypothermia research.

REFERENCES

1. Gilchrist, R. K.; Medal, R.; Shorey, W. D.; Hanselman, R. C.; Parrott, J. C.; Taylor, C. B. Selective Inductive Heating of Lymph Nodes. *Annals of Surgery* **1957**, *146*, 596.
2. Pankhurst, Q.; Connolly, J.; Jones, S.; Dobson, J. Applications of Magnetic Nanoparticles in Biomedicine. *Journal of Physics D: Applied Physics* **2003**, *36*, R167.
3. Muthana, M.; Multhoff, G.; Graham Pockley, A. Tumour Infiltrating Host Cells and Their Significance for Hyperthermia. *Int J Hyperthermia* **2010**, *26*, 247–255.
4. Le Renard, P.-E.; Jordan, O.; Faes, A.; Petri-Fink, A.; Hofmann, H.; Rüfenacht, D.; Bosman, F.; Buchegger, F.; Doelker, E. The in Vivo Performance of Magnetic Particle-Loaded Injectable, in Situ Gelling, Carriers for the Delivery of Local Hyperthermia. *Biomaterials* **2010**, *31*, 691–705.
5. Latorre-Esteves, M.; Cortés, A.; Torres-Lugo, M.; Rinaldi, C. Synthesis and Characterization of Carboxymethyl Dextran-Coated Mn/Zn Ferrite for Biomedical Applications. *Journal of Magnetism and Magnetic Materials* **2009**, *321*, 3061–3066.
6. Aronov, O.; Horowitz, A.; Gabizon, A. Folate-Targeted PEG as a Potential Carrier for Carboplatin Analogs. Synthesis and in Vitro Studies. *Bioconjugate Chemistry* **2003**, *14*, 563–574.
7. Yan, Q.; Purkayastha, A.; Kim, T.; Kröger, R.; Bose, A.; Ramanath, G. Synthesis and Assembly of Monodisperse High-Coercivity Silica-Capped FePt Nanomagnets of Tunable Size, Composition, and Thermal Stability From Microemulsions. *Advanced Materials* **2006**, *18*, 2569–2573.
8. Chen, M.; Liu, J.; Sun, S. One-Step Synthesis of FePt Nanoparticles with Tunable Size. *J. Am. Chem. Soc* **2004**, *126*, 8394–8395.
9. Sun, S.; Anders, S.; Thomson, T.; Baglin, J.; Toney, M.; Hamann, H.; Murray, C.; Terris, B. Controlled Synthesis and Assembly of FePt Nanoparticles. *J. Phys. Chem. B* **2003**, *107*, 5419–5425.
10. Kim, J.; Rong, C.; Liu, J.; Sun, S. Dispersible Ferromagnetic FePt Nanoparticles. *Advanced Materials* **2009**, *21*, 906–909.
11. Hou, Y.; Kondoh, H.; Kogure, T.; Ohta, T. Preparation and Characterization of Monodisperse FePd Nanoparticles. *Chem. Mater* **2004**, *16*, 5149–5152.

12. Tzitzios, V.; Niarchos, D.; Margariti, G.; Fidler, J.; Petridis, D. Synthesis of CoPt Nanoparticles by a Modified Polyol Method: Characterization and Magnetic Properties. *Nanotechnology* **2005**, *16*, 287.
13. Chinnasamy, C.; Jeyadevan, B.; Shinoda, K.; Tohji, K. Polyol-Process-Derived CoPt Nanoparticles: Structural and Magnetic Properties. *Journal of Applied Physics* **2003**, *93*, 7583.
14. Ghosh, M.; Sampathkumaran, E.; Rao, C. Synthesis and Magnetic Properties of CoO Nanoparticles. *Chem. Mater* **2005**, *17*, 2348–2352.
15. Oh, J.; Park, J. Iron Oxide-Based Superparamagnetic Polymeric Nanomaterials: Design, Preparation, and Biomedical Application. *Progress in Polymer Science* **2010**.
16. Ghosh, M.; Biswas, K.; Sundaresan, A.; Rao, C. MnO and NiO Nanoparticles: Synthesis and Magnetic Properties. *J. Mater. Chem.* **2006**, *16*, 106–111.
17. Weissleder, R.; Stark, D.; Engelstad, B.; Bacon, B.; Compton, C.; White, D.; Jacobs, P.; Lewis, J. Superparamagnetic Iron Oxide: Pharmacokinetics and Toxicity. *American Journal of Roentgenology* **1989**, *152*, 167.
18. Sun, S.; Zeng, H. Size-Controlled Synthesis of Magnetite Nanoparticles. *J. Am. Chem. Soc* **2002**, *124*, 8204–8205.
19. Hyeon, T.; Lee, S.; Park, J.; Chung, Y.; Na, H. Synthesis of Highly Crystalline and Monodisperse Maghemite Nanocrystallites Without a Size-Selection Process. *J. Am. Chem. Soc* **2001**, *123*, 12798–12801.
20. Babes, L.; Denizot, B.; Tanguy, G.; Le Jeune, J.; Jallet, P. Synthesis of Iron Oxide Nanoparticles Used as MRI Contrast Agents: a Parametric Study* 1. *Journal of Colloid and Interface Science* **1999**, *212*, 474–482.
21. Bulte, J.; Kraitchman, D. Iron Oxide MR Contrast Agents for Molecular and Cellular Imaging. *NMR in Biomedicine* **2004**, *17*, 484–499.
22. Kuhara, M.; Takeyama, H.; Tanaka, T.; Matsunaga, T. Magnetic Cell Separation Using Antibody Binding with Protein a Expressed on Bacterial Magnetic Particles. *Anal. Chem* **2004**, *76*, 6207–6213.
23. McCloskey, K.; Chalmers, J.; Zborowski, M. Magnetic Cell Separation: Characterization of Magnetophoretic Mobility. *Anal. Chem* **2003**, *75*, 6868–6874.

24. Ito, A.; Shinkai, M.; Honda, H.; Kobayashi, T. Medical Application of Functionalized Magnetic Nanoparticles. *Journal of bioscience and bioengineering* **2005**, *100*, 1–11.
25. Foy, S.; Manthe, R.; Foy, S.; Dimitrijevic, S. Optical Imaging and Magnetic Field Targeting of Magnetic Nanoparticles in Tumors. *ACS Nano* **2010**.
26. Habib, A. H.; Ondeck, C. L.; Chaudhary, P.; Bockstaller, M. R.; McHenry, M. E. Evaluation of Iron-Cobalt/Ferrite Core-Shell Nanoparticles for Cancer Thermotherapy. *Journal of Applied Physics* **2008**, *103*, 07A307.
27. Lu, J.; Ma, S.; Sun, J.; Xia, C.; Liu, C.; Wang, Z.; Zhao, X.; Gao, F.; Gong, Q.; Bin Song; *et al.* Manganese Ferrite Nanoparticle Micellar Nanocomposites as MRI Contrast Agent for Liver Imaging. *Biomaterials* **2009**, *30*, 2919–2928.
28. Ahamed, M.; Akhtar, M. J.; Siddiqui, M. A.; Ahmad, J.; Musarrat, J.; Al-Khedhairy, A. A.; AlSalhi, M. S.; Alrokayan, S. A. Oxidative Stress Mediated Apoptosis Induced by Nickel Ferrite Nanoparticles in Cultured A549 Cells. *Toxicology* **2011**, 1–8.
29. Pradhan, P.; Giri, J.; Samanta, G.; Sarma, H. D.; Mishra, K. P.; Bellare, J.; Banerjee, R.; Bahadur, D. Comparative Evaluation of Heating Ability and Biocompatibility of Different Ferrite-Based Magnetic Fluids for Hyperthermia Application. *J. Biomed. Mater. Res.* **2007**, *81B*, 12–22.
30. Buckley, P. R.; Mckinley, G. H.; Wilson, T. S.; Small, W.; Benett, W. J.; Bearinger, J. P.; Mcelfresh, M. W.; Maitland, D. J. Inductively Heated Shape Memory Polymer for the Magnetic Actuation of Medical Devices. *IEEE Trans. Biomed. Eng.* **2006**, *53*, 2075–2083.
31. Mandal, M.; Kundu, S.; Ghosh, S.; Panigrahi, S.; Sau, T.; Yusuf, S.; Pal, T. Magnetite Nanoparticles with Tunable Gold or Silver Shell. *Journal of Colloid and Interface Science* **2005**, *286*, 187–194.
32. Neouze, M.; Schubert, U. Surface Modification and Functionalization of Metal and Metal Oxide Nanoparticles by Organic Ligands. *Monatshefte für Chemie/Chemical Monthly* **2008**, *139*, 183–195.
33. Dulkeith, E.; Ringler, M.; Klar, T.; Feldmann, J. Gold Nanoparticles Quench Fluorescence by Phase Induced Radiative Rate Suppression. *Nano Letters* **2005**, *5*, 585–589.
34. Jain, P. K.; El-Sayed, I. H.; El-Sayed, M. A. Au Nanoparticles Target Cancer. *nanotoday* **2007**, *2*, 18–29.

35. Wang, L.; Park, H.; Lim, S.; Schadt, M.; Mott, D.; Luo, J.; Wang, X.; Zhong, C. Core@ Shell Nanomaterials: Gold-Coated Magnetic Oxide Nanoparticles. *J. Mater. Chem.* **2008**, *18*, 2629–2635.
36. Salgueirino-Maceira, V.; Correa-Duarte, M.; Farle, M.; Lopez-Quintela, A.; Sieradzki, K.; Diaz, R. Bifunctional Gold-Coated Magnetic Silica Spheres. *Chem. Mater* **2006**, *18*, 2701–2706.
37. Sperling, R. A.; Rivera Gil, P.; Zhang, F.; Zanella, M.; Parak, W. J. Biological Applications of Gold Nanoparticles. *Chemical Society Reviews* **2008**, *37*, 1896.
38. Cheng, F.; Su, C.; Yang, Y.; Yeh, C.; Tsai, C.; Wu, C.; Wu, M.; Shieh, D. Characterization of Aqueous Dispersions of Fe₃O₄ Nanoparticles and Their Biomedical Applications. *Biomaterials* **2005**, *26*, 729–738.
39. Gass, J.; Poddar, P.; Almand, J.; Srinath, S.; Srikanth, H. Superparamagnetic Polymer Nanocomposites with Uniform Fe₃O₄ Nanoparticle Dispersions. *Advanced Functional Materials* **2006**, *16*, 71–75.
40. Goya, G.; Lima, E.; Arelaro, A.; Torres, T.; Rechenberg, H.; Rossi, L.; Marquina, C.; Ibarra, M. Magnetic Hyperthermia with Fe₃O₄ Nanoparticles: the Influence of Particle Size on Energy Absorption. *Magnetics, IEEE Transactions on* **2008**, *44*, 4444–4447.
41. Kallumadil, M.; Tada, M.; Nakagawa, T.; Abe, M.; Southern, P.; Pankhurst, Q. Suitability of Commercial Colloids for Magnetic Hyperthermia. *Journal of Magnetism and Magnetic Materials* **2009**, *321*, 1509–1513.
42. Dennis, C.; Jackson, A.; Borchers, J.; Ivkov, R.; Foreman, A.; Lau, J.; Goernitz, E.; Gruettner, C. The Influence of Collective Behavior on the Magnetic and Heating Properties of Iron Oxide Nanoparticles. *Journal of Applied Physics* **2009**, *103*, 07A319.
43. Eggeman, A.; Majetich, S.; Farrell, D.; Pankhurst, Q. Size and Concentration Effects on High Frequency Hysteresis of Iron Oxide Nanoparticles. *Magnetics, IEEE Transactions on* **2007**, *43*, 2451–2453.
44. Rosensweig, R. Heating Magnetic Fluid with Alternating Magnetic Field. *Journal of Magnetism and Magnetic Materials* **2002**, *252*, 370–374.
45. Gonzales-Weimuller, M.; Zeisberger, M.; Krishnan, K. Size-Dependant Heating Rates of Iron Oxide Nanoparticles for Magnetic Fluid Hyperthermia. *Journal of Magnetism and Magnetic Materials* **2009**, *321*, 1947–1950.

46. Mornet, S.; Vasseur, S.; Grasset, F.; Duguet, E. Magnetic Nanoparticle Design for Medical Diagnosis and Therapy. *J. Mater. Chem.* **2004**, *14*, 2161–2175.
47. Tabatabaei, S. Hyperthermia via Ac Electromagnetic Field and Magnetic Nanoparticles Integrated in Micro-Carriers Navigable in Blood Vessels. *wiki.polymtl.ca*.
48. Ma, M.; Wu, Y.; Zhou, J.; Sun, Y.; Zhang, Y.; Gu, N. Size Dependence of Specific Power Absorption of Fe₃O₄ Particles in AC Magnetic Field. *Journal of Magnetism and Magnetic Materials* **2004**, *268*, 33–39.
49. Ivkov, R.; DeNardo, S.; Daum, W.; Foreman, A.; Goldstein, R.; Nemkov, V.; DeNardo, G. Application of High Amplitude Alternating Magnetic Fields for Heat Induction of Nanoparticles Localized in Cancer. *Clinical Cancer Research* **2005**, *11*, 7093s.
50. Zhang, L.; Gu, H.; Wang, X. Magnetite Ferrofluid with High Specific Absorption Rate for Application in Hyperthermia. *Journal of Magnetism and Magnetic Materials* **2007**, *311*, 228–233.
51. Jordan, A.; Wust, P.; Fähling, H.; John, W.; Hinz, A.; Felix, R. Inductive Heating of Ferrimagnetic Particles and Magnetic Fluids: Physical Evaluation of Their Potential for Hyperthermia. *Int J Hyperthermia* **2009**, *25*, 499–511.
52. Kim, D.; Nikles, D.; Johnson, D.; Brazel, C. Heat Generation of Aqueously Dispersed CoFe₂O₄ Nanoparticles as Heating Agents for Magnetically Activated Drug Delivery and Hyperthermia. *Journal of Magnetism and Magnetic Materials* **2008**, *320*, 2390–2396.
53. Johannsen, M.; Gneveckow, U.; Eckelt, L.; Feussner, A.; Waldöfner, N.; Scholz, R.; Deger, S.; Wust, P.; Loening, S. A.; Jordan, A. Clinical Hyperthermia of Prostate Cancer Using Magnetic Nanoparticles: Presentation of a New Interstitial Technique. *Int J Hyperthermia* **2005**, *21*, 637–647.
54. Vadala, M.; Thompson, M.; Ashworth, M.; Lin, Y.; Vadala, T.; Ragheb, R.; Riffle, J. Heterobifunctional Poly(Ethylene Oxide) Oligomers Containing Carboxylic Acids. *Biomacromolecules* **2008**, *9*, 1035–1043.
55. Lin, H.; Watanabe, Y.; Kimura, M.; Hanabusa, K.; Shirai, H. Preparation of Magnetic Poly (Vinyl Alcohol)(PVA) Materials by in Situ Synthesis of Magnetite in a PVA Matrix. *Journal of Applied Polymer Science* **2003**, *87*, 1239–1247.

56. Aslam, M.; Schultz, E.; Sun, T.; Meade, T.; Dravid, V. Synthesis of Amine-Stabilized Aqueous Colloidal Iron Oxide Nanoparticles. *Crystal Growth & Design* **2007**, *7*, 471–475.
57. Goff, J.; Huffstetler, P.; Miles, W.; Pothayee, N.; Reinholz, C.; Ball, S.; Davis, R.; Riffle, J. Novel Phosphonate-Functional Poly (Ethylene Oxide)-Magnetite Nanoparticles Form Stable Colloidal Dispersions in Phosphate-Buffered Saline. *Chemistry of Materials* **2009**, *21*, 4784–4795.
58. Sahoo, Y.; Pizem, H.; Fried, T.; Golodnitsky, D.; Burstein, L.; Sukenik, C.; Markovich, G. Alkyl Phosphonate/Phosphate Coating on Magnetite Nanoparticles: a Comparison with Fatty Acids. *Langmuir* **2001**, *17*, 7907–7911.
59. Grüttner, C.; Müller, K.; Teller, J.; Westphal, F.; Foreman, A.; Ivkov, R. Synthesis and Antibody Conjugation of Magnetic Nanoparticles with Improved Specific Power Absorption Rates for Alternating Magnetic Field Cancer Therapy. *Journal of Magnetism and Magnetic Materials* **2007**, *311*, 181–186.
60. Huang, P.; Wang, M.; Chiu, C. Soil Mineral-Organic Matter-Microbe Interactions: Impacts on Biogeochemical Processes and Biodiversity in Soils. *Pedobiologia* **2005**, *49*, 609–635.
61. McCash, E. M. *Surface Chemistry*; New York: Oxford University Press, 2001; Vol. 62.
62. Amstad, E.; Gillich, T.; Bilecka, I.; Textor, M.; Reimhult, E. Ultrastable Iron Oxide Nanoparticle Colloidal Suspensions Using Dispersants with Catechol-Derived Anchor Groups. *Nano Letters* **2009**, *9*, 4042–4048.
63. Qu, H.; Caruntu, D.; Liu, H.; O Connor, C. J. Water-Dispersible Iron Oxide Magnetic Nanoparticles with Versatile Surface Functionalities. *Langmuir* **2011**, *27*, 2271–2278.
64. Basti, H.; Ben Tahar, L.; Smiri, L. S.; Herbst, F.; Vaulay, M. J.; Chau, F.; Ammar, S.; Benderbous, S. Catechol Derivatives-Coated Fe₃O₄ and γ -Fe₂O₃ Nanoparticles as Potential MRI Contrast Agents. *Journal of Colloid and Interface Science* **2010**, *341*, 248–254.
65. Gu, H.; Xu, K.; Yang, Z.; Chang, C.; Xu, B. Synthesis and Cellular Uptake of Porphyrin Decorated Iron Oxide Nanoparticles—a Potential Candidate for Bimodal Anticancer Therapy. *Chem. Commun.* **2005**, *2005*, 4270–4272.

66. Amstad, E.; Zurcher, S.; Mashaghi, A.; Wong, J. Y.; Textor, M.; Reimhult, E. Surface Functionalization of Single Superparamagnetic Iron Oxide Nanoparticles for Targeted Magnetic Resonance Imaging. *Small* **2009**, *5*, 1334–1342.
67. Mefford, O.; Vadala, M.; Goff, J.; Carroll, M.; Mejia-Ariza, R.; Caba, B.; Pierre, T.; Woodward, R.; Davis, R.; Riffle, J. Stability of Polydimethylsiloxane-Magnetite Nanoparticle Dispersions Against Flocculation: Interparticle Interactions of Polydisperse Materials. *Langmuir* **2008**, *24*, 5060–5069.
68. Harris, L.; Goff, J.; Carmichael, A.; Riffle, J.; Harburn, J.; Pierre, T.; Saunders, M. Magnetite Nanoparticle Dispersions Stabilized with Triblock Copolymers. *Chem. Mater* **2003**, *15*, 1367–1377.
69. Latham, A.; Williams, M. Versatile Routes Toward Functional, Water-Soluble Nanoparticles via Trifluoroethylester– PEG– Thiol Ligands. *Langmuir* **2006**, *22*, 4319–4326.
70. Tan, H.; Xue, J.; Shuter, B.; Li, X.; Wang, J. Synthesis of PEOlated Fe₃O₄@SiO₂ Nanoparticles via Bioinspired Silification for Magnetic Resonance Imaging. *Advanced Functional Materials* **2010**, *20*, 722–731.
71. Liu, X.; Guan, Y.; Ma, Z.; Liu, H. Surface Modification and Characterization of Magnetic Polymer Nanospheres Prepared by Miniemulsion Polymerization. *Langmuir* **2004**, *20*, 10278–10282.
72. Chen, S.; Li, Y.; Guo, C.; Wang, J.; Ma, J.; Liang, X.; Yang, L.; Liu, H. Temperature-Responsive Magnetite/PEO– PPO– PEO Block Copolymer Nanoparticles for Controlled Drug Targeting Delivery. *Langmuir* **2007**, *23*, 12669–12676.
73. Chiappetta, D.; Sosnik, A. Poly (Ethylene Oxide)-Poly (Propylene Oxide) Block Copolymer Micelles as Drug Delivery Agents: Improved Hydrosolubility, Stability and Bioavailability of Drugs. *European Journal of Pharmaceutics and Biopharmaceutics* **2007**, *66*, 303–317.
74. Fan, L.; Du, Y.; Wang, X.; Huang, R.; Zhang, L.; Hu, L. Preparation and Characterization of Alginate/Poly(Vinyl Alcohol) Blend Fibers. *J. of Macromolecular Sc., Part A* **2005**, *42*, 41–50.
75. Ditsch, A.; Laibinis, P.; Wang, D.; Hatton, T. Controlled Clustering and Enhanced Stability of Polymer-Coated Magnetic Nanoparticles. *Langmuir* **2005**, *21*, 6006–6018.

76. Cammas, S.; Nagasaki, Y.; Kataoka, K. Heterobifunctional Poly (Ethylene Oxide): Synthesis of. Alpha.-Methoxy-. Omega.-Amino and. Alpha.-Hydroxy-. Omega.-Amino PEOs with the Same Molecular Weights. *Bioconjugate Chemistry* **1995**, *6*, 226–230.
77. Yang, B.; Guo, C.; Chen, S.; Ma, J.; Wang, J.; Liang, X.; Zheng, L.; Liu, H. Effect of Acid on the Aggregation of Poly (Ethylene Oxide)– Poly (Propylene Oxide)– Poly (Ethylene Oxide) Block Copolymers. *J. Phys. Chem. B* **2006**, *110*, 23068–23074.
78. Gil, E.; Hudson, S. Stimuli-Responsive Polymers and Their Bioconjugates. *Progress in Polymer Science* **2004**, *29*, 1173–1222.
79. Meyer, D.; Shin, B.; Kong, G.; Dewhirst, M.; Chilkoti, A. Drug Targeting Using Thermally Responsive Polymers and Local Hyperthermia. *Journal of Controlled Release* **2001**, *74*, 213–224.
80. Mørup, S.; Hansen, M. F.; Frandsen, C. Magnetic Interactions Between Nanoparticles. *Beilstein journal of nanotechnology* **2010**, *1*, 182–190.
81. Mornet, S.; Vasseur, S.; Grasset, F.; Veverka, P.; Goglio, G.; Demourgues, A.; Portier, J.; Pollert, E.; Duguet, E. Magnetic Nanoparticle Design for Medical Applications. *Progress in Solid State Chemistry* **2006**, *34*, 237–247.
82. Tong, S.; Hou, S.; Zheng, Z.; Zhou, J.; Bao, G. Coating Optimization of Superparamagnetic Iron Oxide Nanoparticles for High T2 Relaxivity. *Nano Letters* **2010**.
83. Kim, T.; Lee, K.; Gong, M.; Joo, S. Control of Gold Nanoparticle Aggregates by Manipulation of Interparticle Interaction. *Langmuir* **2005**, *21*, 9524–9528.
84. Viudez, A. J.; Madueño, R.; Pineda, T.; Blázquez, M. Stabilization of Gold Nanoparticles by 6-Mercaptopurine Monolayers. Effects of the Solvent Properties. *J. Phys. Chem. B* **2006**, *110*, 17840–17847.
85. Wiogo, H. T. R.; Lim, M.; Bulmus, V.; Yun, J.; Amal, R. Stabilization of Magnetic Iron Oxide Nanoparticles in Biological Media by Fetal Bovine Serum (FBS). *Langmuir* **2011**, *27*, 843–850.
86. Harris, J. M.; Chess, R. B. Effect of Pegylation on Pharmaceuticals. *Nature Reviews Drug Discovery* **2003**, *2*, 214–221.

87. Caliceti, P.; Veronese, F. M. Pharmacokinetic and Biodistribution Properties of Poly (Ethylene Glycol)–Protein Conjugates. *Advanced Drug Delivery Reviews* **2003**, *55*, 1261–1277.
88. Bailon, P.; Berthold, W. Polyethylene Glycol-Conjugated Pharmaceutical Proteins. *Pharmaceutical Science & Technology Today* **1998**, *1*, 352–356.
89. Abuchowski, A.; McCoy, J. R.; Palczuk, N. C.; van Es, T.; Davis, F. F. Effect of Covalent Attachment of Polyethylene Glycol on Immunogenicity and Circulating Life of Bovine Liver Catalase. *Journal of Biological Chemistry* **1977**, *252*, 3582–3586.
90. Kozlowski, A.; Milton Harris, J. Improvements in Protein PEGylation: Pegylated Interferons for Treatment of Hepatitis C. *Journal of Controlled Release* **2001**, *72*, 217–224.
91. Li, W.; Zhan, P.; De Clercq, E.; Lou, H.; Liu, X. Current Drug Research on PEGylation with Small Molecular Agents. *Progress in Polymer Science* **2012**.
92. Marcucci, F.; Lefoulon, F. Active Targeting with Particulate Drug Carriers in Tumor Therapy: Fundamentals and Recent Progress. *Drug Discovery Today* **2004**, *9*, 219–228.
93. Yang, S.-J.; Lin, F.-H.; Tsai, K.-C.; Wei, M.-F.; Tsai, H.-M.; Wong, J.-M.; Shieh, M.-J. Folic Acid-Conjugated Chitosan Nanoparticles Enhanced Protoporphyrin IX Accumulation in Colorectal Cancer Cells. *Bioconjugate Chemistry* **2010**, *21*, 679–689.
94. Jayant, S.; Khandare, J. J.; Wang, Y.; Singh, A. P.; Vorsa, N.; Minko, T. Targeted Sialic Acid–Doxorubicin Prodrugs for Intracellular Delivery and Cancer Treatment. *Pharmaceutical research* **2007**, *24*, 2120–2130.
95. Veronese, F. M.; Pasut, G. PEGylation, Successful Approach to Drug Delivery. *Drug Discovery Today* **2005**, *10*, 1451–1458.
96. Duncan, R. Polymer Conjugates as Anticancer Nanomedicines. *Nature Reviews Cancer* **2006**, *6*, 688–701.
97. Ranjan, A.; Pothayee, N.; Seleem, M.; Jain, N.; Sriranganathan, N.; Riffle, J. S.; Kasimanickam, R. Drug Delivery Using Novel Nanoplexes Against a Salmonella Mouse Infection Model. *J Nanopart Res* **2010**, *12*, 905–914.
98. Kolb, H.; Finn, M.; Sharpless, K. Click Chemistry: Diverse Chemical Function From a Few Good Reactions. *Angew. Chem. Int. Ed.* **2001**, *40*, 2004–2021.

99. Kolb, H. C.; Sharpless, K. B. The Growing Impact of Click Chemistry on Drug Discovery. *Drug Discovery Today* **2003**, *8*, 1128–1137.
100. Padwa, A. *1,3-Dipolar Cycloaddition Chemistry*; Padwa, A., Ed. 2nd ed. Wiley, 1984; Vol. 1.
101. Rostovtsev, V.; Green, L.; Fokin, V.; Sharpless, K. A Stepwise Huisgen Cycloaddition Process: Copper(I)-Catalyzed Regioselective TMLigation] of Azides and Terminal Alkynes. *Angew. Chem. Int. Ed.* **2002**, *41*, 2596.
102. Tornøe, C.; Christensen, C.; Meldal, M. Peptidotriazoles on Solid Phase:[1, 2, 3]-Triazoles by Regiospecific Copper (I)-Catalyzed 1, 3-Dipolar Cycloadditions of Terminal Alkynes to Azides. *J. Org. Chem* **2002**, *67*, 3057–3064.
103. Hein, C. D.; Liu, X.-M.; Wang, D. Click Chemistry, a Powerful Tool for Pharmaceutical Sciences. *Pharmaceutical research* **2008**, *25*, 2216–2230.
104. Wang, Q.; Chan, T. R.; Hilgraf, R.; Fokin, V. V.; Sharpless, K. B.; Finn, M. G. Bioconjugation by Copper (I)-Catalyzed Azide-Alkyne [3+ 2] Cycloaddition. *Journal of the American Chemical Society* **2003**, *125*, 3192–3193.
105. Seo, T. S.; Li, Z.; Ruparel, H.; Ju, J. Click Chemistry to Construct Fluorescent Oligonucleotides for DNA Sequencing. *The Journal of Organic Chemistry* **2003**, *68*, 609–612.
106. Isaacman, M. J.; Corigliano, E. M. Stealth Polymeric Vesicles via Metal-Free Click Coupling. *Biomacromolecules* **2013**.
107. Cheng, G.; Fan, X.; Tian, W.; Liu, Y.; Kong, J. Synthesis of Three-Arm Poly(Ethylene Glycol) by Combination of Controlled Anionic Polymerization and “Click” Chemistry. *Polym. Int.* **2010**, *59*, 543–551.
108. Das, M.; Bandyopadhyay, D.; Mishra, D.; Datir, S.; Dhak, P.; Jain, S.; Maiti, T. K.; Basak, A.; Pramanik, P. “Clickable,” Trifunctional Magnetite Nanoparticles and Their Chemoselective Biofunctionalization. *Bioconjugate Chemistry* **2011**, *22*, 1181–1193.
109. Avti, P.; Maysinger, D.; Kakkar, A. Alkyne-Azide “Click” Chemistry in Designing Nanocarriers for Applications in Biology. *Molecules* **2013**, *18*, 9531–9549.
110. Rungta, P.; Bandera, Y. P.; Tsyalkovsky, V.; Foulger, S. H. Designing Fluoroprobes Through Förster Resonance Energy Transfer: Surface Modification of Nanoparticles Through “Click” Chemistry. *Soft Matter* **2010**, *6*, 6083–6095.

111. Krovi, S. A.; Smith, D.; Nguyen, S. T. “Clickable” Polymer Nanoparticles: a Modular Scaffold for Surface Functionalization. *Chem. Commun.* **2010**, *46*, 5277.
112. Iehl, J.; Nierengarten, J.-F. Sequential Copper Catalyzed Alkyne–Azide and Thiol–Ene Click Reactions for the Multiple Functionalization of Fullerene Hexaadducts. *Chem. Commun.* **2010**, *46*, 4160–4162.
113. Baranov, D.; Kadnikova, E. N. Synthesis and Characterization of Azidoalkyl-Functionalized Gold Nanoparticles as Scaffolds for “Click-”Chemistry Derivatization. *J. Mater. Chem.* **2011**, *21*, 6152.
114. Thompson, M.; Vadala, T.; Vadala, M.; Lin, Y.; Riffle, J. Synthesis and Applications of Heterobifunctional Poly (Ethylene Oxide) Oligomers. *Polymer* **2007**, *49*, 345–373.
115. FE Bailey, J.; Koleske, J. V. *Poly (Ethylene Oxide)*; Academic Press, 1976.
116. Kim, Y. J.; Nagasaki, Y.; Kataoka, K.; Kato, M.; Yokoyama, M.; Okano, T.; Sakurai, Y. Heterobifunctional Poly (Ethylene Oxide). *Polym. Bull.* **1994**, *33*, 1–6.
117. Gervais, M.; Labbe, A.; Carlotti, S.; Deffieux, A. Direct Synthesis of α -Azido, ω -Hydroxypolyethers by Monomer-Activated Anionic Polymerization. *Macromolecules* **2009**, *42*, 2395–2400.
118. Dufresne, M.-H.; Gauthier, M. A.; Leroux, J.-C. Thiol-Functionalized Polymeric Micelles: From Molecular Recognition to Improved Mucoadhesion. *Bioconjugate Chemistry* **2010**, *16*, 1027–1033.
119. Hiki, S.; Kataoka, K. Versatile and Selective Synthesis of “Click Chemistry” Compatible Heterobifunctional Poly (Ethylene Glycol) S Possessing Azide and Alkyne Functionalities. *Bioconjugate Chemistry* **2010**, *21*, 248–254.
120. ISHII, T.; YAMADA, M.; HIRASE, T. New Synthesis of Heterobifunctional Poly (Ethylene Glycol) Possessing a Pyridyl Disulfide at One End and a Carboxylic Acid at the Other End. *Polymer Journal* **2005**.
121. Qu, L.; Gu, L.; Li, H.; Taylor, S.; Elkin, T.; Luo, P. G.; Tzeng, T.-R. J.; Jiang, X.; Latour, R. A.; Stutzenberger, F.; *et al.* Galactosylated Polymeric Nanoparticles: Synthesis and Adhesion Interactions with Escherichia Coli. *J. Nanosci. Nanotech.* **2005**, *1*, 61–67.

122. Bhattacharya, D.; Das, M.; Mishra, D.; Banerjee, I.; Sahu, S. K.; Maiti, T. K.; Pramanik, P. Folate Receptor Targeted, Carboxymethyl Chitosan Functionalized Iron Oxide Nanoparticles: a Novel Ultradispersed Nanoconjugates for Bimodal Imaging. *Nanoscale* **2011**, *3*, 1653–1662.
123. Hiki, S.; Kataoka, K. A Facile Synthesis of Azido-Terminated Heterobifunctional Poly (Ethylene Glycol) S for “Click” Conjugation. *Bioconjugate Chemistry* **2007**, *18*, 2191–2196.
124. Labbe, A.; Carlotti, S.; Billouard, C.; Desbois, P.; Deffieux, A. Controlled High-Speed Anionic Polymerization of Propylene Oxide Initiated by Onium Salts in the Presence of Triisobutylaluminum. *Macromolecules* **2010**, *40*, 7842–7847.
125. He, X.; Liang, L.; Xie, M.; Zhang, Y.; Lin, S.; Yan, D. Synthesis of Novel Linear PEO-B-PS-B-PCL Triblock Copolymers by the Combination of ATRP, ROP, and a Click Reaction. *Macromolecular Chemistry and Physics* **2007**, *208*, 1797–1802.
126. Johnson, J. A.; Lu, Y. Y.; Burts, A. O.; Lim, Y.-H.; Finn, M. G.; Koberstein, J. T.; Turro, N. J.; Tirrell, D. A.; Grubbs, R. H. Core-Clickable PEG-Branch-Azide Bivalent-Bottle-Brush Polymers by ROMP: Grafting-Through and Clicking-to. *Journal of the American Chemical Society* **2010**, *133*, 559–566.
127. Wuts, P. G.; Greene, T. W. *Greene's Protective Groups in Organic Synthesis*; 4 ed. John Wiley & Sons, Inc., 2006.
128. Yokoyama, M.; Okano, T.; Sakurai, Y.; Kikuchi, A.; Ohsako, N.; Nagasaki, Y.; Kataoka, K. Synthesis of Poly (Ethylene Oxide) with Heterobifunctional Reactive Groups at Its Terminals by an Anionic Initiator. *Bioconjugate Chemistry* **1992**, *3*, 275–276.
129. Zeng, F.; Allen, C. Synthesis of Carboxy-Functionalized Heterobifunctional Poly (Ethylene Glycol) by a Thiol-Anionic Polymerization Method. *Macromolecules* **2006**, *39*, 6391–6398.
130. Amstad, E.; Gehring, A. U.; Fischer, H.; Nagaiyanallur, V. V.; Hähner, G.; Textor, M.; Reimhult, E. Influence of Electronegative Substituents on the Binding Affinity of Catechol-Derived Anchors to Fe₃O₄ Nanoparticles. *The Journal of Physical Chemistry C* **2011**, *115*, 683–691.
131. Saville, S. L.; Stone, R.; Qi, B.; Mefford, O. T. Investigation of the Stability of Magnetite Nanoparticles Functionalized with Catechol Based Ligands in Biological Media. *J. Mater. Chem.* **2012**.

132. Majeed, M. I.; Lu, Q.; Yan, W.; Li, Z.; Hussain, I.; Tahir, M. N. Highly Water-Soluble Magnetic Iron Oxide (Fe₃O₄) Nanoparticles for Drug Delivery: Enhanced in Vitro Therapeutic Efficacy of Doxorubicin and MION Conjugates. *J. Mater. Chem.* **2013**.
133. Park, K. M.; Lee, Y.; Son, J. Y.; Oh, D. H.; Lee, J. S.; Park, K. D. Synthesis and Characterizations of in Situ Cross-Linkable Gelatin and 4-Arm-PPO-PEO Hybrid Hydrogels via Enzymatic Reaction for Tissue Regenerative Medicine. *Biomacromolecules* **2012**, *13*, 604–611.
134. Roberts, M.; Bentley, M.; Harris, J. Chemistry for Peptide and Protein PEGylation. *Advanced Drug Delivery Reviews* **2002**, *54*, 459–476.
135. Binder, W. “Click” Chemistry in Polymer and Materials Science. *Macromolecular rapid ...* **2007**.
136. Deng, Y.; Zhang, S.; Lu, G.; Huang, X. Constructing Well-Defined Star Graft Copolymers. *Polym. Chem.* **2013**, *4*, 1289.
137. Huang, J.; Wan, S.; Guo, M.; Yan, H. Preparation of Narrow or Mono-Disperse Crosslinked Poly ((Meth) Acrylic Acid)/Iron Oxide Magnetic Microspheres. *J. Mater. Chem.* **2006**, *16*, 4535–4541.
138. Yen, S. K.; Janczewski, D.; Lakshmi, J. L.; Dolmanan, S. B. Design and Synthesis of Polymer Functionalized NIR Fluorescent Dyes–Magnetic Nanoparticles for Bioimaging. *ACS Nano* **2013**.
139. Stone, R.; Willi, T.; Rosen, Y.; Mefford, O. T.; Alexis, F. Targeted Magnetic Hyperthermia. *Therapeutic Delivery* **2011**, *2*, 815–838.
140. Kohler, N.; Fryxell, G.; Zhang, M. A Bifunctional Poly (Ethylene Glycol) Silane Immobilized on Metallic Oxide-Based Nanoparticles for Conjugation with Cell Targeting Agents. *J. Am. Chem. Soc* **2004**, *126*, 7206–7211.
141. Benyettou, F.; Chebbi, I.; Motte, L.; Seksek, O. Magnetoliposome for Alendronate Delivery. *J. Mater. Chem.* **2011**, *21*, 4813–4820.
142. Ma, M.; Zhang, Y.; Yu, W.; Shen, H. Y.; Zhang, H.; Gu, N. Preparation and Characterization of Magnetite Nanoparticles Coated by Amino Silane. *Colloids and Surfaces A: Physicochemical and Engineering Aspects* **2003**, *212*, 219–226.

143. Miles, W. C.; Goff, J. D.; Huffstetler, P. P.; Reinholz, C. M.; Pothayee, N.; Caba, B. L.; Boyd, J. S.; Davis, R. M.; Riffle, J. Synthesis and Colloidal Properties of Polyether– Magnetite Complexes in Water and Phosphate-Buffered Saline. *Langmuir* **2008**, *25*, 803–813.
144. Lee, H.; Scherer, N.; Messersmith, P. Single-Molecule Mechanics of Mussel Adhesion. *Proceedings of the National Academy of Sciences* **2006**, *103*, 12999.
145. Chirdon, W.; O'Brien, W.; Robertson, R. Adsorption of Catechol and Comparative Solutes on Hydroxyapatite. *J. Biomed. Mater. Res.* **2003**, *66B*, 532–538.
146. Amstad, E.; Textor, M.; Reimhult, E. Stabilization and Functionalization of Iron Oxide Nanoparticles for Biomedical Applications. *Nanoscale* **2011**.
147. Zhang, Y.; Kohler, N.; Zhang, M. Surface Modification of Superparamagnetic Magnetite Nanoparticles and Their Intracellular Uptake. *Biomaterials* **2002**, *23*, 1553–1561.
148. Yang, X.; Hong, H.; Grailer, J. J.; Rowland, I. J.; Javadi, A.; Hurley, S. A.; Xiao, Y.; Yang, Y.; Zhang, Y.; Nickles, R. J.; *et al.* cRGD-Functionalized, DOX-Conjugated, and ⁶⁴Cu-Labeled Superparamagnetic Iron Oxide Nanoparticles for Targeted Anticancer Drug Delivery and PET/MR Imaging. *Biomaterials* **2011**, *32*, 4151–4160.
149. Sun, S.; Zeng, H.; Robinson, D.; Raoux, S.; Rice, P.; Wang, S.; Li, G. Monodisperse MFe₂O₄ (M= Fe, Co, Mn) Nanoparticles. *J. Am. Chem. Soc* **2004**, *126*, 273–279.
150. Giustini, A. J.; Ivkov, R.; Hoopes, P. J. Magnetic Nanoparticle Biodistribution Following Intratumoral Administration. *Nanotechnology* **2011**, *22*, 345101.
151. Amiji, M.; Park, K. Surface Modification of Polymeric Biomaterials with Poly (Ethylene Oxide), Albumin, and Heparin for Reduced Thrombogenicity. *Journal of Biomaterials Science, Polymer Edition* **1993**, *4*, 217–234.
152. Pavlin, M.; Bregar, V. B. Stability of Nanoparticle Suspensions in Different Biologically Relevant Media. *Dig J Nanomater Bios* **2012**, *7*, 1389–1400.
153. Daniele, M. A.; Shaughnessy, M. L.; Roeder, R.; Childress, A.; Bandera, Y. P.; Foulger, S. Magnetic Nanoclusters Exhibiting Protein-Activated Near-Infrared Fluorescence. *ACS Nano* **2012**, *7*, 203–213.

154. Daniele, M. A.; Bandera, Y. P.; Sharma, D.; Rungta, P.; Roeder, R.; Sehorn, M. G.; Foulger, S. H. Substrate-Baited Nanoparticles: a Catch and Release Strategy for Enzyme Recognition and Harvesting. *Small* **2012**, *8*, 2083–2090.
155. Chekina, N.; Horák, D.; Jendelová, P.; Trchová, M. Fluorescent Magnetic Nanoparticles for Biomedical Applications. *J. Mater. Chem.* **2011**.
156. Balivada, S.; Rachakatla, R.; Wang, H.; Samarakoon, T. N.; Dani, R.; Pyle, M.; Kroh, F. O.; Walker, B.; Leaym, X.; Koper, O. B.; *et al.* A/C Magnetic Hyperthermia of Melanoma Mediated by Iron(0)/Iron Oxide Core/Shell Magnetic Nanoparticles: a Mouse Study. *BMC Cancer* **2010**, *10*, 119.
157. Susumu, K.; Uyeda, H. T.; Medintz, I. L.; Pons, T.; Delehanty, J. B.; Mattoussi, H. Enhancing the Stability and Biological Functionalities of Quantum Dots via Compact Multifunctional Ligands. *Journal of the American Chemical Society* **2007**, *129*, 13987–13996.
158. Mei, B. C.; Susumu, K.; Medintz, I. L.; Delehanty, J. B.; Mountziaris, T. J.; Mattoussi, H. Modular Poly (Ethylene Glycol) Ligands for Biocompatible Semiconductor and Gold Nanocrystals with Extended pH and Ionic Stability. *J. Mater. Chem.* **2008**, *18*, 4949–4958.
159. Bagaria, H. G.; Xue, Z.; Neilson, B. M.; Worthen, A. J.; Yoon, K. Y.; Nayak, S.; Cheng, V.; Lee, J. H.; Bielawski, C. W.; Johnston, K. P. Iron Oxide Nanoparticles Grafted with Sulfonated Copolymers Are Stable in Concentrated Brine at Elevated Temperatures and Weakly Adsorb on Silica. *ACS Appl. Mater. Interfaces* **2013**, *5*, 3329–3339.
160. Bagaria, H. G.; Neilson, B. M.; Worthen, A. J.; Xue, Z.; Yoon, K. Y.; Cheng, V.; Lee, J. H.; Velagala, S.; Huh, C.; Bryant, S. L.; *et al.* Journal of Colloid and Interface Science. *Journal of Colloid and Interface Science* **2013**, *398*, 217–226.
161. Goff, J. D.; Huffstetler, P. P.; Miles, W. C.; Pothayee, N.; Reinholz, C. M.; Ball, S.; Davis, R. M.; Riffle, J. S. Novel Phosphonate-Functional Poly (Ethylene Oxide)-Magnetite Nanoparticles Form Stable Colloidal Dispersions in Phosphate-Buffered Saline. *Chemistry of Materials* **2009**, *21*, 4784–4795.
162. Ling, D.; Park, W.; Park, Y. I.; Lee, N.; Li, F.; Song, C.; Yang, S. G.; Choi, S. H.; Na, K.; Hyeon, T. Multiple-Interaction Ligands Inspired by Mussel Adhesive Protein: Synthesis of Highly Stable and Biocompatible Nanoparticles. *Angew. Chem. Int. Ed.* **2011**, *50*, 11360–11365.

163. Na, H. B.; Palui, G.; Rosenberg, J. T.; Ji, X.; Grant, S. C.; Mattoussi, H. Multidentate Catechol-Based Polyethylene Glycol Oligomers Provide Enhanced Stability and Biocompatibility to Iron Oxide Nanoparticles. *ACS Nano* **2012**, *6*, 389–399.
164. Tessmar, J. K.; Mikos, A. G.; Gopferich, A. Amine-Reactive Biodegradable Diblock Copolymers. *Biomacromolecules* **2001**, *3*, 194–200.
165. Fan, X.; Huang, B.; Wang, G.; Huang, J. Synthesis of Amphiphilic Heteroeight-Shaped Polymer Cyclic-[Poly (Ethylene Oxide)-B-Polystyrene] 2 via “Click” Chemistry. *Macromolecules* **2012**, *45*, 3779–3786.
166. Berry, C. C.; Curtis, A. S. Functionalisation of Magnetic Nanoparticles for Applications in Biomedicine. *Journal of Physics D: Applied Physics* **2003**, *36*, R198.
167. Gupta, A. K.; Wells, S. Surface-Modified Superparamagnetic Nanoparticles for Drug Delivery: Preparation, Characterization, and Cytotoxicity Studies. *NanoBioscience, IEEE Transactions on* **2004**, *3*, 66–73.
168. Scudiero, D. A.; Shoemaker, R. H.; Paull, K. D.; Monks, A.; Tierney, S.; Nofziger, T. H.; Currens, M. J.; Seniff, D.; Boyd, M. R. Evaluation of a Soluble Tetrazolium/Formazan Assay for Cell Growth and Drug Sensitivity in Culture Using Human and Other Tumor Cell Lines. *Cancer research* **1988**, *48*, 4827–4833.
169. Santhosh, P. B.; Ulrih, N. P. Multifunctional Superparamagnetic Iron Oxide Nanoparticles: Promising Tools in Cancer Theranostics. *CANCER LETTERS* **2013**.
170. Guo, J.; Meng, F.; Li, X.; Wang, M. PEGylated Click Polypeptides Synthesized by Copper-Free Microwave-Assisted Thermal Click Polymerization for Selective Endotoxin Removal From Protein *Macromolecular ...* **2012**.
171. Hafelli, U. O.; Riffle, J. S.; Harris-Shekhawat, L.; Carmichael-Baranauskas, A.; Mark, F.; Dailey, J. P.; Bardenstein, D. Cell Uptake and in Vitro Toxicity of Magnetic Nanoparticles Suitable for Drug Delivery. In; 2009; Vol. 6, pp. 1417–1428.
172. Kim, D.-H.; Kim, K.-N.; Kim, K.-M.; Lee, Y.-K. Targeting to Carcinoma Cells with Chitosan- and Starch-Coated Magnetic Nanoparticles for Magnetic Hyperthermia. *Journal of Biomedical Materials Research Part A* **2009**, *88A*, 1–11.

173. Mahmoudi, M.; Sant, S.; Wang, B.; Laurent, S.; Sen, T. Superparamagnetic Iron Oxide Nanoparticles (SPIONs): Development, Surface Modification and Applications in Chemotherapy. *Advanced Drug Delivery Reviews* **2010**.
174. Frangioni, J. In Vivo Near-Infrared Fluorescence Imaging. *Current opinion in chemical biology* **2003**, *7*, 626–634.
175. Luo, P. G.; Tzeng, T.-R.; Qu, L.; Lin, Y.; Caldwell, E.; Latour, R. A.; Stutzenberger, F.; Sun, Y.-P. Quantitative Analysis of Bacterial Aggregation Mediated by Bioactive Nanoparticles. *J. Nanosci. Nanotech.* **2005**, *1*, 291–296.
176. Raftery, T. D.; Kerscher, P.; Hart, A. E.; Saville, S. L.; Qi, B.; Kitchens, C. L.; Mefford, O. T.; McNealy, T. L. Discrete Nanoparticles Induce Loss of *Legionella Pneumophila* Biofilms From Surfaces. *Nanotoxicology* **2013**, 1–8.
177. Misri, R.; Saatchi, K.; Häfeli, U. O. Nanoprobes for Hybrid SPECT/MR Molecular Imaging. *Nanomedicine* **2012**, *7*, 719–733.
178. Litchman, E. Invisible Invaders: Non-Pathogenic Invasive Microbes in Aquatic and Terrestrial Ecosystems. *Ecology letters* **2010**, *13*, 1560–1572.
179. Ferré, M. S.; Arias, C.; Oliva, J. M.; Pedrol, A.; Garcia, M.; Pellicer, T.; Roura, P.; Dominguez, A. A Community Outbreak of Legionnaires' Disease Associated with a Cooling Tower in Vic and Gurb, Catalonia (Spain) in 2005. *European journal of clinical microbiology & infectious diseases* **2009**, *28*, 153–159.
180. Fields, B. S.; Benson, R. F.; Besser, R. E. Legionella and Legionnaires' Disease: 25 Years of Investigation. *Clinical Microbiology Reviews* **2002**, *15*, 506–526.
181. WHITE, P. S.; GRAHAM, F. F.; Harte, D.; BAKER, M. G.; AMBROSE, C. D.; Humphrey, A. Epidemiological Investigation of a Legionnaires' Disease Outbreak in Christchurch, New Zealand: the Value of Spatial Methods for Practical Public Health. *Epidemiol. Infect.* **2013**, *141*, 789–799.
182. Raftery, T. D.; Lindler, H.; McNealy, T. L. Altered Host Cell–Bacteria Interaction Due to Nanoparticle Interaction with a Bacterial Biofilm. *Microb Ecol* **2012**, *65*, 496–503.
183. Gallagher, F. A. An Introduction to Functional and Molecular Imaging with MRI. *Clinical radiology* **2010**, *65*, 557–566.
184. Prata, M.; Santos, A. C.; Geraldés, C.; De Lima, J. Structural and in Vivo Studies of Metal Chelates of Ga (III) Relevant to Biomedical Imaging. *Journal of Inorganic Biochemistry* **2000**, *79*, 359–363.

185. Szijjártó, C.; Pershagen, E.; Borbas, K. E. Functionalisation of Lanthanide Complexes via Microwave-Enhanced Cu (I)-Catalysed Azide–Alkyne Cycloaddition. *Dalton Transactions* **2012**, *41*, 7660–7669.
186. Wade, S. A.; Collins, S. F.; Baxter, G. W. Fluorescence Intensity Ratio Technique for Optical Fiber Point Temperature Sensing. *Journal of Applied Physics* **2003**, *94*, 4743.
187. Sudimack, J. Targeted Drug Delivery via the Folate Receptor. *Advanced Drug Delivery Reviews* **2000**.
188. Wuts, P. G.; Greene, T. W. Greene's Protective Groups in Organic Synthesis. **2006**.
189. Lutz, J.-F.; Hoth, A. Preparation of Ideal PEG Analogues with a Tunable Thermosensitivity by Controlled Radical Copolymerization of 2-(2-Methoxyethoxy) Ethyl Methacrylate and Oligo (Ethylene Glycol) Methacrylate. *Macromolecules* **2006**, *39*, 893–896.
190. Saville, S. L.; Woodward, R.; House, M.; Tokarev, A. The Effect of Magnetically Induced Linear Aggregates on Proton Transverse Relaxation Rates of Aqueous Suspensions of Polymer Coated Magnetic Nanoparticles. *Nanoscale* **2013**.
191. Sondjaja, R.; Alan Hatton, T.; Tam, M. K. Clustering of Magnetic Nanoparticles Using a Double Hydrophilic Block Copolymer, Poly (Ethylene Oxide)-B-Poly (Acrylic Acid). *Journal of Magnetism and Magnetic Materials* **2009**, *321*, 2393–2397.
192. Huang, J.; Bu, L.; Xie, J.; Chen, K.; Cheng, Z.; Li, X.; Chen, X. Effects of Nanoparticle Size on Cellular Uptake and Liver MRI with Polyvinylpyrrolidone-Coated Iron Oxide Nanoparticles. *ACS Nano* **2010**, *4*, 7151–7160.
193. Wilhelm, C.; Billotey, C.; Roger, J.; Pons, J. N.; Bacri, J. C.; Gazeau, F. Intracellular Uptake of Anionic Superparamagnetic Nanoparticles as a Function of Their Surface Coating. *Biomaterials* **2003**, *24*, 1001–1011.